# FUNCTIONAL STUDIES OF NUSAP IN MICROTUBULE STABILITY, CHROMOSOME OSCILLATION AND MIDZONE FORMATION DURING MITOSIS

**CHENYU LI**

**(B.Sc., Fudan University, China)**

**A THESIS SUBMITTED FOR THE DEGREE OF DOCTOR OF PHILOSOPHY**

**DEPARTMENT OF BIOLOGICAL SCIENCES**

**NATIONAL UNIVERSITY OF SINGAPORE**

**2015**

**DECLARATION**

I here by declare that this thesis is my original work and it has been written by me in its entirety. I have duly acknowledged all the sources of information which have been used in this thesis.

This thesis has also not been submitted for any degree in any university previously.

_____

Chenyu Li

December, 2014

**Acknowledgements**

The work presented in this thesis was carried out at L.Y-.C.'s Lab, Department of Biological Science, National University of Singapore, from July 2010 to January 2015. I am so blessed to have so many kind, helpful and brilliant people to wholeheartedly help me in my graduate studies. Their efforts contribute so much to this manuscript and a big acknowledgement must precede the contents of this thesis.

First of all, I greatly thank Dr. Liou Yih-Cherng, my mentor from the very bottom of my heart. It is his continuous support and encouragements that help me go through all the failings to continue chasing my career goal. His innovative insights, valuable guidance and unsurpassed knowledge contribute the most to the work presented here. Moreover, his unfaltering devotion to developing independent scientific minds and his never-giving-up character that I appreciate and learn most.

I am very lucky to work with all the lab members in L.Y-.C. lab and very grateful to have the pleasure of being around a friendly and helpful gang of people. A big thankful to Yang Qiaoyun, Xiao Lin, Xiao Bin, Zhang Yajun, Bhavani K, Zhang Rui, Xian Hongxu and our previous lab members, Lai Chengyu, Chang Jawshin

and Xia Yun for having their moral support, valuable suggestions and making my lab life joyful. I want to specifically thank Dr. Ye Fan for his contributions in sharing his scientific opinions and discussions which I benefit a lot. Also, my collaborators Xue Chenyi and Le Beilin deserve a special mention for their consistent help to reach the collaborative scientific goal, only with which the work can be done. Great thanks to Xia Han and Chen Shi for their important advices and our friendship will be cherished most.

In addition, I particularly thank Dr. Chen Ee Sin and Dr. Cynthia He for their time and effort in guiding my research, and Dr. Alexander Bershadsky, Dr. Low Boon Chuan, Dr. Deng Lih wen, Dr. Artem Yefremov and Dr. Cheng-Han Yu for their instructive suggestions and criticism. I would like to thank the Center of BioImaging Sciences (CBIS) at National University of Singapore, especially to Ms. Yan Tong and Dr. Jian Shi for the technical support, James Zhao and Weijuan Wong from Advanced Bio-Imaging Core Singhealth, Dr. Adam Cliffe from Leica and Dr. Clement Khaw and Jian Chow Soo from Nikon for their great help with the imaging systems.

It is my family to whom I am so grateful beyond words for their unconditional support, which is the motive for me to continue pursuing my scientific research goals. Hence, I dedicate my thesis to my dearest mom Luo Li and dad Li Jun.

Last but not least, I would like to acknowledge the Department of Biological Science and the National University of Singapore for supporting the course of my study.

Chenyu LI

December, 2014

## Table of Contents

**Summary**

Mitosis is critical to multiple aspects of life in mammalian cells, which defects lead to cancer. During mitosis, an accurate spindle formation with a precise chromosome alignment is the pre-conditions for precise chromosome separation into two daughter cells and the process is under tightly control of microtubule associated proteins, kinesins and kinases. Despite its importance, the mechanism of mitosis is still a mystery.

NuSAP (Nucleolar and Spindle Associated Protein), a microtubule associated protein, plays a critical role in stabilizing microtubules both in vitro and in vivo. Previous studies indicate the depletion of NuSAP leads to severe mitotic defects. However, the function of NuSAP in mitosis is still largely unknown.

To address this question, we first dissect the function of NuSAP in kinetochore microtubules. Our study identifies NuSAP as a novel negative regulator of the microtubule depolymerizer-MCAK (Mitotic Centromere-Associated Kinesin). NuSAP tightly regulates both the localization and depolymerization activity of MCAK. Moreover, we demonstrate that the interaction of NuSAP with MCAK and the regulation of NuSAP on MCAK are positively modulated by the mitotic

kinase—Aurora B. Our results elucidate a vital mechanism that NuSAP controls kinetochore microtubule dynamics by modulating MCAK, in an Aurora B kinase-dependent manner. Furthermore, our finding shows that NuSAP pivotally functions in chromosome alignment, orientation and oscillation through its regulation of a chromokinesin—Kif22. Furthermore, we specifically investigated the impact of NuSAP on the polar ejection force generated by Kif22. We also found that NuSAP disrupts the kinesin—Kif4a localization at midzone region during anaphase, which indicates its important role in midzone formation during mitosis.

Taken together, our findings reveal that NuSAP has major roles in mitosis through the spatially and temporally regulation of different kinesins during different mitotic stages. Thus, our study provides new insights into the complicated regulations of a microtubule associated protein in mitosis to ensure precise chromosome segregation during cell division.

**List of Figures**

**List of Tables**

**List of Abbreviations**

| | |
|---|---|
| NuSAP | Nuclear and spindle associated protein |
| MCAK | Mitotic and Centromere Associated Protein |
| Kif22 | Kinesin 22, kid, kinesin like DNA binding protein |
| ACA | Anti-Centromere Antibody |
| APC | anaphase promoting complex |
| CENP-A | centromere protein A |
| RanGTP | GTP bound form of Ran |
| RNAi | RNA interference |
| 3D | three-dimensional |
| MAP | Microtubule associated protein |
| MT | microtubule |
| KT | kinetochore |
| kMT | kinetochore microtubules |
| iMT | interpolar microtubules |
| PEF | polar ejection force |
| ICD | inter-centromere distance |
| CIN | chromosome instability |

**List of publications**

Publications relating to the research works from the current thesis

**1.** Li, C. Zhang, Y. Yang, Q. Ye, F. Sun, Y. Chen E.S. Liou Y.C. (2015). NuSAP stabilizes kinetochore microtubules by attenuating MCAK depolymerization activity. (Scientific Reports)

**2.** Li, C. Xue, C. Yang, Q. Low B.C. Liou Y.C. (2015). NuSAP governs centrosome oscillation by regulating Kif22 generated polar ejection force. (under revision)

Oral or poster presentations presented in conference from the current thesis

**1.** The 2015 ASBMB annual meeting (Poster presentation). ASBMB, Boston, USA. March 2015.

**2.** The 2014 ASCB annual meeting (ePoster talk). ASCB, Philadelphia, USA. December 2014. Graduate Travel Award from ASCB. Graduate Travel Grant from Lee Foundation.

**3.** EMBO microtubule structure, regulation and functions conference (Poster presentation). EMBL, Germany. April 2014. Graduate Travel award from Department of Biological Science, National University of Singapore

**4.** The 7$^{th}$ Asian Pacific Organization For Cell Biology (APOCB) conference (Poster presentation and volunteer). Biopolis, Singapore. February 2014.

**5.** The 2012 ASCB annual meeting (Poster presentation). ASCB, San Francisco, USA. December 2012.

**6.** The 16th Biological Sciences Graduate Congress (Poster presentation). Department of Biological Science, National University of Singapore. December 2011.

Publications from other projects not included in the current thesis

**1.** Ruan, K[1]. Ye, F[1]. Li, C[1]. Liou, Y. C. Lin, S. C. Lin, S. Y. * (2012). PLK1 interacts and phosphorylates Axin that is essential for proper centrosome formation. Plos One ([1] the authors contributed equally )

**2.** Ye, J. Shi, H. Shen, Y. Peng, C. Liu, Y. Li, C. Deng , K. Geng, J. Xu,T. Zhuang, Y. Zheng, B. Tao, W. * (2014). *PP6* controls T cell development and homeostasis by negatively regulating distal TCR signaling. Journal of Immunology.

**3.** Peng, C. Ye, J. Yan, S. Kong, S. Shen, Y. Li, C. Li, Q. Zheng, Y. Deng, K. Xu, T. Tao, W. (2012). Ablation of vacuole protein sorting 18 (Vps18) gene leads to neurodegeneration and impaired neuronal migration by disrupting multiple vesicle transport pathways to lysosomes. Journal of Biological Chemistry.

# CHAPTER 1 Introduction

## 1.1 Mitotic spindle

### 1.1.1 Microtubules and mitotic spindle

Microtubules are hollow, cylindrical polymers assembled from alpha and beta tubulin heterodimers approximately 25nm in diameter with 13 linear protofilaments. Beta tubulin subunits are exposed at the faster polymerizing plus end and alpha tubulins are exposed at the slower polymerizing minus ends of the microtubules. In addition, a third type of tubulin gamma tubulin is concentrated at centrosomes for microtubule initiation.

Both the polarity and dynamics are unique features of microtubules and microtubules undergo continual assembly and disassembly with two distinct ends within the cell, a fast-growing plus ends and a slow-growing minus end. This polarity is important for determining the direction of the movement along the microtubules, for example, dyneins to the minus end and kinesins to the plus end of the microtubules. The dyanmics instability indicates individual microtubules alternate between cycles of growth and shrinkage with rapid GTP hydrolysis on beta tubulin. The high concentration of tubulin bound to GTP leads to the growth of microtubules and the presence of GDP-tubulin at microtubule ends leads to

depolymerization of the microtubules. The function of microtubules determines the shape of the cell and in a variety of cell movements, including intracellular transport of organelles and separation of chromosomes during mitosis (Gall, 1966).

The spindle is a structure formed during chromosome seperation in mitosis or meiosis, which is essential to distribute the hereditary mateial into the two daughter cells. sThe mitotic spindle is made up of microtubules extending from two opposing spindle poles. The minus ends of these microtubules accurate together to form two centrosomes, while the plus ends extend away from poles (Inoue, 1960). There are three kinds of microtubules in the mitotic spindle—kinetochore microtubules, interpolar microtubules and astral microtubules (Rieder, 1990). Kinetochore microtubules directly attach to the chromosomes and function to align or separate the chromosomes during mitosis. Interpolar microtubules from two spindle poles overlap at the metaphase plate to enable spindle pole separation during late mitotic stage. Astral microtubules are the microtubules extend from centrosomes towards cell membrane and important to position mitotic spindle (Chapman et al., 2000; Schaerer-Brodbeck and Riezman, 2000; Walczak, 2000).

### 1.1.2 Kinetochore microtubule

Kinetochore microtubules are critical and directly connect to kinetochores on sister chromatids to generate proper tension and ensure error-free chromosome separation (Biggins and Walczak, 2003; Kline-Smith et al., 2005). Before chromosomes segregation occurs, a bipolar mitotic spindle is assembled into two overlapping microtubule arrays that attach to the kinetochores and align chromosomes at the metaphase plate. One commonly accepted mechanism of this progress is the "search and capture" model (Hinkle et al., 2000; Maddox et al., 1999). A higher RanGTP gradient at the metaphase plate region accelerates microtubules polymerization to increase the efficiency of microtubules to capture kinetochores. Kinetochore microtubule arrangements that generate normal tension are selectively stabilized (Desai and Hyman, 1999; Kalab et al., 1999; Nishimoto, 1999; Wilde and Zheng, 1999; Zhang et al., 1999).

During metaphase, the dynamics of kinetochore microtubules is tightly controlled by microtubule associated proteins, motor proteins and mitotic kinases in order to precisely align chromosomes at the metaphase plate (Cimini, 2007; Joglekar et al., 2010; Slep and Vale, 2007). When incidence of impropriate chromosome-microtubule binding happens, such as mono-oriented attachment or lagging chromosomes, the error correction system in spindle will be activated. To date,

Aurora B complex has been reported to detect the inappropriate attachments based on the tension of the microtubules. The complex can specifically recognize and depolymerize the kinetochore microtubules that are syntelically or merotically attached (Toso et al., 2009; Zhang and Walczak, 2006). Disruption of this process leads to chromosome instability, which is considered to be one of the main causes of carcinogenesis (Bakhoum et al., 2009; Sanhaji et al., 2011; Sudakin and Yen, 2007).

### 1.1.3 Chromosome oscillation

In vertebrate cells, chromosomes oscillate to align at metaphase plate during metaphase (Lewis, 1939). The oscillation can be divided into two processes according the direction of the chromosomes—towards the pole and away from the pole (Skibbens et al., 1993a). The poleward motion is mainly generated by the depolymerization of the kinetochore microtubules (kinetochore microtubules) (Hays and Salmon, 1990b) and the anti-poleward motion largely depends on the motors sliding chromosome arms at interpolar microtubules (Rieder et al., 1986b). Many studies investigated the possible involved factors during chromosome oscillation. One of the predicted models is the tug-of-war mechanism between the opposing motors that changes the course of chromosome oscillation (Sutradhar and Paul, 2014), for example kinesins (Gardner et al., 2008; Stumpff et al., 2008)

and dyneins (King et al., 2000a). The major forces are from the net polar force that generated on kinetochore microtubules and the polar ejection force generated on interpolar microtubules (Rieder et al., 1986a). The polar force is positively related to kinetochore-to-pole distance, the number and dynamics of kinetochore microtubules (Hays and Salmon, 1990a). On the other hand, the polar ejection force is negatively related with the kinetochore-to-pole distance and directly correlated with the microtubule density (Joglekar and Hunt, 2002; Ke et al., 2009; Skibbens et al., 1993b). One portion of the force imbalance upon the chromosome is absolved by the kinetochore besides the mechanical tug-of-war mechanism (Liu et al., 2007) and the KMN complex couples the oscillation at kinetochore-microtubule attachment (McClelland et al., 2007). Previous investigations suggest the integrity of the spindle pole may also involve in the forces balancing during the oscillation (Gordon et al., 2001). Microtubule associated proteins plays vital roles in regulating chromosome oscillation by tightly maintaining both the dynamics of kinetochore microtubules and the surface properties of interpolar microtubules (Maiato et al., 2004).

### 1.1.4 Central spindle

At anaphase, the sister chromatids are separated by the shortening of the attached kinetochore microtubules and the interpolar microtubules are bundled at the

middle part of the spindle between the separated daughter chromosome (Rieder, 1990). The two masses of parallel microtubule bundles with opposite directionalities in the center of the inter-chromosomal region are referred as central spindle (spindle midzone) (McDonald et al., 1979). In anaphase, multiple mitotic kinesins and microtubule associated proteins are recruited to the antiparallel array of microtubules at the central spindle (Saxton and McIntosh, 1987). The region recruits several key midzone components, such as the chromosome passenger complex, polo-like kinase 1, PRC1 and Kif4a (Hornick et al., 2010). The stability and length of the central spindle microtubules are critical for accurate chromosome separation at telophase and cell division at cytokinesis.

## 1.2 Roles of NuSAP

### 1.2.1 NuSAP functional domains

NuSAP (Nucleolar and Spindle Associated Protein) is a microtubule associated protein and plays an important role in the spindle assembly (Hussain et al., 2009; Raemaekers et al., 2003b). Human NuSAP locates on 15q 15.1, and the cDNA of NuSAP encodes 441 amino acids. The amino acid sequence of human NuSAP shows a highly resistant homology among different species (Raemaekers et al., 2003a). NuSAP has a number of functional domains (Figure 1.2.1) (Iyer et al., 2011a).

The SAP domain (hydrophobic, polar, aliphatic and bulky) has been defined by Aravind and Koonin in 2000 (Aravind and Koonin, 2000). This domain is responsible for chromosome binding (Verbakel et al., 2011). The nuclear localization signal (NLS) is a short sequence motif which is critical for the nucleo-cytoplasmic targeting of proteins. This sequence can be recognized by importin alpha or beta and the binding between importin proteins and NLS is further regulated by RanGTP proteins. KEN box, containing the amino acid sequence KEN, is important for directing target protein for APC/C (anaphase-promoting ubiquitin ligase complex) which further degraded the KEN box containing protein through ubiquitin-proteolysis pathway. Moreover, the KEN

box can be recognized by Cdh1/Hct1 and the binding between KEN box containing protein and Cdc20 or Cdh1 subsequently stimulate the recruitment of APC and thus leads to protein degradation. The CHhD domain (Charged helical domain) is well conserved among different species in microtubule associated protein families, until now the function of this motif is still unclear (Lara-Chacon et al., 2010; Levin et al., 1990).

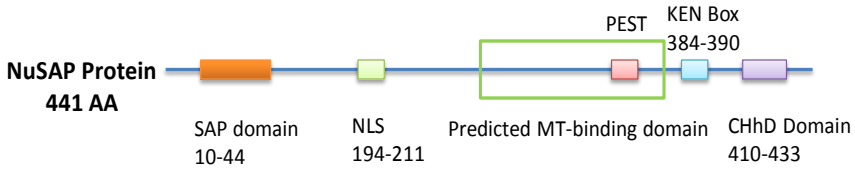


**Figure 1.2.1 Potential functional domains on human NuSAP**

Five potential domains are predicted in NuSAP, SAP domain from 10-44AA, NLS domain 194-211, predicted microtubules-binding domain 233-383AA, KEN box 384-390AA, CHhD domain 410-433 AA.

### 1.2.2 NuSAP modification

There are around 50 possible phosphorylation sites on NuSAP are predicted using bioinformatics prediction, as shown in Figure 1.2.2. However, so far only three phosphorylation sites are identified. The residue S240 of NuSAP was shown to be phosphorylated by a proteomics study, but its impact is still unknown (Sardon et

al., 2010). On the other hand, the residues T300 and T338 of NuSAP were identified to be phosphorylated by cdk1 regulate its microtubule binding ability (Chou et al., 2011). One recent study also indicates that NuSAP is presented as a novel PARP1 target and can be modified by poly (ADP-ribosyl) ation (Jungmichel et al., 2013). NuSAP is demonstrated to undergo PARylation under a specific genotoxic stress treatment with nocodazole.

**NuSAP protein sequence**

```
MIIPSLEELDSLKYSDLQNLAKSLGLRANLRATKLLKALKGYIKHEARKGNENQDESQTSASSCDETEIQISNQEEAERQ   80
PLGHVTKTRRRCKTVRVDPDSQQNHSEIKISNPTEFQNHEKQESQDLRATAKVPSPPDEHQEAENAVSSGNRDSKVPSEG  160
KKSLYTDESSKPGKNKRTAITTPNFKKLHEAHFKEMESIDQYIERKKKHFEEHNSMNELKQQPINKGGVRTPVPPRGRLS  240
VASTPISQRRSQGRSCGPASQSTLGLKGSLKRSAISAAKTGVRFSAATKDNEHKRSLTKTPARKSAHVTVSGGTPKGEAV  320
LGTHKLKTITGNSAAVITPFKLTTEATQTPVSNKKPVFDLKASLSRPLNYEPHKGKLKPWGQSKENNYLNQHVNRINFYK  400
KTYKQPHLQTKEEQRKKREQERKEKKAKVLGMRRGLILAED                                           441
. . . . S . . . . . S . . Y . . . . . . . . . . . . . . . . . . . . . . . . . . . . . . . . . . . . . . . . . . . . S . T S . S S . . . . . . . . S . . . . . . . .   8 0
. . . . . . . T . . . . . T . . . . . . S . . . . S . . . . . . . . . . . . . . . . . . . . T . . . . S . . . . . . . . . . . . S S . . . . S . . . S . .   1 6 0
. . S . Y . . . S . . . . . . . . . . . . . . . . . . . . . . . . . . . . . . . . . . . . . . . . Y . . . . . . . . . . . . S . . . . . . . . . . . . . . . T . . . . . . . . S   2 4 0
. . . . . . S . . . S . . . S . . . . . . . . . . . . . S . . . S . . S . . . T . . . . S . . . . . . . . . . S . T . . . . . . S . . . . . . . . . T . . . . . .   3 2 0
. . . . . . . . . . . . . . . . . . . T . . . . T . . . . . T . . S . . . . . . . . . . S . . . . . . . . . . . . . . . . . . . . S . . . . Y . . . . . . . . . . . .   4 0 0
. . Y . . . . . . T . . . . . . . . . . . . . . . . . . . . . . . . . . . . . . . . . . . . . . . . . . . . . . . . . . . . . . . . . . . . . . . . . . . . . . . . . . . .   4 4 1
```

**Phosphorylation sites predicted:** **Ser: 30** **Thr: 12** **Tyr: 5**

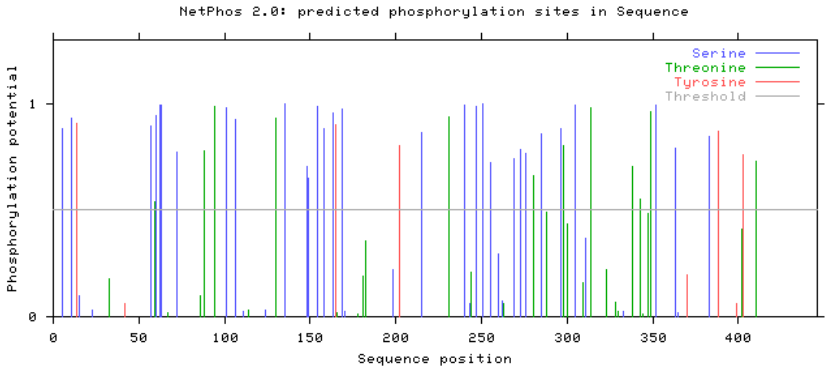


**Figure 1.2.2. Phosphorylation sites prediction on NuSAP**

The possible phosphorylation sites on NuSAP are predicted using NetPhos 2.0 (Technology University of Denmark).

### 1.2.3 NuSAP in mitosis

NuSAP, a 55 kDa microtubule associated protein, is primarily nucleolar in interphase and localizes prominently to central spindle microtubules during mitosis in cells (Raemaekers et al., 2003a). The expression of NuSAP is tightly controlled during the cell cycle by the APC complex (Song and Rape, 2010b). The protein level of NuSAP peaks at the transition of G2 to mitotic phase and rapidly decreases after cell division (Song and Rape, 2010b). The deletion of NuSAP results in aberrant mitotic spindles, defective chromosome segregation and cytokinesis (Raemaekers et al., 2003a), suggesting that NuSAP plays an important role in different stages of mitosis.

NuSAP functions as a microtubule stabilizer both bundles and crosslink microtubule (Ribbeck et al., 2006b). In vitro studies show that NuSAP, which is the RanGTP target, can directly link microtubules to chromosomes under the regulation of importin 7, importin α and importin β (Ribbeck et al., 2006b; Ribbeck et al., 2007a). Importin α and importin β can block the microtubule stabilizing activity of NuSAP, while importin β specifically suppresses the crosslinking activity of NuSAP.

### 1.2.4 NuSAP in model organisms

The protein level of NuSAP displays tissue specificity. NuSAP is highly expressed in the retina, forebrain, hindbrain and neural crest in zebrafish, thymus, long bones and colon in mice, and thymus and testis in human (Vanden Bosch et al., 2010). Taken together, these data indicate that NuSAP is highly expressed in tissues that contain a considerable population of proliferating cells.

The function of NuSAP is investigated in zebrafish and mice. Overexpression of NuSAP induces cell apoptosis and its deletion results in neural crest cell migration defects in zebrafish (Nie et al., 2010). In mice, the deletion of NuSAP causes early embryonic lethality (Vanden Bosch et al., 2010). As a conclusion, NuSAP plays an essential in embryo genesis and neuron cell migration.

### 1.2.5 NuSAP and cancer

NuSAP is up-regulated in various kinds of cancer—pancreatic adenocarcinoma, melanoma, glioblastoma, breast cancer, hepatocellular carcinoma, acute lymphoblastic leukemia and acute myelogenous leukemia (Fujiwara et al., 2006; Gulzar et al., 2013; Iyer et al., 2011b; Kokkinakis et al., 2005b; Wadia et al., 2010; Xie et al., 2011). Recent studies have reported a correlation between the

protein levels of NuSAP and the progression in various cancers (Gulzar et al., 2013). NuSAP has a malignancy-risk gene signature and the expression levels of NuSAP can be utilized as a pre-diagnosis marker for cancer (Iyer et al., 2011a; Kokkinakis et al., 2005a; Zhang et al., 2013). Other study reveals that the expression of NuSAP may help to predict the effectiveness of chemotherapy treatment (Kokkinakis et al., 2005a).

## 1.3 Roles of kinesins in mitosis

### 1.3.1 The microtubule depolymerizer-MCAK

Two major kinesin families function as the microtubule depolymerizers—kinesin 8 and kinesin 13. Compare to kinesin 8, the kinesin 13 family drastically depolymerizes microtubules (Endow, 1991). Three members in the kinesin 13 family—Kif2A, Kif2B and kif2C. MCAK (Kif2C, Mitotic Centromere Associated Kinesin) is a member of the kinesin-13 family and targets at both ends of the microtubules (Wordeman and Mitchison, 1995). MCAK is kinesin I with the microtubule depolymerization motor domain in the middle of the protein. The major function of MCAK in mitosis is to depolymerize and regulate the dynamics of microtubules from both the plus ends of the microtubules and the minus ends. MCAK diffuses and directly binds both the plus-end and minus-end of microtubules to efficiently depolymerize the microtubules independent on the

length of the microtubules (Helenius et al., 2006; Hunter et al., 2003; Maney et al., 1998).

The localization of MCAK is essential for its function as a microtubule depolymerizer. The targeting of the MCAK to microtubule tips dependents on its association with EB1 (End Binding protein) thoguh its SKIP domain on N terminal of MCAK. MCAK-EB bining is necessary for the depolymerization activity of MCAK with the regulation of its targeting to the microtubule tip, though the catalytic domain of MCAK is not altered by binding to EB. During mitosis, the localization of MCAK is changed from inner centromere at prometaphase to the inner kinetochore region at metaphase (Kline-Smith et al., 2004; Lan et al., 2004). The inner kinetochore localization of MCAK is critical to remove the mis-connected kinetochore microtubules through the microtubule depolymerization activity of MCAK (Gorbsky, 2004; Kline-Smith et al., 2004; Lan et al., 2004). MCAK has different functions on spindle microtubules and kinetochore microtubules. The previous study from Walzak group (Rizk et al., 2009) indicates that MCAK specifically regulates the turnover rate of kinetochore microtubules, but not the interpolar microtubules.

The localization and depolymerization activity of MCAK are tightly regulated by the mitotic kinase—Aurora B kinase (Andrews et al., 2004; Gorbsky, 2004;

Knowlton et al., 2006; Lan et al., 2004; Ohi et al., 2004; Parra et al., 2006). Aurora B is the catalytic subunit of the Chromosomal Passenger Complex (CPC) (Vader et al., 2006). From prometaphase to metaphase, Aurora B concentrates between sister chromosomes in the inner centromere region (Carmena and Earnshaw, 2003; Ruchaud et al., 2007). The phosphorylation of Aurora B on MCAK is essential to correct the imprecise attachment of kinetochore microtubules during metaphase and regulate kinetochore microtubules dynamics (Andrews et al., 2003; Welburn et al., 2010). Two recent studies also indicate that Aurora B can phosphorylate C terminal of MCAK, which regulates its conformation during microtubule depolymerization (Ems-McClung et al., 2013; Talapatra et al., 2015).

### 1.3.2 The chromokinesin-Kif22

Chromokinesins are plus-end directed motors contributing to the anti-poleward movement (Heald, 2000; Mazumdar and Misteli, 2005; Vanneste et al., 2011). Kif22 (Kinesin-like DNA binding protein, Kid) is a chromokinesin with an N-terminal microtubule binding domain and a C-terminal chromosome interacting domain (Tokai et al., 1996). Kif22 associated with chromosome arms to associate with chromosome congression and establish spindle bipolarity (Vernos and Karsenti, 1996). Kif22 contributes to spindle morphogenesis by mediating

imprecise chromosome alignment at metaphase and the onset of anaphase (Tokai-Nishizumi et al., 2005).

Kif22, as a weak motor protein, functions as the principle force producing agent for polar ejection force (Brouhard and Hunt, 2005). Kif22 is also a plus end-directed microtubule-based motor with an average speed of 160nm/s in vitro (Yajima et al., 2003). The RanGTP gradient further promotes the accumulation of Kif22 on chromosomes (Tahara et al., 2008a). The protein level of Kif22 during the cell cycle is regulated by APC/C (Feine et al., 2007). Previous studies identified several regulators of Kif22. For example, NuMA (Nuclear Mitotic Apparatus Protein) functions at the spindle morphology and chromosome alignment with the regulation of Kif22 (Levesque et al., 2003). The localization of Kif22 on the mitotic spindle was mediated by CHICA (Santamaria et al., 2008).

Kif22 mutations at P148 and R149 are important in maintaining hydrogen bonds in the ATP binding and motor domains of kif22, which are found in SEMDJL (spondyloepimetaphyseal dysplasia with joint laxity) and leptodactylic (lepto-SEMDJL) skeletal diseases (Boyden et al., 2011; Min et al., 2011). The protein level of Kif22 has been found to be up-regulated in cancers and the inhibition of kif22 arrests cell at G2/M stage which suppresses cancer proliferation (Yu et al., 2014)

### 1.3.3 The central spindle regulator-Kif4a

Kif4a is a kinesin-4 family chromokinesin member (Oh et al., 2000). During interphase, Kif4a localizes at the nuclear matrix and associates with chromosome during early mitosis (Lee et al., 2001). The DNA methyltransferase DNMT3D binds with Kif4a and the complex functions in chromosome condensation machinery (Geiman et al., 2004). Kif4a also majorly functions as a microtubule depolymerizer to regulate the length of the microtubules at the central spindle region during anaphase and cytokinesis (Hu et al., 2011).

During cytokinesis, Kif4a interacts with PRC1 to recruit at the midzone and control the formation of central spindle under the regulation of Aurora B and cdk1 (Hu et al., 2012; Kurasawa et al., 2004; Zhu and Jiang, 2005; Zhu et al., 2006). During anaphase, Kif4a binds with PRC1 to specifically target at the midzone microtubule ends and organize central spindle formation (Kurasawa et al., 2004). The depletion of Kif4a results in dramatic central spindle disorganization and loosened interpolar microtubule arrays (Mazumdar et al., 2004). The co-depletion of both Kif4a and PRC1 leads to the dis-localization of the essential midzone proteins from the midlines, such as chromosome passenger proteins, plk1and CENPE (Centromere Protein E) (Kurasawa et al., 2004). The function of Kif4a at

midzone is tightly regulated by mitotic kinases. Cdk1 phosphorylates Kif4a during the early mitosis to target Kif4a to the chromosomes and Aurora B phosphorylation on Kif4a enhances the association and depolymerization activity of Kif4a at the plus-ends of the midzone microtubules (Hu et al., 2011; Nunes Bastos et al., 2013; Zhu et al., 2006).

## 1.4 Objectives

Mitosis is the unique feature in eukaryote cells and the fidelity of chromosome segregation is essential for consistent genetic material in daughter cells. The precise chromosome segregation depends on the accurate bipolar spindle formation with the proper microtubule dynamics, chromosome oscillation and normal midzone formation during anaphase. However, the detailed mechanisms on these essential cellular processes are still largely unknown.

MAPs (microtubule associated protein) facilitate the spindle formation through modulating the feature of microtubules. NuSAP, as a MAP, plays an important role in mitosis and the depletion leads to severe mitotic defects. Though several study indicates NuSAP functions as a microtubule stabilizer both in vitro and in cells, the underlying molecular mechanisms on how NuSAP involves in the regulation of mitosis remains unclear.

To fully address the question, my graduate study aims exploring three functions of NuSAP during mitosis: **(1)** the mechanism of NuSAP in the dynamics of kinetochore microtubules during metaphase, **(2)** the role of NuSAP in chromosome oscillation and **(3)** the function of NuSAP in midzone formation during anaphase.

# CHAPTER 2 Material and Methods

## 2.1 Plasmid construction and siRNAs

The cDNAs of NuSAP, MCAK, Kif22, Kif4a and CENPA were amplified from a cDNA library extracted from HEK 293T cells and inserted into a pXJ40 vector, tagged with GFP, mCherry, HA, FLAG, or PAGFP. The truncation mutants of NuSAP were constructed using the PfuTurbo$^{TM}$ polymerase (Stratagene). The mammalian cell expression plasmids of GFP-MCAK-His, GFP-MCAK 5A-His and GFP-MCAK 5E-His mutants were obtained from Addgene (#13987, #23108, #23109 (Andrews et al., 2004); contributed by Dr. Linda Wordeman's group). The GFP-centrin1 was a gift from Dr. Maki Murata-Hori. The mCherry α-tubulin was obtained from Addgene (#49149 (Friedman et al., 2010)) and constructed into the pXJ40 vector tagged with GFP or HA.

The sequences of NuSAP siRNA (5′-AAGCACCAAGAAGCTGAGAAT-3′ (Raemaekers et al., 2003b)), MCAK siRNA (5′-GCAATAAACCCAGAACTCT-3′) and Nuf2 siRNA (5'-AAGCATGCCGTGAAACGTATA-3' (Cai et al., 2009)) were described previously and synthesized by Sigma. The siRNA oligonucleotide for Kif22 was synthesized by Santa Cruz Biotechnology (#sc-44350) and control siRNA were treated with Silencer Negative Control #1 siRNA (Ambion).

## 2.2 Cell culture, transfection and synchronization

HeLa and HEK 293T cells (ATCC) were cultured in Dulbecco's modified Eagle Medium (DMEM, Sigma), supplemented with 10% fetal bovine serum (Gibco) and 1% penicillin/streptomycin at 37°C, 5% $CO_2$. Stable H2B-mCherry HeLa cells were generated using pcDNA3-H2B-mCherry vector from Addgene (#20972 (Nam and Benezra, 2009)) and cultured in the presence of 0.2mg/ml G418 (Sigma).

The HEK 293T and HeLa cells were transfected using either calcium phosphate or Effectene$^{TM}$ (Qiagen) to introduce target genes. For siRNA transfections, stable H2B-mCherry HeLa cells were transfected at 30-50% confluence using Lipofectamine 2000 (Invitrogen) according to the manufacturer's protocol with 20 nM each siRNA. For experiments involving double-depletions, control cells were treated with 40nM negative control siRNA.

To synchronize cells at G2/M stage, HeLa cells were treated with 100ng/ml nocodazole (Sigma) for 16 hr and washed with 1×PBS for three times and released in DMEM medium with 10μM MG132 (Sigma) for 2 hr prior to fixation or live-imaging. For monopolar spindle experiments, cells were treated with 100 μM monastrol (Sigma) for 2 hr prior to fixation or live-imaging. To analyze the protein levels and interaction of NuSAP and Kif22 during cell cycle, HeLa cells

were treated with 2mM thymidine (Sigma) for 24h, released for 3h, and treated with 100ng/ml nocodazole for 11h following 10μM MG132 for 2h. Cells were released by 3-5 times washing with prewarmed medium, and plated into fresh DMEM, 10%FBS. Samples were taken at the indicated time points and processed for Western blot analysis. For the monastrol-flavopiridol treatment, HeLa cells were treated with 100uM monastrol for 3 hours and 10uM flavopiridol for 30min in DMEM medium.

### 2.3 Protein expression and purification

GST-NuSAP or His-NuSAP was expressed in *E. coli* BL21 (DE3) pLysS at 20°C overnight after IPTG induction; while His-NuSAP$^{1\text{-}233}$ or His-NuSAP$^{233\text{-}441}$ was expressed at 37°C, 3 hours after IPTG induction. Proteins were purified using glutathione-Sepharose 4B (Amersham Biosciences) or Ni-NTA agarose (Qiagen). MCAK WT, 5A, and 5E-His were constructed into a pFastBac Dual vector and transfected into SF9 cells with Cellfectin$^{TM}$ (Invitrogen) and expressed at 28°C for 3 days. MCAK, 5A and 5E were expressed and purified as previous studies.

## 2.4 Mass Spectrometry and GST Pull-down

For mass spectrometry to identify possible NuSAP binding partners, anti-FLAG-M2 agrose beads (Sigma) were incubated with FLAG-NuSAP- or FLAG vector-expressing HEK 293T cell lysate for 3 hours at 4°C. The beads were washed 5 times in mammalian cell lysis buffer (50mM HEPES, 100mM $NaCl_2$, 1mM EDTA, 1%EDTA, 1% Triton X-100 and 10% glycerol), and bound species were separated with 10% SDS-PAGE gel and Coomassie blue stained. The selected bands were analyzed with Triple TOF 5600 (ABSciex) and data was analyzed with ProteinPilot 4.0 (ABSciex).

The GST pull-down assay with purified proteins *in vitro* were performed in 50mM Tris-HCl, pH 7.4, 150mM NaCl, 2mM EGTA and 0.5% Triton X-100 with 5 μg GST fusion protein and 1 μg target protein. After 3h incubation at 4°C, the GST beads were washed for 3 times and protein samples were separated by SDS-PAGE and analyzed by Coomassie blue staining.

## 2.5 Immunoprecipitation and Western blot

For immunoprecipitation assay, HEK 293T cells were lysed in M-PER™ (Thermo scientific) with phosphatases inhibitors including 1mM $Na_3VO_4$, 10μg/ml aprotinin, 1mM pepstatin, 1mM leupeptin and 1mM PMSF. Nocodazole (10μg/ml) was added to completely depolymerize microtubules. 10μl FLAG M2

beads (Sigma) were incubated with cell lysate for 1h at 4°C and washed 3-5 times in mammalian cell lysis buffer (50mM Hepes, 100mM NaCl, 1.5mM $MgCl_2$, 1mM EDTA, 1% Triton X-100 and 10% glycerol).

Protein samples were separated on 10% SDS gel and detected by primary antibodies (rabbit anti-FLAG (Santa Cruz Biotechnology), rabbit anti-HA (Santa Cruz Biotechnology), rabbit anti-GFP (Sigma), rabbit anti-α-tubulin (Sigma), rabbit anti-Aurora B (Cell Signalling), mouse anti-GAPDH (Santa Cruz Biotechnology), rabbit anti-cyclinB1 (Santa Cruz Biotechnology), rabbit anti-kif22 (Abcam), rabbit anti-NuSAP (Abcam), rabbit anti-MCAK (Cytoskeleton), goat anti-Kif4a (Abcam)) and horseradish peroxidase (HRP) conjugated second antibodies (Santa Cruz Biotechnology).

### 2.6 Immunofluorescence

HeLa cells were cultured on ethanol-sterilized coverslips in 12-well plates and synchronized before fixed with ice-cold methanol at -20°C for 10min, and then were rehydrated with 1×PBS at room temperature for 10 min (Ye et al., 2011). The fixed cells were permeabilized with 0.3% Triton X-100 in 1×PBS for 15min and blocked with 2% BSA for 30min at room temperature.

Mouse anti-α-tubulin 1:2000 (Sigma), mouse anti-acetylated α-tubulin 1:200 (Sigma), rabbit anti-γ-tubulin 1:200 (sigma), human anti-CREST antibody 1:2000 (ImmunoVIsion), rabbit anti-MCAK (Cytoskeleton), rabbit anti-NuSAP (Abcam), rabbit anti-Kif22 1:200 (Abcam) were utilized to stain the respective proteins in cells, respectively. DNA was stained with Hoechst 33342 (Invitrogen). Alexa Fluor dye-conjugated goat anti-mouse, goat anti-rabbit or goat anti-human IgG (Invitrogen) were used as the secondary antibodies. Cells were mounted in FluorSave™ reagent (Calbiochem).

The enlarged images of MCAK localization were captured from single z-stack and noise removal was achieved by convolving the raw images with the Gaussian filter after background correction. The line profiles presented the original fluorescence intensity. For MCAK localization analysis, HeLa cells were synchronized at the metaphase stage and kinetochore pairs with MCAK signal at 2×8μm region on metaphase plate were analyzed. For the monastrol-cold treatment, the average of all the kinetochore microtubule length at ¼ of the region in cells was identified as the kinetochore microtubule length of the cells. The line profiles presented the original fluorescence intensity. The images were processed using Volocity™ software (PerkinElmer) or Image J (National Institutes of Health, Bethesda, MD).

## 2.7 Live-cell imaging

HeLa cells were cultured on 35 mm glass bottom petri dish (Greiner Bio-one) and imaging was conducted at 37 °C. For nocodazole treatment experiment, a final concentration of 10μM nocodazole was added into cultured cells and images were acquired at 10-second intervals for 3 min. The imaging was collected using UltraVIEW Vox Spinning disc confocal system (PerkinElmer) using an Olympus Uplan SApo 100✕1.4 oil lens and EMCCD camera C9100-50 (Hamamatsu). The images were processed using either Volocity™ software (PerkinElmer) or Image J. (National Institutes of Health, Bethesda, MD), depending on the needs.

For FLIP experiments, synchronized mCherry-α-tubulin stable HeLa cells were cultured on glass bottom dish and imaged by an UltraVIEW Vox spinning disc confocal system (PerkinElmer) in a 37 °C humid chamber supplied with 5% $CO_2$. Photobleaching laser (405nm, 50mW) was utilized with two spots (2×2μm) away from mitotic spindle. Images were acquired at 5-second intervals for 3 min with 20 mitotic cells for each transfection. The 568nm fluorescence signal intensity was background corrected and normalized to 100% at the first time point by Volocity™ software (PerkinElmer). The turnover $T_{1/2}$ of mCherry α-tubulin was calculated by linear regression as we previously described (Ye et al., 2011).

For FRAP experiments, GFP-MCAK-expressed HeLa cells were synchronized at the metaphase stage and cultured in a 37 °C humid chamber supplied with 5% $CO_2$ and imaged using a UltraVIEW Vox spinning disc confocal system (PerkinElmer). A 1×1μm photobleaching spot was placed at the kinetochore region and GFP fluorescence intensities were photobleaching corrected and background corrected and analyzed by Volocity$^{TM}$ 3D imaging analysis software (PerkinElmer).

For photoactivation experiments, PAGFP-α-tubulin-expressed HeLa cells were synchronized and identified by labeling Hoechst 33342 (2.5ng/ml, 10min) before photoactivation. A 405nm laser at 15% intensity was focused on the selected area for 1s and images were acquired at 15-second intervals for 10min. Kymographs were analyzed with Image J (National Institutes of Health, Bethesda, MD). Fluorescence intensity of the activated region was photobleaching and background corrected by Volocity$^{TM}$ (PerkinElmer) and analysed by double exponential regression analysis using Sigmaplot software (Jandel Scientific) to fit the data to the equation $F(t)=A_1e^{-k1t}+ A_2e^{-k2t}$, where F(t) stands for fluorescence intensity overtime, $A_1$ and $A_2$ represent the proportion of interpolar microtubules and kinetochore microtubules with regression rate $k_1$ and $k_2$. Kinetochore microtubule turnover half-life time was calculated by the equation $T_{1/2}=Ln2/k_2$ (DeLuca, 2010; Zhai et al., 1995).

For 3D live cell imaging, stable H2B-mCherry HeLa cells were cultured on 35 mm glass bottom petri dish (Greiner Bio-one) and synchronized or monastrol-treated before imaging. The imaging was collected with the UltraviewVox Spinning disc confocal system (PerkinElmer) which includes a CSD-X1 spinning disk head (Yokogawa), a solid state diode laser with both diode and DPSS modules (25-50mM) and an EMCCD camera C9100-50 (Hamamatsu). The images were taken with an Olympus Uplan SApo 100✕1.4 oil lens controlled by Volocity software (PerkinElmer) and conducted at 37°C.

Previous studies indicate that the movement of centromeres at the periphery of the spindle is different from the KT in the middle (Cimini et al., 2004; Civelekoglu-Scholey et al., 2013; Stumpff et al., 2012). Also, the imaging conditions are based on the phototoxic effects on cells and KT detection quality especially in 3D live-imaging (Jaqaman et al., 2010; Kitajima et al., 2011; Magidson et al., 2011), thus only the centromeres in the middle region of the spindle were imaged and analyzed. To avoid aliasing on motion characteristics analysis, the motion should be sampled at least two times faster than its frequency (Dorn et al., 2008). The KT oscillation in HeLa cells is about 60s per period, thus, the sampling interval should be less than 30s. To compromise all these conditions, the time points comprised of 0.5 μm each z sections for 3 μm within the center of the spindle

were acquired every 15s for 10 mins. Only cells with spindles oriented about parallel to the plane of focus were analyzed and the focal plane at the center of the spindle was chosen.

### 2.8 *In vitro* microtubule assays

For *in vitro* MT stabilization assay, a final concentration of 20μM tubulin (Cytoskeleton) in BRB80 buffer (80 mM PIPES, pH 6.9; 1 mM $MgCl_2$; 1 mM EGTA) with 1mM GTP was incubated at 37°C for 10min with certain protein concentrations (Ribbeck et al., 2006a). For *in vitro* microtubule destabilization assays, tubulins were first polymerized in the BRB80 buffer with 1mM GTP at 37°C for 15min. NuSAP protein and MCAK WT, 5A, and 5E were preincubated in the BRB80 buffer with 1mM ATP at room temperature for 5min and then added to a reaction mixture containing 1.5μM polymerized microtubules with 10μM taxol. After the reaction for a further 10min, the microtubule samples were fixed on cover glass in ice-cold methanol at -20°C for 5min and stained with mouse anti-α-tubulin 1:2000 (Sigma). Images were taken by an Axio Imager II system using Zeiss 63×1.4 oil lens (Zeiss) and number of microtubules were analyzed by Image J (National Institutes of Health, Bethesda, MD).

## 2.9 Quantitative Analyses of 3D Chromosome Movements

The 3D images were first background corrected with the background image in Volocity software (PerkinElmer) and noise removal was achieved by convolving the raw images with the 3D Gaussian filter in Imaris (Bitplane). Chromosomes were tracked using the Imaris (Bitplane) 3D surface detection function, followed by manual corrections. The velocity and acceleration of chromosome were analyzed by Imaris with center projection function and the images were processed with Volocity software (PerkinElmer) and Image J (National Institutes of Health, Bethesda, MD).

## 2.10 Quantitative Analyses of 3D Centromere oscillation

To correctly detect the centromeres, the images were first background corrected with the background image in Volocity software (PerkinElmer) and noise removal was achieved by convolving the raw images with the 3D Gaussian filter in Imaris (Bitplane). Centromeres in bipolar metaphase cells and monopolar cells were tracked using the Imaris (Bitplane) 3D spot detection function, followed by manual corrections. The centromere trajectories were constructed using the single particle tracking (SPT) algorithm within the center of the spindle to avoid track interruptions resulted from temporary centromere disappearance by movement out of the imaging volume or detection failure. Tracking was detected with a

Brownian motion model, since the centromere oscillation is neither linear or with any merging and splitting events. Based on the approximate parameters of the centromere movement, we set the maximum gap-closing time window as 1, the search radius upper limit as 1.5. Only the tracks with over than 20 timepoints detected were analyzed. To correct cell movement during the process of imaging, KT positions (x, y, z, t) were registered to the relative 3D position compared with spindle pole ($x_o$, $y_o$, $z_o$, t) over time as (x-$x_o$, y-$y_o$, z-$z_o$, t).

The 3D position information of each centromere track was extracted from Imaris and the data was analyzed with custom scripts in Perl (Perl, Inc.) and run from the Perl command line. Sister pairing was based on the average distance and the distance variation using both 3D spatial and temporal information of the centromere tracks (Jaqaman et al., 2010). The average of sister track pair should be closer and the distance variation within each track should be smaller, compared with other nonsisters. Thus, we calculated the average distance $d_{ij}$ ($d_{ij,t} = \sqrt{(x_{i,t} - x_{j,t})^2 + (y_{i,t} - y_{j,t})^2 + (z_{i,t} - z_{j,t})^2}$ , $d_{ij} = \frac{1}{n}\sum_{t=1}^{n} d_{ij,t}$ ) and the variance of the distance $v_{ij}$ ($v_{ij} = \frac{1}{n-1}\sum_{t=1}^{n}\left(d_{ij,t} - d_{ij}\right)^2$) between each pair i ($x_i$, $y_i$, $z_i$, t) and j ($x_j$, $y_j$, $z_j$, t) tracks over the course of the imaging. The cost of the sister pairing counts the two criteria together and was defined as $d_{ij} \times v_{ij}$. The acceptable bounds were set as 1.5 and the combination of the trajectory pairings

was taken with the minimum global cost as the assignment of the sister tracks. Only the paired tracks with over 20 timepoints matched of the total 41 timepoints were analyzed. The ICD was calculated as the average distance between the sister pairs ($\mathrm{ICD}_{ij,t} = \sqrt{(\mathrm{x}_{i,t} - \mathrm{x}_{j,t})^2 + (\mathrm{y}_{i,t} - \mathrm{y}_{j,t})^2 + (\mathrm{z}_{i,t} - \mathrm{z}_{j,t})^2}$, $\mathrm{ICD} = \overline{ICD_{ij,t}}$).

The direction of the movement was set based on the change of the distances between each centromere in the sister tracks to the spindle pole ($x_o$, $y_o$, $z_o$, t) during two timepoints ($\mathrm{dp}_{i,t} = \sqrt{(\mathrm{x}_{i,t} - \mathrm{x}_{o,t})^2 + (\mathrm{y}_{i,t} - \mathrm{y}_{o,t})^2 + (\mathrm{z}_{i,t} - \mathrm{z}_{o,t})^2}$). In bipolar cells, if the centromere i of a sister pair i ($x_i$, $y_i$, $z_i$, t) and j ($x_j$, $y_j$, $z_j$, t) that is near the certain spindle pole ($dp_i<dp_j$), the sign for centromere i was set as positive ($Sign_{i,t}=+1$) of the movement to the pole ($dp_{i,t}>dp_{i,t+1}$) and negative ($Sign_{i,t}=-1$) of the movement away from the pole ($dp_{i,t}<dp_{i,t+1}$); for the other centromere j that far from the certain spindle pole, the sign was the opposite, ($Sign_{j,t}=+1$) of the movement away from the pole ($dp_{j,t}<dp_{j,t+1}$) and negative ($Sign_{j,t}=-1$) of the movement to the pole ($dp_{j,t}>dp_{j,t+1}$). In monopolar cells, the sign was set as positive ($Sign_{m,t}=+1$) of the movement to the pole ($dp_{m,t}>dp_{m,t+1}$) and negative ($Sign_{m,t}=-1$) of the movement away from the pole ($dp_{m,t}<dp_{m,t+1}$). The half-period was calculated as the time between two directional switching points based on the sign change (if $\mathrm{Sign}_{\mathrm{switch}+1} \neq \mathrm{Sign}_{\mathrm{switch}}$, $\mathrm{T}_{half} = \frac{1}{n} \sum_1^n (\mathrm{t}_{\mathrm{switch}+1} - \mathrm{t}_{\mathrm{switch}})$).

The mimick center track of sister pair i ($x_i$, $y_i$, $z_i$, t) and j ($x_j$, $y_j$, $z_j$, t) was set as (($x_i$+$x_j$)/2, ($y_i$+$y_j$)/2, ($z_i$+$z_j$)/2, t). The oscillation amplitude was set as the distance of the projected center moved between directional switch points ($Amp = \frac{1}{n}\sqrt{\sum_1^n((\mathrm{x_{switch+1}} - \mathrm{x_{switch}})^2 + (\mathrm{y_{switch+1}} - \mathrm{y_{switch}})^2 + (\mathrm{z_{switch+1}} - \mathrm{z_{switch}})^2}$, Amp= $\overline{Amp_t}$). The average ($\mathrm{V}_t = \frac{1}{\Delta \mathrm{t}}\sqrt{(\mathrm{x}_{t+1} - \mathrm{x}_t)^2 + (\mathrm{y}_{t+1} - \mathrm{y}_t)^2 + (\mathrm{z}_{t+1} - \mathrm{z}_t)^2}$, V= $\overline{V_t}$) and the distribution of the center velocity were calculated by the absolute value. The sign of the presented center velocity overtime shows the direction of the center oscillation. The sign was set as positive ($Sign_{c,t}$=+1) of the movement to the pole ($dp_{c,t}$>$dp_{c,t+1}$) and negative ($Sign_{c,t}$=-1) of the movement away from the pole ($dp_{c,t}$<$dp_{c,t+1}$). The statistical analysis of the correlation, standard error of mean and confidence was previously described (Ye et al., 2011).

### 2.11 Mathematical calculation of $K_{NuSAP}$ and $I_{NuSAP}$

Taken together our result of the velocity of the center point (Table 1 and Figure 3-6F), the force in bipolar metaphase cells can be analyzed as:

Control siRNA: $F = \Delta \mathrm{PF_{kMT}} - \Delta \mathrm{PEF_{iMT}} = \mathrm{k}\times \mathrm{v_1}$ (1)

NuSAP siRNA: $F = \Delta \mathrm{PF'_{kMT}} - \Delta \mathrm{PEF'_{iMT}} = \mathrm{k}\times \mathrm{v_2}$ (2)

Kif22 siRNA: $F = \Delta \mathrm{PF_{kMT}} - (\Delta \mathrm{PEF_{iMT}} - \Delta \mathrm{PEF_{Kif22}}) = \mathrm{k}\times \mathrm{v_3}$ (3)

Nuf2 siRNA: $F = \Delta \mathrm{PEF_{iMT}} = \mathrm{k}\times \mathrm{v_4}$ (4)

NuSAP/Nuf2 siRNA: $F = \Delta PEF'_{iMT} = k \times v_5$ (5)

Kif22/Nuf2 siRNA: $F = \Delta PEF_{iMT} - \Delta PEF_{Kif22} = k \times v_6$ (6)

The force in monopolar metaphase cells can be analyzed as:

Control siRNA: $F = PF_{kMT} - PEF_{iMT} = k \times v_7$ (7)

NuSAP siRNA: $F = PF'_{kMT} - PEF'_{iMT} = k \times v_8$ (8)

Kif22 siRNA: $F = PF_{kMT} - (PEF_{iMT} - PEF_{Kif22}) = k \times v_9$ (9)

Nuf2 siRNA: $F = PEF_{iMT} = k \times v_{10}$ (10)

NuSAP/Nuf2 siRNA: $F = PEF'_{iMT} = k \times v_{11}$ (11)

Kif22/Nuf2 siRNA: $F = PEF_{iMT} - PEF_{Kif22} = k \times v_{12}$ (12)

Based on the simplified scenario, the influence of NuSAP on the force during chromosome oscillation is proposed to be liner as $K_{NuSAP}$ on kMT generated force, $I_{NuSAP}$ on the PEF generated by Kif22 on iMT and the possible influence of NuSAP on the other force on iMT as $I'_{NuSAP}$.

Thus, $\Delta PF'_{kMT} = \Delta PF_{kMT} - K_{NuSAP} \times \Delta PF_{kMT}$ (13)

$PF'_{kMT} = PF_{kMT} - K_{NuSAP} \times PF_{kMT}$ (14)

$\Delta PEF'_{iMT} = \Delta PEF_{iMT} - I_{NuSAP} \times \Delta PEF_{Kif22} - I'_{NuSAP} \times (\Delta PEF_{iMT} - \Delta PEF_{Kif22})$ (15)

$PEF'_{iMT} = PEF_{iMT} - I_{NuSAP} \times PEF_{Kif22} - I'_{NuSAP} \times (PEF_{iMT} - PEF_{Kif22})$ (16)

Combining the equations, we have:

Eqs.4 $\Delta PEF_{iMT} = k \times v_4$

Eqs.1+Eqs.4 $\Delta PF_{kMT} = k \times (v_1 + v_4)$

Eqs.1-Eqs.3 & Eqs.4-Eqs.6 (average) $\Delta PEF_{Kif22} = k \times \frac{v_1 - v_3 + v_4 - v_6}{2}$

Eqs.2+Eqs.5 $\Delta PF'_{kMT} = k \times (v_2 + v_5)$

Eqs.5 $\Delta PEF'_{iMT} = k \times v_5$

Eqs.6 $\Delta PEF_{iMT} - \Delta PEF_{Kif22} = k \times v_6$

Eqs.13 $k \times (v_2 + v_5) = k \times (v_1 + v_4) - K_{NuSAP} \times k \times (v_1 + v_4)$ (17)

Eqs.15 $k \times v_5 = k \times v_4 - I_{NuSAP} \times k \times \frac{v_1 - v_3 + v_4 - v_6}{2} - I'_{NuSAP} \times k \times v_6$ (18)

Eqs.10 $PEF_{iMT} = k \times v_{10}$

Eqs.7+Eqs.10 $PF_{kMT} = k \times (v_7 + v_{10})$

Eqs.7-Eqs.9 & Eqs.10-Eqs.12 (average) $PEF_{Kif22} = k \times \frac{v_7 - v_9 + v_{10} - v_{12}}{2}$

Eqs.8+Eqs.11 $PF'_{kMT} = k \times (v_8 + v_{11})$

Eqs.11 $PEF'_{iMT} = k \times v_{11}$

Eqs.6 $PEF_{iMT} - PEF_{Kif22} = k \times v_{12}$

Eqs.14 $k \times (v_8 + v_{11}) = k \times (v_7 + v_{10}) - K_{NuSAP} \times k \times (v_7 + v_{10})$ (19)

Eqs.16 $k \times v_{11} = k \times v_{10} - I_{NuSAP} \times k \times \frac{v_7 - v_9 + v_{10} - v_{12}}{2} - I'_{NuSAP} \times k \times v_{12}$ (20)

Combining Eqs. 17 & 19 and taking the average, we have

$$K_{NuSAP} = 1 - \frac{(v_2 + v_5)(v_7 + v_{10}) + (v_1 + v_4)(v_8 + v_{11})}{2v_1v_7 + 2v_4v_7 + 2v_1v_{10} + 2v_4v_{10}}$$

$$I_{NuSAP} = \frac{2v_4v_{12} - 2v_5v_{12} - 2v_6v_{10} + 2v_6v_{11}}{v_1v_{12} + v_4v_{12} - v_3v_{12} - v_6v_7 - v_6v_{10} + v_6v_9}$$

$$I'_{NuSAP} = \frac{(v_4 - v_5)(v_7 - v_9 + v_{10} - v_{12}) - (v_{10} - v_{11})(v_1 - v_3 + v_4 - v_6)}{v_6(v_7 - v_9 + v_{10}) - v_{12}(v_1 - v_3 + v_4)}$$

Taking in the velocity values in Table 1, thus

$K_{NuSAP} = 0.20$

$I_{NuSAP} = 0.88$

$I'_{NuSAP} = 0.09$

# CHAPTER 3 NuSAP stabilizes kinetochore microtubules by attenuating MCAK depolymerization activity

## 3.1 Abstract

NuSAP (Nucleolar and Spindle Associated Protein), a microtubule associated protein, functions as a microtubule stabilizer. Depletion of NuSAP leads to severe mitotic defects. However, it remains unclear how NuSAP stabilizes microtubules at mitosis. In this study, we dissect the function of NuSAP in kinetochore microtubules and identify MCAK (Mitotic Centromere-Associated Kinesin), a microtubule depolymerizer, as a novel binding partner of NuSAP. NuSAP tightly regulates the localization and depolymerization activity of MCAK. Moreover, we demonstrate that Aurora B significantly enhances the interaction of NuSAP with MCAK and modulates the effects of NuSAP on the localization and depolymerization activity of MCAK. Our results elucidate an underlying mechanism in which NuSAP controls kinetochore microtubule dynamics spatially and temporally by modulating the localization and function of MCAK, in an Aurora B kinase-dependent manner. Hence, this study provides new insights into a pivotal role of NuSAP in maintaining the fidelity of chromosome segregation during mitosis.

## 3.2 Introduction

Kinetochore microtubules are critical and directly connect to kinetochores on sister chromatids to generate proper tension and ensure error-free chromosome separation(Biggins and Walczak, 2003; Kline-Smith et al., 2005). During metaphase, the dynamics of kinetochore microtubules is tightly controlled by microtubule associated proteins, motor proteins and mitotic kinases in order to precisely align chromosomes at the metaphase plate(Cimini, 2007; Joglekar et al., 2010; Slep and Vale, 2007). Disruption of this process leads to chromosome instability, which is considered to be one of the main causes of carcinogenesis(Bakhoum et al., 2009; Sanhaji et al., 2011; Sudakin and Yen, 2007). However, it remains unclear how this complex system is coordinated to regulate kinetochore microtubule dynamics.

NuSAP is a microtubule associated protein and plays an important role in the spindle assembly(Hussain et al., 2009; Raemaekers et al., 2003b). Previous studies indicated that depletion of NuSAP in cells led to severe defects in mitotic spindle formation, chromosome segregation and cytokinesis(Raemaekers et al., 2003b). NuSAP was identified as a microtubule stabilizer because of its role in inducing microtubule crosslink, bundling, and attachment to chromosomes(Ribbeck et al., 2006a; Ribbeck et al., 2007b). The protein levels of NuSAP are tightly regulated by APC/C (Anaphase-Promoting

Complex/Cyclosome) during the cell cycle (Li et al., 2007b; Song and Rape, 2010a). In addition, NuSAP was found to be highly expressed in several types of cancers (Fujiwara et al., 2006; Gulzar et al., 2013; Iyer et al., 2011b; Kokkinakis et al., 2005b; Wadia et al., 2010; Xie et al., 2011). Even though several studies have identified the vital role of NuSAP, the underlying mechanism of how NuSAP functions at mitosis remains largely unknown.

MCAK is a member of the kinesin-13 family (Wordeman and Mitchison, 1995) and an important microtubule depolymerizer (Helenius et al., 2006; Hunter et al., 2003; Maney et al., 1998). During mitosis, the localization of MCAK is changed from inner centromere at prometaphase to the inner kinetochore region at metaphase (Kline-Smith et al., 2004; Lan et al., 2004). This translocalization is critical for MCAK to remove the mis-connected kinetochore microtubules through its microtubule depolymerization activity (Gorbsky, 2004; Kline-Smith et al., 2004; Lan et al., 2004). Aurora B kinase phosphorylates MCAK to tightly regulate its localization and depolymerization activity (Andrews et al., 2004; Gorbsky, 2004; Knowlton et al., 2006; Lan et al., 2004; Ohi et al., 2004; Parra et al., 2006). Aurora B behaves as the catalytic subunit of the Chromosomal Passenger Complex (CPC) (Vader et al., 2006), which concentrates between sister chromosomes in the inner centromere region at prometaphase to metaphase (Carmena and Earnshaw, 2003; Ruchaud et al., 2007). The critical functions of

Aurora B are to correct the imprecise attachment of kinetochore microtubules during metaphase and regulate kinetochore microtubules dynamics through phosphorylation of MCAK to ensure accurate chromosome alignment (Andrews et al., 2003; Welburn et al., 2010). However, it is still elusive whether there is an additional regulator of MCAK in modulating its function during mitosis.

In this study, we report for the first time that the role of NuSAP, as a kinetochore microtubule stabilizer, regulates the dynamics and depolymerization activity of MCAK. Our results also elucidate an underlying mechanism in which NuSAP controls kinetochore microtubule dynamics by modulating the localization and function of MCAK, in an Aurora B kinase-dependent manner. Our findings provide new insights into a pivotal role of NuSAP in maintaining the fidelity of chromosome segregation during mitosis.

## 3.3 Results

### 3.3.1 NuSAP stabilizes spindle microtubule during metaphase

To obtain insights into the function of NuSAP during metaphase, we constructed vectors-expressing the full-length NuSAP, the N-terminal (1-233 aa, $NuSAP^{1-233}$) domain, which includes a chromosome binding domain, and the C-terminal (233-441 aa, $NuSAP^{233-441}$) domain, which contains a microtubule binding domain (MTBD), and were ectopically expressed in synchronized HeLa cells (Figure 3.3.1 A,B). Interestingly, overexpression of the full-length NuSAP and $NuSAP^{233-441}$, but not $NuSAP^{1-233}$, displayed a range of mitotic defects including spindle elongation (Figure 3.3.1 C), wider metaphase plate (Figure 3.3.2 A) and misaligned chromosomes (Figure 3.3.2 B) that have not yet been reported previously, though overexpression of $NuSAP^{1-233}$ slightly increased the percentage of cells with misaligned chromosomes. Our quantitative results showed that the average spindle length for the full-length NuSAP and $NuSAP^{233-441}$-overexpressing cells was approximately 13.49±0.91μm and 13.45±0.87μm, respectively, which were almost twice the length of control (7.12±0.30μm, consistent with previous study (Ye et al., 2011) and $NuSAP^{1-233}$-overexpressing HeLa cells (7.45±0.43μm) (Figure 3.3.1 C). Taken together, the results indicate that overexpression of NuSAP elongated the mitotic spindle length, probably through its C-terminal domain.

We next assessed whether the elongated mitotic spindle in NuSAP-overexpressing cells was a consequence of over-stabilized spindle microtubules. To test this possibility, metaphase cells were treated with nocodazole for 5 mins to depolymerize dynamic spindle microtubules. The result showed that HeLa cells overexpressing with the full-length NuSAP (1.44 times) or NuSAP$^{233-441}$ (1.36 times) retained more stable spindle microtubules in the nocodazole-treated cells but not NuSAP$^{1-233}$-overexpressing cells (1.04 times), compared to control (Figure 3.3.1 D,E). Moreover, live-cell imaging showed that in the presence of nocodazole, NuSAP- or NuSAP$^{233-441}$-overexpressing cells retained 60% of the original spindle microtubules up to 180 seconds; on the other hand, the GFP-vector control and NuSAP$^{1-233}$-overexpressing cells retained only by approximately 100 seconds (Figure 3.3.2 C, indicated by arrows). To further investigate the role of NuSAP in bundling microtubules, the microtubules were incubated with NuSAP protein *in vitro* and the results show that in the presence of NuSAP, prominent microtubule bundle was detected (Figure 3.3.2 D). Taken together, these findings indicate that NuSAP stabilizes microtubules through its C terminus that contains a microtubule binding domain in metaphase cells.

To further decipher the function of NuSAP in stabilizing microtubules, we hypothesized that NuSAP might stabilize spindle microtubules by decreasing the depolymerization of microtubules. To test this, we performed the Fluorescence Loss In Photobleaching (FLIP) assay using HeLa cells stably expressing mCherry-tagged α-tubulin. Photobleaching laser (405nm) was utilized with two spots (2×2μm) away from mitotic spindle and the fluorescence intensity of the microtubules at the spindle region was analyzed. As shown in Figure 3.3.1F and G, the half-life ($T_{1/2}$) of spindle microtubules in the full-length and $NuSAP^{233-441}$-overexpressing cells was 67.46±6.32s and 92.49±9.32s respectively, which were considerably higher than that in the control (44.06±4.93s) and $NuSAP^{1-233}$-transfected cells (40.73±6.56s). The FLIP data indicate that NuSAP and $NuSAP^{233-441}$ stabilize spindle microtubules probably by decreasing the turnover rates of microtubules. Taken together, our results demonstrate that NuSAP functions as a microtubules stabilizer, through its C-terminal microtubule domain, by decreasing the turnover rate of microtubules.

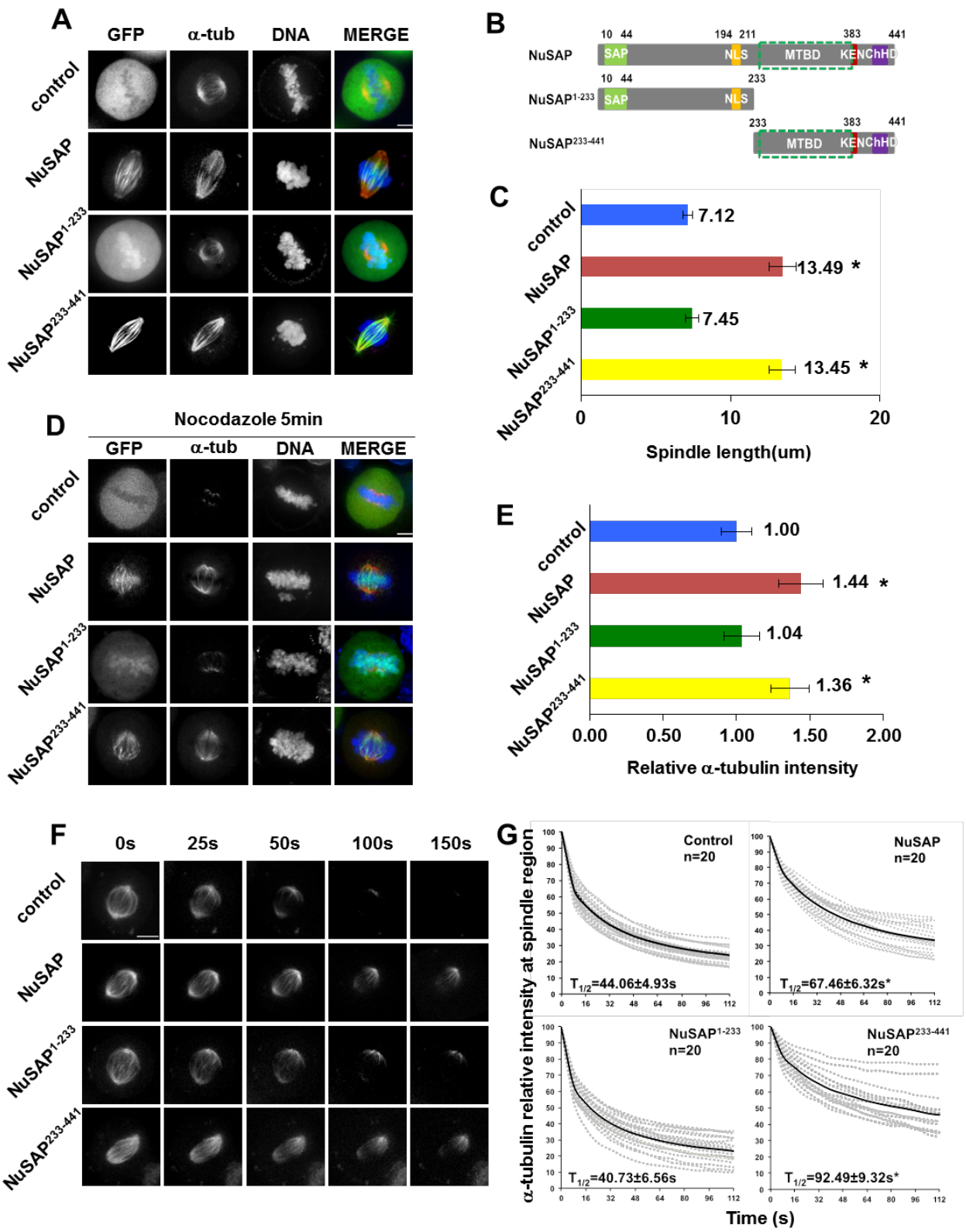
A
GFP
α-tub
DNA
MERGE
control
NuSAP
NuSAP1-233
NuSAP233-441
B
NuSAP
10 44
194 211
383
441
SAP
NLS
MTBD
KENCh
HD
NuSAP1-233
233
NuSAP233-441
C
7.12
13.49 *
7.45
13.45 *
0
10
20
Spindle length(um)
D
Nocodazole 5min
E
1.00
1.44 *
1.04
1.36 *
0.00
0.50
1.00
1.50
2.00
Relative α-tubulin intensity
F
0s
25s
50s
100s
150s
G
Control
n=20
NuSAP
n=20
NuSAP1-233
n=20
NuSAP233-441
n=20
T1/2=44.06±4.93s
T1/2=67.46±6.32s*
T1/2=40.73±6.56s
T1/2=92.49±9.32s*
α-tubulin relative intensity at spindle region
Time (s)

**Figure 3.3.1 NuSAP stabilizes spindle microtubules during metaphase.**

(A) Fluorescent images of metaphase HeLa cells expressing GFP-vector (control), GFP-NuSAP, GFP-NuSAP$^{1-233}$ or GFP-NuSAP$^{233-441}$. Mitotic spindles were labeled with an anti-α-tubulin antibody and DNA with Hoechst 333342. Scale bar, 5μm. (B) A schematic diagram of NuSAP and its truncation mutants NuSAP$^{1-233}$, NuSAP $^{233-441}$. Previously identified functional domains on NuSAP are indicated. SAP: 10-44 aa, chromosome binding domain; NLS domain: 194-211 aa, Nuclear Localization Signal; predicted microtubule binding domain (dotted line square): 233-383 aa; KEN box: 384-390 aa, APC/C binding domain; ChHD domain: 410-433 aa, Charged Helical Domain(Iyer et al., 2011b). (C) A bar charts representing the average of spindle length of cells expressing GFP-NuSAP, GFP-NuSAP$^{1-233}$, GFP-NuSAP$^{233-441}$ and GFP-vector only (control). The number of cells quantified: n (GFP)=37/3 independent experiments, n (GFP-NuSAP)=30/3, n (GFP-NuSAP$^{1-233}$)=36/3, n (GFP-NuSAP$^{233-441}$)=32/3. Error bars represent ±SD. * $p<0.001$. (D) Stable spindle microtubules in metaphase HeLa cells expressing GFP-vector (control), GFP-NuSAP, GFP-NuSAP$^{1-233}$ and GFP-NuSAP$^{233-441}$ after nocodazole treatment (10μM, 5min). Mitotic spindles were labeled with an anti-α-tubulin antibody and DNA with Hoechst 333342. Scale bar, 5μm. (E) A bar charts representing the average of α-tubulin immunofluorescence intensity on metaphase spindles stained as in D in cells expressing GFP-NuSAP, GFP-NuSAP$^{1-233}$, GFP-NuSAP$^{233-441}$ and GFP-vector only (control). The number of cells quantified: n (GFP)=40/3 independent experiments, n (GFP-NuSAP)=41/3, n (GFP-NuSAP$^{1-233}$)=39/3, n (GFP-NuSAP$^{233-441}$)=36/3. Error bars represent ±SD. * $p<0.001$. (F) Representative images of spindle microtubules signal loss in mCherry-α-tubulin stable metaphase HeLa cells and HeLa cells expressing GFP-NuSAP, GFP-NuSAP$^{1-233}$ or GFP-NuSAP$^{233-441}$ with FLIP assays. Scale bar, 5μm. (G) Normalized signal decreasing curves of mCherry-α-tubulin signal intensity at the metaphase spindle region in FLIP assays. Dotted gray lines represent each individual measurement and black lines for the mean value of each group. Turnover $T_{1/2}$ was calculated by linear regression. Data were collected from 3 independent experiments and "n" indicates the number of mitotic spindles analyzed. Error bars represent ±SD. * $p<0.001$.

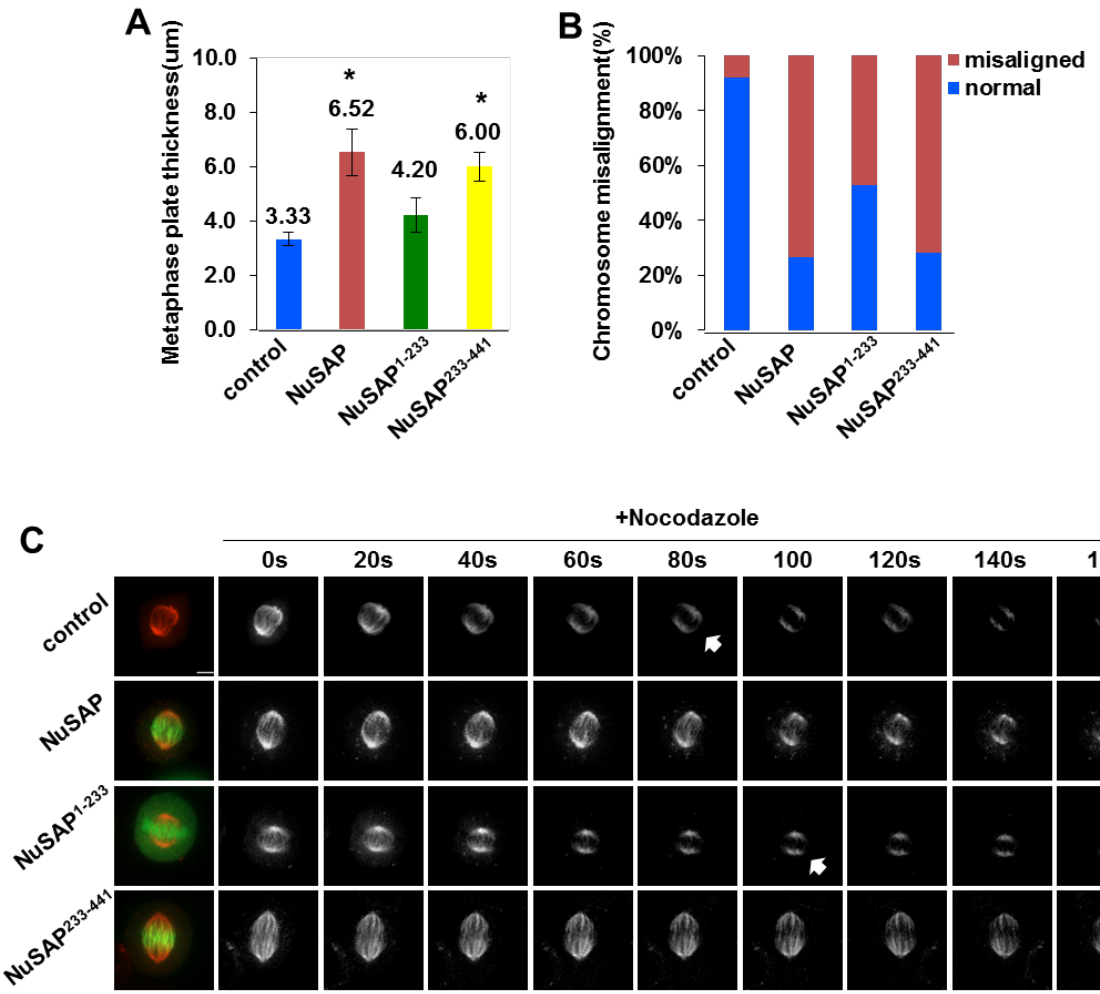
A
Metaphase plate thickness(um)
10.0
8.0
6.0
4.0
2.0
0.0
3.33
6.52
4.20
6.00
*
*
control
NuSAP
NuSAP1-233
NuSAP233-441
B
Chromosome misalignment(%)
100%
80%
60%
40%
20%
0%
misaligned
normal
control
NuSAP
NuSAP1-233
NuSAP233-441
C
+Nocodazole
0s
20s
40s
60s
80s
100
120s
140s
180s
control
NuSAP
NuSAP1-233
NuSAP233-441
D
microtubules
NuSAP+microtubules
100 nm

**Figure 3.3.2. Overexpression of NuSAP leads to severe mitotic defects and stabilized microtubules**

(A-B) Bar charts representing the average of metaphase plate thickness A and the percentage of cells with misaligned chromosomes expressing GFP-NuSAP, GFP-NuSAP$^{1-233}$, GFP-NuSAP$^{233-441}$ and GFP-vector only (control) B. The number of cells quantified: n (GFP)=37/3 independent experiments, n (GFP-NuSAP)=30/3, n (GFP-NuSAP$^{1-233}$)=36/3, n (GFP-NuSAP$^{233-441}$)=32/3. Error bars represent ±SD. * $p<0.001$. (C) Representative time-lapse images of spindle microtubules in mCherry-α-tubulin stable metaphase HeLa cells and HeLa cells expressing GFP-NuSAP, GFP-NuSAP$^{1-233}$ or GFP-NuSAP$^{233-441}$ after treated with nocodazole (10μM). White arrows indicate the time point that reaches 60% of original α-tubulin fluorescence intensity at spindle region. Scale bar, 5μm. (D) NuSAP bundles microtubules *in vitro*. Purified tubulin (1.5 μM) was incubated either alone or with 1 μM recombinant NuSAP for 10 min and fixed for electron microscopy. In the presence of NuSAP, microtubule bundles were detectable. Bars, 100nm.

### 3.3.2 NuSAP modulates the localization of MCAK at the kinetochore region

To understand the molecular mechanism of how NuSAP regulates the stability of microtubules, immunoprecipitation and proteomic analysis were utilized to search the binding partners of NuSAP and MCAK was identified (Figure 3.3.3 A and Figure 3.3.4 A). To verify our proteomic results, we examined whether NuSAP could interact directly with MCAK *in vitro*. As shown in 3.3.4 B, His-tagged recombinant MCAK protein was pulled-down by GST-NuSAP protein, but not the GST control, indicating that MCAK is a novel NuSAP binding partner both *in vitro* and in metaphase cells. To decipher the MCAK binding domain(s) of NuSAP, we constructed a series of truncation mutants of NuSAP and performed immunoprecipitation assays. Interestingly, our results showed that the interacting domain of MCAK laid within the C-terminal 433-441 aa (MCAK binding domain, MCBD) in NuSAP (Figure 3.3.3 B and C), suggesting that MCAK is a novel NuSAP binding partner. Moreover, deletion of the MCAK binding region ($NuSAP^{delMCBD}$), encompassing 433-441 aa in NuSAP, resulted in a marked abolishment of the interaction between NuSAP and MCAK, suggesting that the 433-441 aa region of NuSAP is responsible for MCAK binding (Figure 3.3.3 C).

The localization of MCAK at the inner kinetochore region is essential for its function as a microtubule depolymerizer during metaphase and the collapse of the

MCAK at inner centromere region leads to weak depolymerization activity on kinetochore microtubules(Andrews et al., 2004). We next questioned whether the interaction of MCAK and NuSAP would alter the localization of MCAK. To do this, we ectopically expressed mCherry-vector (control), mCherry-NuSAP, mCherry-NuSAP$^{1\text{-}233}$, mCherry-NuSAP$^{233\text{-}441}$ or mCherry-NuSAP$^{delMCBD}$ in metaphase synchronized cells and examined if NuSAP affects the localization of the endogenous MCAK at the metaphase plate. As shown in Figure 3.3.3 D, MCAK localized at the inner kinetochore region in the control metaphase cells (Figure 3.3.3 D, row 1) and aligned well with ACA (Anti-CREST Antibody; an inner kinetochore marker)(Waters et al., 1996), which is consistent with the previous study(Andrews et al., 2004). In contrast, in NuSAP (Figure 3.3.3 D, row 2)- or NuSAP$^{233\text{-}441}$ (Figure 3.3.3 D, row 4)-overexpressing metaphase cells, the majority of MCAK was spread to the inner centromere region, judged by the localization between ACA staining sites (enlarged single z-stack images). However, both NuSAP$^{1\text{-}233}$ (Figure 3.3.3 D, row 3) and NuSAP$^{delMCBD}$ (Figure 3.3.3 D, row 5) truncation mutants, which do not contain a MCAK binding domain, did not disturb the inner kinetochore localization of MCAK (Figure 3.3.3 D). Consistently, the MTBD domain (NuSAP$^{MTBD}$; 233-383 aa), without a MCAK binding domain, could not affect its localization (Figure 3.3.4 C, row 4). On the other hand, all other NuSAP truncation mutants (*ie*. NuSAP$^{delKEN}$,

NuSAP$^{del390-410}$, NuSAP$^{delChHD}$), which contain a MCAK binding domain, significantly affected the localization of MCAK (Figure 3.3.4 C, rows 1-3).

Furthermore, the visual impression gained in Figure 3.3.3 D and Figure 3.3.4 B was quantified and summarized in Figure 3.3.3 E and Figure 3.3.4 D, respectively. To this end, since the overexpression of NuSAP and its truncation mutants leads to severe chromosome misalignment phenotypes, we then specifically analyzed a region of 2×8μm at the metaphase plate in metaphase synchronized HeLa cells to rule out the misaligned kinetochore pairs. Based on the ACA staining, we classify the localization of MCAK into three categories—inner centromere localization, asymmetrical kinetochore localization and inner kinetochore localization. As shown in Figure 3.3.3 E, our results showed that overexpression of the full-length NuSAP or NuSAP$^{233-441}$ significantly increased the inner centromere localization of MCAK between the kinetochore pairs in approximately 69.37±3.37%, 67.59±1.02% cells, respectively, but NuSAP$^{1-233}$ or NuSAP$^{delMCBD}$ did not have significant effect with approximately 21.59±2.53% and 23.08±1.61% cells respectively, as compared to 14.13±3.02% the control cells. Relatively, the percentage of asymmetrical kinetochore localized MCAK was not significantly changed in NuSAP-, NuSAP$^{1-233}$-, NuSAP$^{233-441}$- or NuSAP$^{delMCBD}$-overexpressing cells (14.41±1.79%, 15.91±1.59%, 21.30±2.85%, 22.12±2.12% respectively), compared to that in control cells (18.48±1.78%)

(Figure 3.3.3 E). Correspondingly, the proportion of inner kinetochore localized MCAK was decreased in the NuSAP (16.22±2.31%)- or $NuSAP^{233\text{-}441}$ (11.11±2.78%)- overexpressing cells, but not in the control (67.39±1.23%), $NuSAP^{1\text{-}233}$- (62.50±1.55%) or $NuSAP^{delMCBD}$ (54.81±1.44%)- overexpressing cells. (Figure 3.3.3 E).

Furthermore, we also intensively studied other truncation mutants of NuSAP and found consistently that the majority of MCAK delocalized to the inner centromere region in the cells overexpressing MCAK-binding-domain containing mutants (*ie*. $NuSAP^{delKEN}$, $NuSAP^{del390\text{-}410}$, $NuSAP^{delChHD}$), except the $NuSAP^{MTBD}$, for it does not contain a MCAK binding domain (Figure 3.3.4 D). To further confirm the effect of NuSAP on MCAK was specific, we examined whether NuSAP would affect the localizations of the other two members of kinesin-13 family—Kif2a (Figure 3.3.5 A) and Kif2b (Figure 3.3.5 B). Our results markedly indicated that the localizations of these kinesins were not affected by the overexpression of NuSAP, suggesting that NuSAP specifically regulates the localization of MCAK at the kinetochore region during metaphase.

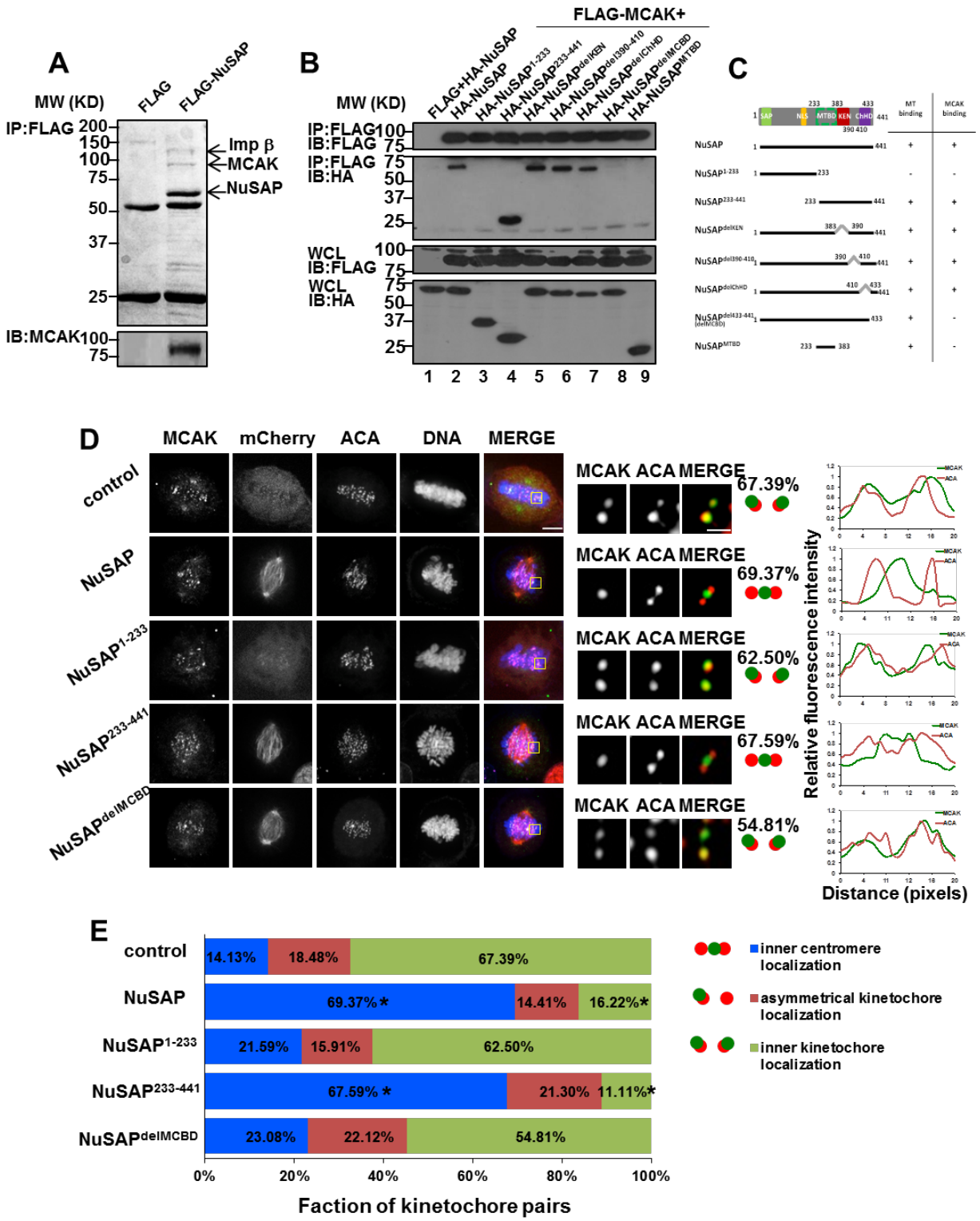
A
MW (KD)
FLAG
FLAG-NuSAP
IP:FLAG
IB:MCAK
Imp β
MCAK
NuSAP
B
FLAG-MCAK+
FLAG+HA-NuSAP
HA-NuSAP
HA-NuSAP1-233
HA-NuSAP233-441
HA-NuSAPdelKEN
HA-NuSAPdel390-410
HA-NuSAPdelChHD
HA-NuSAPdelMCBD
HA-NuSAPMTBD
IP:FLAG IB:FLAG
IP:FLAG IB:HA
WCL IB:FLAG
WCL IB:HA
C
MT binding
MCAK binding
D
MCAK
mCherry
ACA
DNA
MERGE
control
NuSAP
NuSAP1-233
NuSAP233-441
NuSAPdelMCBD
67.39%
69.37%
62.50%
67.59%
54.81%
Relative fluorescence intensity
Distance (pixels)
E
14.13%
18.48%
67.39%
69.37%*
14.41%
16.22%*
21.59%
15.91%
62.50%
67.59%*
21.30%
11.11%*
23.08%
22.12%
54.81%
inner centromere localization
asymmetrical kinetochore localization
inner kinetochore localization
Faction of kinetochore pairs

**Figure 3.3.3. NuSAP modulates MCAK localization at the kinetochore region.**

(A) NuSAP immunoprecipitates contain MCAK and Importin β. FLAG and FLAG-NuSAP immunoprecipitates from HEK 293T cell lysate were analyzed by Coomassie blue staining. (B) Identification of the MCAK binding domain on NuSAP. Immunoprecipitated proteins and whole cell lysates were detected with anti-HA and anti-FLAG antibodies. (C) A schematic map of NuSAP and its truncation mutants. The table represents microtubule binding and MCAK binding ability of different truncation mutants. +, positive; -, negative. (D) MCAK localization at the kinetochore region in metaphase HeLa cells expressing mCherry-vector (control), mCherry-NuSAP, mCherry-NuSAP$^{1-233}$, mCherry-NuSAP$^{233-441}$ or mCherry-NuSAP$^{delMCBD}$. Cells were stained with ACA and Hoechst 33342. Four laser channels were used to detect these signal intensities: 405nm for DNA, 488nm for MCAK, 568nm for mCherry, 640nm for ACA staining and seven z-stacks were merged. Scale bar, 5μm. The detailed MCAK localization at the plus-ends of kinetochore microtubules was imaged with single z-stack and enlarged in the middle panel and line profiles were represented in the right graph. Scale bar, 1μm. (E) A bar chart represents the percentage of kinetochore pairs with different types of MCAK localization according to ACA staining in HeLa cells expressing mCherry-NuSAP, mCherry-NuSAP$^{1-233}$, mCherry-NuSAP$^{233-441}$, mCherry-NuSAP$^{delMCBD}$ or mCherry-vector (control) during metaphase. The number of kinetochore pairs quantified: n (mCherry-vector control)=91/13 cells, n (mCherry-NuSAP)=105/15, n (mCherry-NuSAP$^{1-233}$)=86/11, n (mCherry-NuSAP$^{233-441}$)=87/11, n (mCherry-NuSAP$^{delMCBD}$)=93/13. * $p<0.001$.

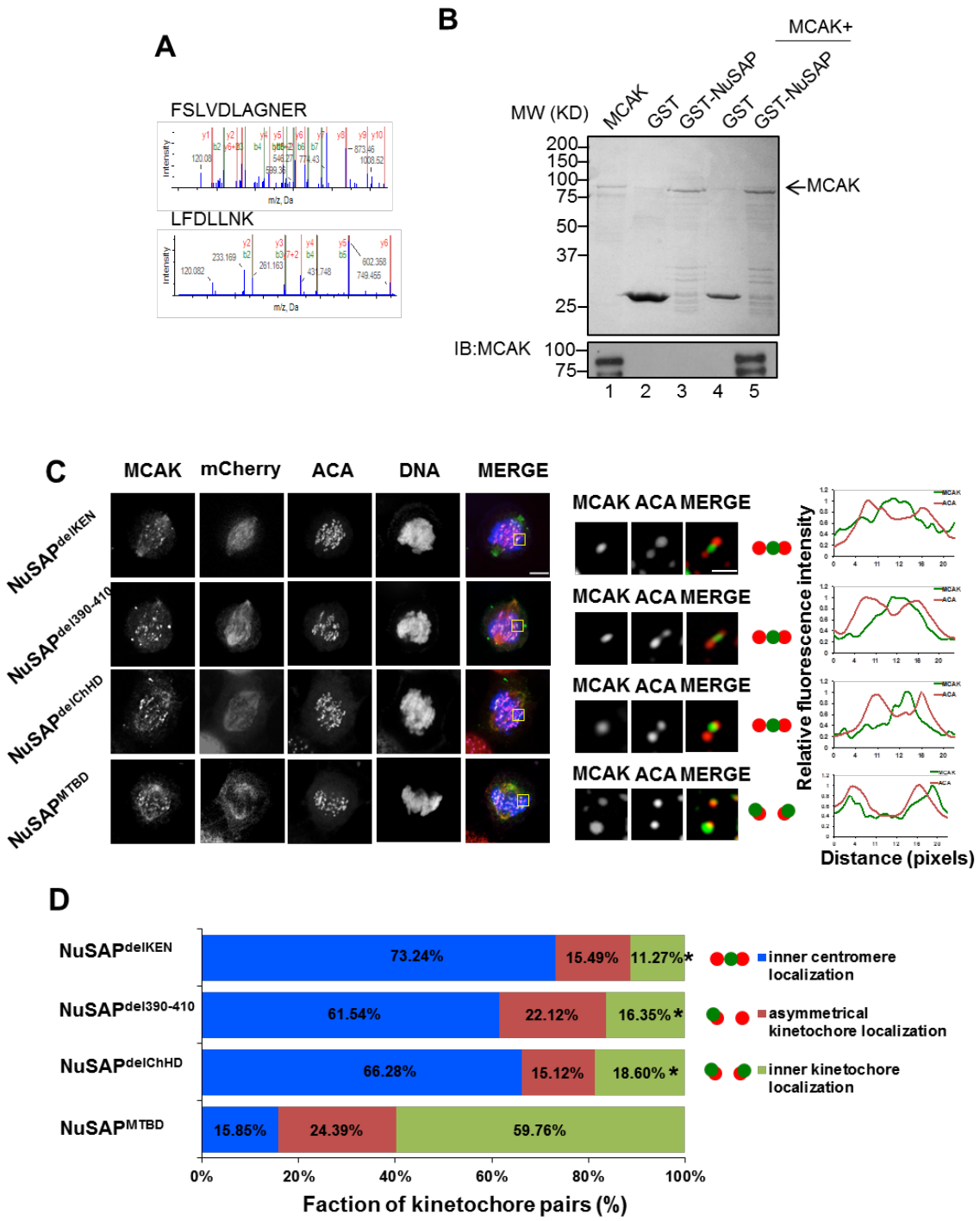
A
FSLVDLAGNER
LFDLLNK
B
MCAK+
MW (KD)
MCAK
GST
GST-NuSAP
GST
GST-NuSAP
200
150
100
75
50
37
25
←MCAK
IB:MCAK
100
75
1 2 3 4 5
C
MCAK
mCherry
ACA
DNA
MERGE
NuSAPdelKEN
NuSAPdel390-410
NuSAPdelChHD
NuSAPMTBD
MCAK ACA MERGE
Relative fluorescence intensity
Distance (pixels)
D
NuSAPdelKEN
NuSAPdel390-410
NuSAPdelChHD
NuSAPMTBD
73.24%
15.49%
11.27%*
61.54%
22.12%
16.35%*
66.28%
15.12%
18.60%*
15.85%
24.39%
59.76%
inner centromere localization
asymmetrical kinetochore localization
inner kinetochore localization
0%
20%
40%
60%
80%
100%
Faction of kinetochore pairs (%)

**Figure 3.3.4. NuSAP influences MCAK kinetochore localization through its interaction with MCAK**

(A) The identified sequences of MCAK by Mass Spectrometry (confidence>99%). (B) MCAK binds with NuSAP in vitro. Purified His-MCAK protein was incubated with GST and GST-NuSAP and detected with Coomassie blue staining and Western blotting. (C) MCAK localization at the kinetochore region during metaphase in HeLa cells expressing NuSAP mutants: mCherry-NuSAP$^{delKEN}$ (deletion of KEN domain), mCherry-NuSAP$^{del390-410}$ (deletion of fragment 390-410 aa), mCherry-NuSAP$^{delChHD}$ (deletion of ChHD domain) and mCherry-NuSAP$^{MTBD}$ (microtubule binding domain). Cells were stained with ACA and Hoechst 33342. Four laser channels were used to detect these signal intensities: 405nm for DNA, 488nm for MCAK, 568nm for mCherry, 640nm for ACA staining and seven z-stacks were merged. Scale bar, 5μm. The detailed MCAK localization at the microtubule plus-ends was imaged with single z-stack and enlarged in the middle panel and line scan profiles were represented in the right graph. Scale bar, 1μm. (D) A bar chart represents the percentage of kinetochore pairs with different types of MCAK localization according to ACA staining in HeLa cells expressing NuSAP mutants: mCherry-NuSAP$^{delKEN}$, mCherry-NuSAP$^{del390-410}$, mCherry-NuSAP$^{delChHD}$, or mCherry-NuSAP$^{MTBD}$ during metaphase. The number of kinetochore pairs quantified: n (mCherry-NuSAP$^{delKEN}$)=69/10 cells, n (mCherry-NuSAP$^{del390-410}$)=90/14, n (mCherry-NuSAP$^{delChHD}$)=75/11, n (mCherry-NuSAP$^{MTBD}$)=71/10. * $p<0.001$.

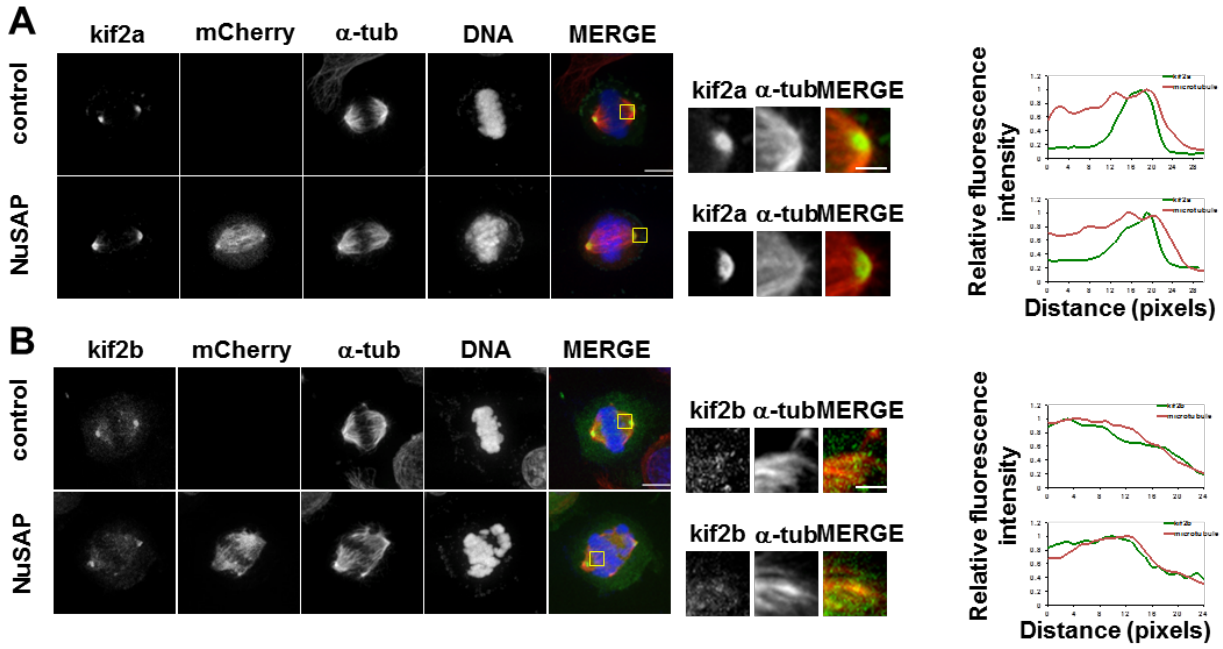


**Figure 3.3.5. NuSAP specifically influences MCAK kinetochore localization, but not other members in kinesin 13 family**

(A-B) Kif2a (A) localization at spindle pole and Kif2b (B) localization at microtubules during metaphase in control-vector- or mCherry-NuSAP-overexpressing HeLa cells. Cells were stained with an anti-α-tubulin antibody and Hoechst 33342. Scale bar, 5μm. The detailed localization was enlarged in the middle panel and line profiles were represented in the right graph. Scale bar, 1μm.

### 3.3.3 NuSAP regulates the dynamics of MCAK on the plus-ends of kinetochore microtubules

Since the localization and dynamics of MCAK are essential for its depolymerization activity, we hypothesized that the interaction between NuSAP and MCAK might also affect the dynamics of MCAK at the plus-ends of kinetochore microtubules resulting in influencing kinetochore microtubule stability. To test this hypothesis, the Fluorescence Recovery After Photobleaching (FRAP) experiment was performed to quantify the dynamics of MCAK at the plus-ends of kinetochore microtubules. The signal of MCAK at the 1×1μm region of the kinetochore region was photobleached and analyzed in the full-length NuSAP- or NuSAP truncation mutants-overexpressing HeLa cells (Figure 3.3.6 A). The kymographs generated from the 1×1μm bleaching region indicated that NuSAP and NuSAP$^{233\text{-}441}$, but not NuSAP$^{1\text{-}233}$ and NuSAP$^{delMCBD}$, noticeably reduced the dynamics of MCAK at the ends of kinetochore microtubules, based on the intensity recovery of MCAK signals from 0-10s after photobleaching (Figure 3.3.6 B). In addition, FRAP analyses were performed to quantify the dynamics of MCAK with normalized intensity fitted into a constrained exponential curve (Figure 3.3.6 C-H). Compared to the $T_{1/2}$ in control cells (0.99±0.05s, Figure 3.3.6 C), the $T_{1/2}$ of MCAK was significantly increased in the full-length NuSAP- or NuSAP$^{233\text{-}441}$-overexpressing cells with 1.45±0.07s and

1.42±0.08s, respectively (Figure 3.3.6 D and F). On the other hand, similar to the $T_{1/2}$ in control cells, the $T_{1/2}$ in NuSAP$^{1-233}$- and NuSAP$^{delMCBD}$- transfected cells was 1.01±0.06s and 1.05±0.07s, respectively (Figure 3.3.6 E and G), suggesting that NuSAP plays a significant role in regulating the dynamics of MCAK at the plus-ends of kinetochore microtubules.

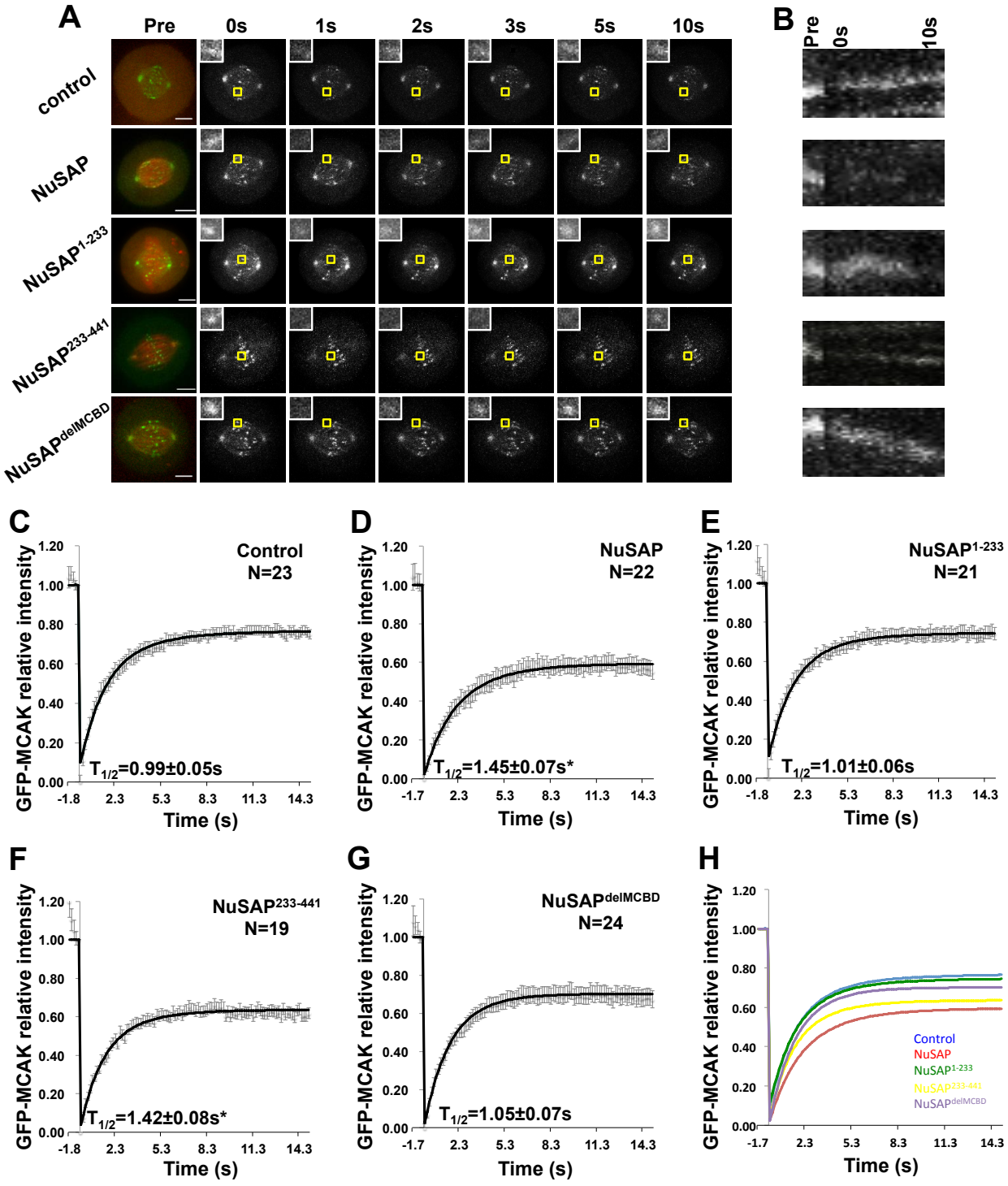
A
Pre
0s
1s
2s
3s
5s
10s
control
NuSAP
NuSAP1-233
NuSAP233-441
NuSAPdelMCBD
B
Pre
0s
10s
C
Control
N=23
T1/2=0.99±0.05s
D
NuSAP
N=22
T1/2=1.45±0.07s*
E
NuSAP1-233
N=21
T1/2=1.01±0.06s
F
NuSAP233-441
N=19
T1/2=1.42±0.08s*
G
NuSAPdelMCBD
N=24
T1/2=1.05±0.07s
H
Control
NuSAP
NuSAP1-233
NuSAP233-441
NuSAPdelMCBD
GFP-MCAK relative intensity
Time (s)

**Figure 3.3.6. NuSAP regulates the dynamics of MCAK on the plus-ends of kinetochore microtubules.**

(A) Representative images and kymographs of MCAK dynamics at kinetochore region in metaphase HeLa cells expressing mCherry-vector (control), mCherry-NuSAP, mCherry-NuSAP$^{1-233}$, mCherry-NuSAP$^{233-441}$, or mCherry-NuSAP$^{delMCBD}$. Yellow squares represent 1×1μm photobleaching region. (B) Kymographs were generated from the photobleaching kinetochore region. Images were acquired in a 0.15-second interval. Scale bar, 5μm. (C-G) Normalized signal recovery curves of FRAP assays in metaphase HeLa cells expressing mCherry-vector C, mCherry-NuSAP D, mCherry-NuSAP$^{1-233}$ E, mCherry-NuSAP$^{233-441}$ F or mCherry-NuSAP$^{delMCBD}$ G. Solid lines represent for the fit values of each group and dots indicate the mean values. Turnover $T_{1/2}$ was calculated using a single constrained exponential curve. Data were collected from 3 independent experiments and "n" indicates the number of mitotic spindles analyzed. Error bars represent ±SD. * $p<0.001$. (H) Normalized recovery curves of FRAP assay were fitted into a single constrained exponential curve to calculate the recovery half-life ($T_{1/2}$).

### 3.3.4 NuSAP stabilizes kinetochore microtubules through its regulation on MCAK depolymerization activity

To investigate whether the interaction between NuSAP and MCAK is essential to regulate the stability of kinetochore microtubules, we performed Fluorescence Dissipation After PhotoActivation (FDAPA) experiment at the kinetochore region (Figure 3.3.8 A). A 405nm laser was focused at a rectangle (1×5μm) around metaphase plate and fluorescence intensity of the activated region was analysed and fitted into a double exponential decay curve ($R^2$>0.99) with the slow depolymerizing populations corresponded to kinetochore microtubules(Zhai et al., 1995). The kymographs and line-scan profiles showed that the intensity of photoactivated PAGFP-α-tubulin rapidly decayed in control- (Figure 3.3.7 A), $NuSAP^{1-233}$- (Figure 3.3.7 C) and $NuSAP^{delMCBD}$- (Figure 3.3.7 E) transfected cells, but was stable in NuSAP- (Figure 3.3.7 B) and $NuSAP^{233-441}$-overexpressing cells (Figure 3.3.7 D). The $T_{1/2}$ of kinetochore microtubules was five-times and three-times longer in NuSAP- and $NuSAP^{233-441}$-overexpressing cells (54.14±6.35min and 30.01±2.72min, respectively), compared to that in control (9.68±0.33min, consistent with previous studies(Bakhoum et al., 2009; Zhai et al., 1995)) and $NuSAP^{1-233}$ (7.56±0.70min)-transfected cells. On the other hand, in $NuSAP^{delMCBD}$-transfected cells, the kinetochore microtubules dynamics (12.72±0.97min) was similar to that in control cells (Figure 3.3.7 F), indicating

that without a MCAK binding domain, NuSAP$^{delMCBD}$ cannot stabilize kinetochore microtubules. Taken together, these results suggest that the interaction with MCAK is essential for NuSAP to stabilize kinetochore microtubules.

To further support our results, we conducted a cold treatment to selectively depolymerize interpolar microtubules and remain the kinetochore microtubules (Figure 3.3.8 B and C). We found that NuSAP (1.54 times) and NuSAP$^{233-441}$ (1.46 times), but not NuSAP$^{1-233}$ (0.94 times) and NuSAP$^{delMCBD}$ (1.11 times), led to higher levels of stable kinetochore microtubules after the cold treatment, compared to control (Figure 3.3.8 B and C, indicated by arrows). To directly investigate the kinetochore microtubule length, a monastrol-cold treatment was utilized to remove interpolar microtubules in monopolar cells and the distance from a kinetochore to the nearest centrosome served as a direct readout for the kinetochore microtubule length (Sturgill and Ohi, 2013). Our results showed that the average of the kinetochore microtubule length was largely increased in NuSAP- and NuSAP$^{233-441}$-, but not NuSAP$^{1-233}$- and NuSAP$^{delMCBD}$-overexpressing cells (Figure 3.3.7 G, indicated by arrows). The quantitative data showed that in NuSAP- and NuSAP$^{233-441}$-overexpressing cells, the average kinetochore microtubule length was 3.67±0.31μm and 3.52±0.24μm respectively, which were significantly longer than the kinetochore microtubule length in

control cells (2.41±0.23μm) (Figure 3.3.7 H). Consistent with our other experiments shown above, NuSAP$^{1-233}$ (2.47±0.23μm) and NuSAP$^{delMCBD}$ (2.50±0.17μm)-transfected cells exhibited similar kinetochore microtubule lengths to that in control cells (Figure 3.3.7 H).

To further support our results, we conducted a cold treatment to specifically investigate the kinetochore microtubules with STED imaging (Figure 3.3.7 I). The line profiles were generated from the enlarged images with 25nm resolution (Figure 3.3.7 I, right panel). We found that NuSAP and NuSAP$^{233-441}$, but not NuSAP$^{1-233}$ and NuSAP$^{delMCBD}$, led to higher levels of stable kinetochore microtubule bundles after the cold treatment, compared to control. To rule out the possible dominant negative effect, we specifically investigate the kinetochore microtubule stability with the depletion assay with NuSAP siRNA (Raemaekers et al., 2003b) and the rescue assay with NuSAP or NuSAP$^{delMCBD}$ with the monastrol-cold treatment (Figure 3.3.8 D and E). The results indicates that the average of the kinetochore microtubule length was largely increased in the cells co-transfected with control siRNA and GFP-NuSAP (3.48±0.27μm) but not GFP-NuSAP$^{delMCBD}$ (2.65±0.26μm), compared to GFP vector control (2.49±0.16μm) (Figure 3.3.7 J, lane 1-3). The depletion of NuSAP significantly decreased the length of kinetochore microtubules (1.77±0.19μm) compared with control siRNA (lane 1 and 4). However, the kinetochore microtubule length was rescued in

NuSAP depleted cells co-transfection with GFP-NuSAP (2.35±0.29μm), but not GFP-NuSAP$^{delMCBD}$ (1.85±0.18μm) (lane 5 and 6). Taken together, our results show that NuSAP stabilizes kinetochore microtubules through its regulation on the activity of MCAK during metaphase.

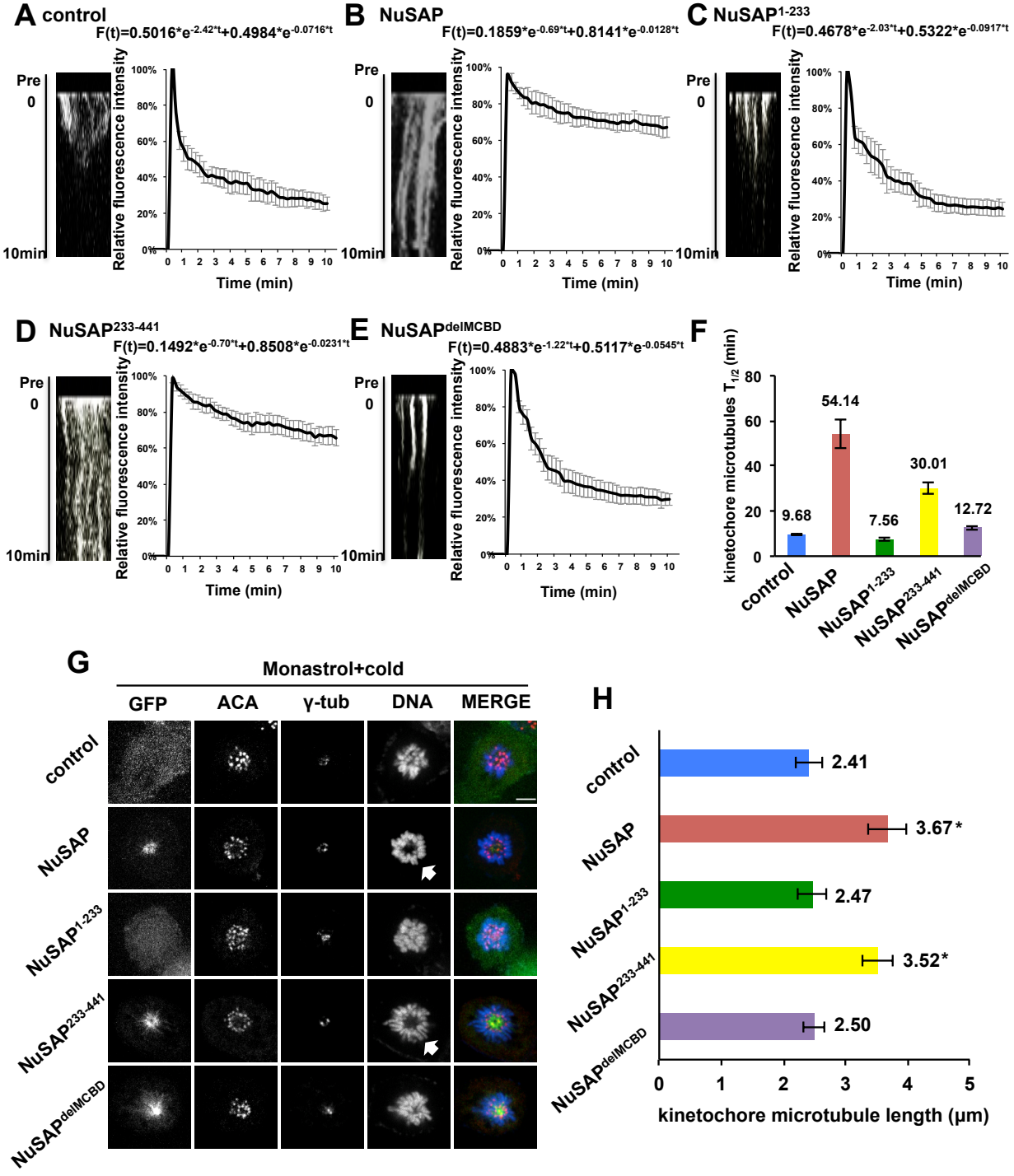
A control
F(t)=0.5016*e-2.42*t+0.4984*e-0.0716*t
B NuSAP
F(t)=0.1859*e-0.69*t+0.8141*e-0.0128*t
C NuSAP1-233
F(t)=0.4678*e-2.03*t+0.5322*e-0.0917*t
D NuSAP233-441
F(t)=0.1492*e-0.70*t+0.8508*e-0.0231*t
E NuSAPdelMCBD
F(t)=0.4883*e-1.22*t+0.5117*e-0.0545*t
Pre
0
10min
Relative fluorescence intensity
Time (min)
F
kinetochore microtubules T1/2 (min)
9.68
54.14
7.56
30.01
12.72
control
NuSAP
NuSAP1-233
NuSAP233-441
NuSAPdelMCBD
G
Monastrol+cold
GFP
ACA
γ-tub
DNA
MERGE
H
2.41
3.67*
2.47
3.52*
2.50
kinetochore microtubule length (μm)

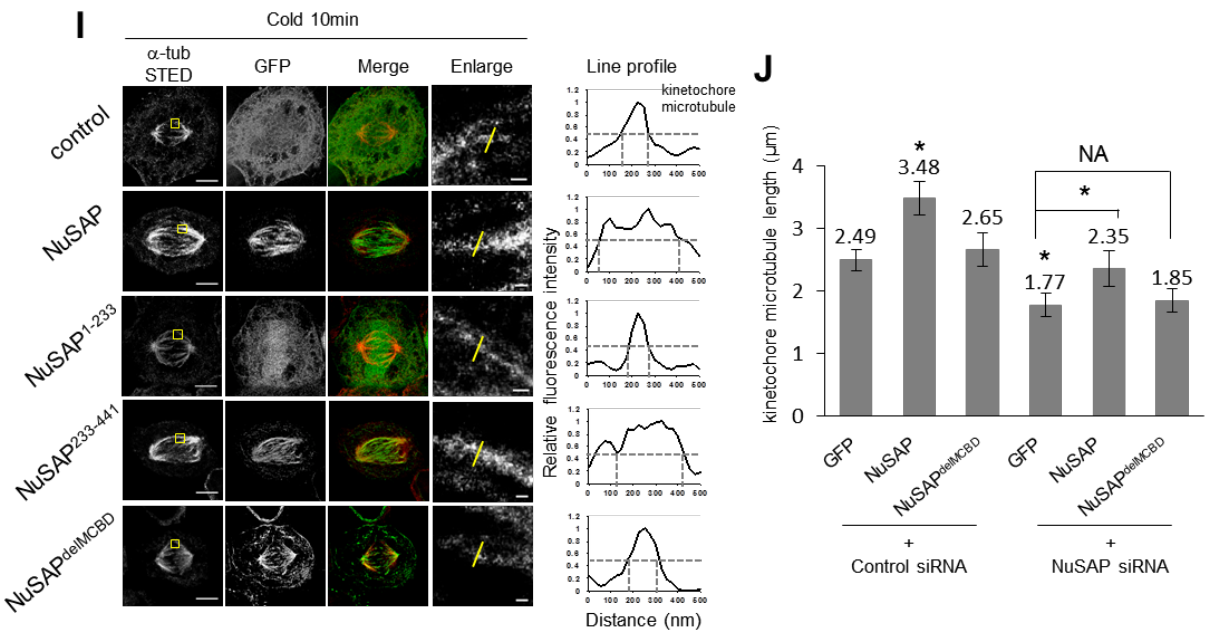


**Figure 3.3.7. NuSAP stabilizes kinetochore microtubules through its regulation on MCAK depolymerization activity.**

(A-E) Representative images of kymographs and normalized signal recovery curves of photoactivation assays in metaphase HeLa cells expressing mCherry-vector (n=12) A, mCherry-NuSAP (n=12) B, mCherry-NuSAP$^{1\text{-}233}$ (n=14) C, mCherry-NuSAP$^{233\text{-}441}$ (n=13) D or mCherry-NuSAP$^{delMCBD}$ (n=14) E. Solid lines represent for the fit values of each group calculated by double exponential regression analysis. $R^2$>0.99.. (F) A bar chart presenting the turnover rate $T_{1/2}$ of the kinetochore microtubules calculated using a double exponential regression curve. Error bars represent ±SD. (G) NuSAP and NuSAP$^{233\text{-}441}$ stabilize kinetochore microtubules, but not NuSAP$^{delMCBD}$. HeLa cells expressing GFP-NuSAP, GFP-NuSAP$^{1\text{-}233}$, GFP-NuSAP$^{233\text{-}441}$, GFP-NuSAP$^{delMCBD}$ or GFP-vector (control) were treated with a monastrol-cold method. Kinetochores were labeled with ACA, spindle poles with anti-γ-tubulin and DNA with Hoechst 333342. Scale bar, 5μm. (H) A bar chart represents the average of kinetochore microtubule length in HeLa cells expressing GFP-NuSAP, GFP-NuSAP$^{1\text{-}233}$, GFP-NuSAP$^{233\text{-}441}$, GFP-NuSAP$^{delMCBD}$ or GFP-vector after monastrol-cold treatment. "n" indicates the number of kinetochore microtubules analyzed. Error bars represents ±SD. * p<0.001. (I) NuSAP and NuSAP$^{233\text{-}441}$ stabilise kinetochore microtubules, but not NuSAP$^{delMCBD}$. HeLa cells expressing GFP-NuSAP, GFP-NuSAP$^{1\text{-}233}$, GFP-NuSAP$^{233\text{-}441}$, GFP-NuSAP$^{delMCBD}$ or GFP-vector (control) were treated with

a cold method to remove interpolar microtubules. Kinetochore microtubules were labeled with anti-α-tubulin and imaged with STED method (Pixel size 25nm). Scale bar, 5μm. The indicated regions were enlarged and analyzed with line profile. Scale bar, 300nm. (J) A bar chart represents the average of kinetochore microtubule length in HeLa cells transfected with control siRNA or NuSAP siRNA together with GFP vector, GFP-NuSAP or GFP-NuSAP$^{delMCBD}$ with monastrol-cold treatment. Error bars represents ±SD. * $p<0.001$. The effectiveness of the NuSAP depletion and the representing images of monastrol-cold treated metaphase cells.

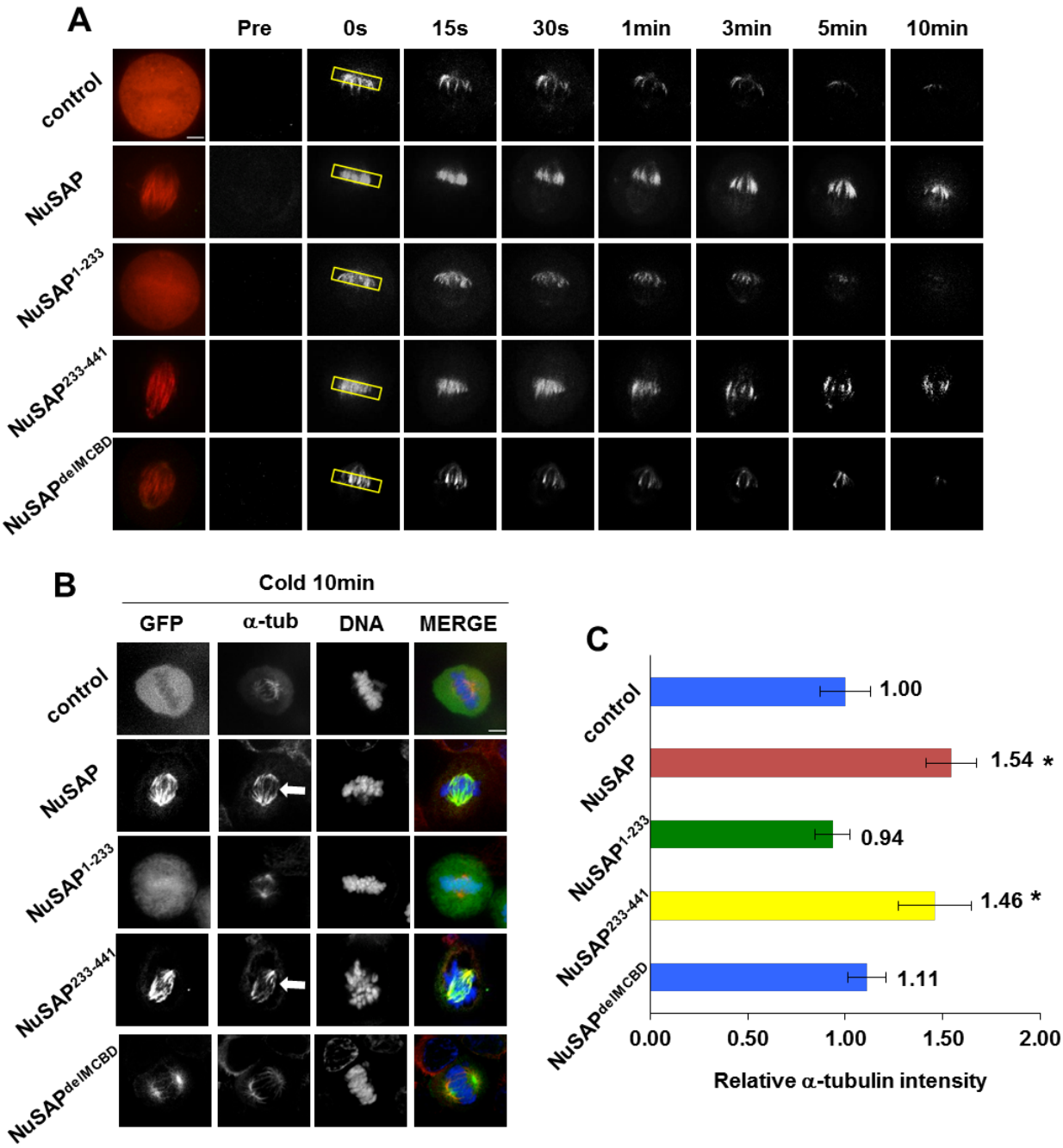
A
Pre
0s
15s
30s
1min
3min
5min
10min
control
NuSAP
NuSAP1-233
NuSAP233-441
NuSAPdelMCBD
B
Cold 10min
GFP
α-tub
DNA
MERGE
control
NuSAP
NuSAP1-233
NuSAP233-441
NuSAPdelMCBD
C
control
NuSAP
NuSAP1-233
NuSAP233-441
NuSAPdelMCBD
1.00
1.54 *
0.94
1.46 *
1.11
0.00
0.50
1.00
1.50
2.00
Relative α-tubulin intensity

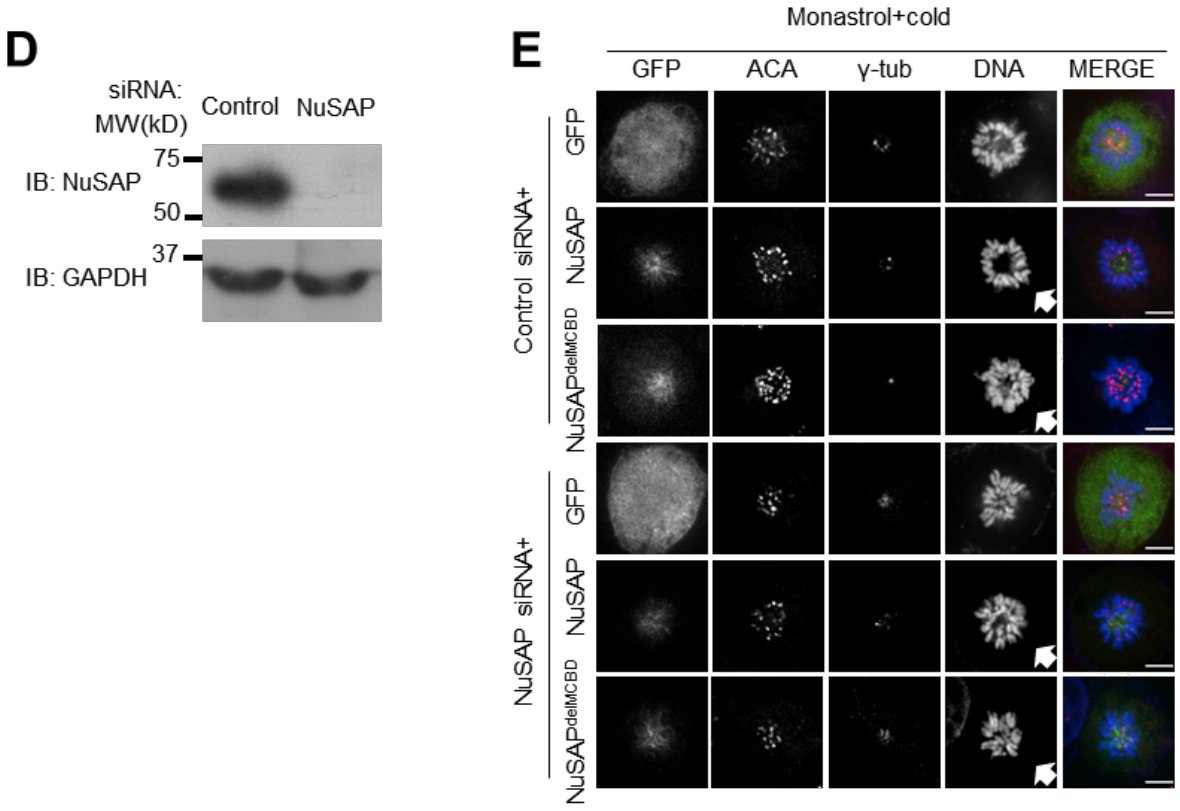


**Figure 3.3.8. NuSAP stabilizes kinetochore microtubules through its binding with MCAK**

(A) Representative images of PAGFP α-tubulin stability at the kinetochore region in metaphase HeLa cells expressing mCherry-NuSAP, mCherry-NuSAP$^{1-233}$, mCherry-NuSAP$^{233-441}$, mCherry-NuSAP$^{delMCBD}$ or mCherry-vector (control) after photoactivation. Yellow squares represent photoactived region. Images were acquired in a 15-second interval for 10min. Scale bar, 5μm. (B) The localization of kinetochore microtubules in cold treated metaphase HeLa cells expressing GFP-NuSAP, GFP-NuSAP$^{1-233}$, GFP-NuSAP$^{233-441}$, GFP-NuSAP$^{delMCBD}$ or GFP-vector (control). Cells were stained with an anti-α-tubulin antibody and DNA with Hoechst 333342. Scale bar, 5μm. (C) A bar charts representing the average of a-tubulin immunofluorescence intensity on metaphase spindles stained as in B in cells expressing GFP-NuSAP, GFP-NuSAP$^{1-233}$, GFP-NuSAP$^{233-441}$, GFP-NuSAP$^{delMCBD}$ and GFP-vector only (control). The number of cells quantified: n (GFP)=37/3 independent experiments, n (GFP-NuSAP)=36/3, n (GFP-NuSAP$^{1-}$

$^{233}$)=35/3, n (GFP-NuSAP$^{233-441}$)=39/3, n (GFP-NuSAP$^{233-441}$)=38/3. Error bars represent ±SD. * $p<0.001$. (D) The effectiveness of NuSAP depletion in HeLa cells was analyzed by western blot 48 hr after siRNA treatment. The cell lysate were blotted for NuSAP. The amount of protein loading was detected using an anti-GAPDH antibody. (E) HeLa cells transfected with control siRNA or NuSAP siRNA together with GFP vector, GFP-NuSAP or GFP-NuSAP$^{delMCBD}$ were treated with a monastrol-cold method. Kinetochores were labeled with ACA, spindle poles with anti-γ-tubulin and DNA with Hoechst 333342. Scale bar, 5μm.

### 3.3.5 Aurora B regulates the interaction and localization between NuSAP and MCAK

The localization and dynamics of MCAK are tightly regulated by Aurora B kinase through its phosphorylation of MCAK at five Serine residues (S92, S106, S108, S112, S186) reported previously (Andrews et al., 2004; Lan et al., 2004). To test whether Aurora B kinase has a role in regulating the interaction between NuSAP and MCAK, we performed immunoprecipitation assays using FLAG-MCAK to pulldown HA-NuSAP in HeLa cells. Strikingly, our data revealed that the association between NuSAP and MCAK was highly enhanced by ectopically expressing Aurora B (Figure 3.3.9 A; lane 3), and this protein-protein association was dramatically abolished by the treatment of ZM447439, a specific inhibitor of Aurora B, in cells (Figure 3.3.9 A; lane 4), demonstrating that Aurora B positively regulated the interaction between MCAK and NuSAP. To further investigate whether the interaction of MCAK and NuSAP may be dependent upon Aurora B-mediated phosphorylation, we utilized phospho-deficient MCAK 5A and phospho-mimicking MCAK 5E mutants (Andrews et al., 2004) to verify the interaction between MCAK and NuSAP. As shown in Figure 3.3.9 B, our result showed that MCAK 5E mutant exhibited an enhanced binding ability with NuSAP. In contrast, MCAK 5A displayed a significant lower affinity to NuSAP.

These results indicate that Aurora B is important in regulating the interaction of NuSAP and MCAK through the phosphorylation of MCAK during metaphase.

To further explore how the Aurora B-mediated phosphorylation-dependent interaction of NuSAP and MCAK contributes to the regulation of MCAK, we examined the localization of MCAK, MCAK 5A and MCAK 5E at the kinetochore region in the control- or NuSAP-overexpressing metaphase HeLa cells. As shown in Figure 3.3.9 C, in overexpression of MCAK WT alone (Figure 3.3.9 C, row 1), MCAK 5A alone (Figure 3.3.9 C, row 2) or MCAK 5A co-transfected with NuSAP (Figure 3.3.9 C, row 5) cells, the localization of MCAK was at the inner kinetochore region, consistent with previous study(Andrews et al., 2004). However, in MCAK 5E transfected cells (Figure 3.3.9 C, row 3), or MCAK WT co-transfected with NuSAP (Figure 3.3.9 C, row 4), or MCAK 5E co-transfected with NuSAP cells (Figure 3.3.9 C, row 6), the localization of MCAK was altered into the inner centromere region as shown by line-scan profiles (Figure 3.3.9 C, right panel, enlarged represented single z-stack images).

Next, we analyzed the relative localization of MCAK to kinetochore in metaphase cells. The results showed that co-overexpression of NuSAP significantly increased the inner centromere localization of MCAK (72.84±0.75%) and MCAK 5E (81.55±0.81%), but not MCAK 5A (10.42±3.99%), compared to the

localization of MCAK, MCAK 5E and MCAK 5A in metaphase cells (14.12±2.14%, 63.16±1.46%, 8.54±4.59%, respectively). Furthermore, co-overexpression of NuSAP also dramatically decreased the inner kinetochore localization of MCAK (12.35±2.57%) and MCAK 5E (4.85±1.56%), but not MCAK 5A (76.04±0.71%), compared to the localization of MCAK (68.24±0.74%), MCAK 5E (19.74±3.07%) and MCAK 5A (75.61±0.86%) in metaphase cells, respectively. Relatively, the asymmetrical kinetochore localizations of MCAK, MCAK 5A and MCAK 5E were not significantly changed by overexpression of NuSAP (Figure 3.3.9 D). Our data suggests that the localization of MCAK mediated by NuSAP is dependent on the activity of Aurora B. Taken together, our results demonstrate that Aurora B plays a pivotal role in regulating the specific function of NuSAP on MCAK to stabilize kinetochore microtubules.

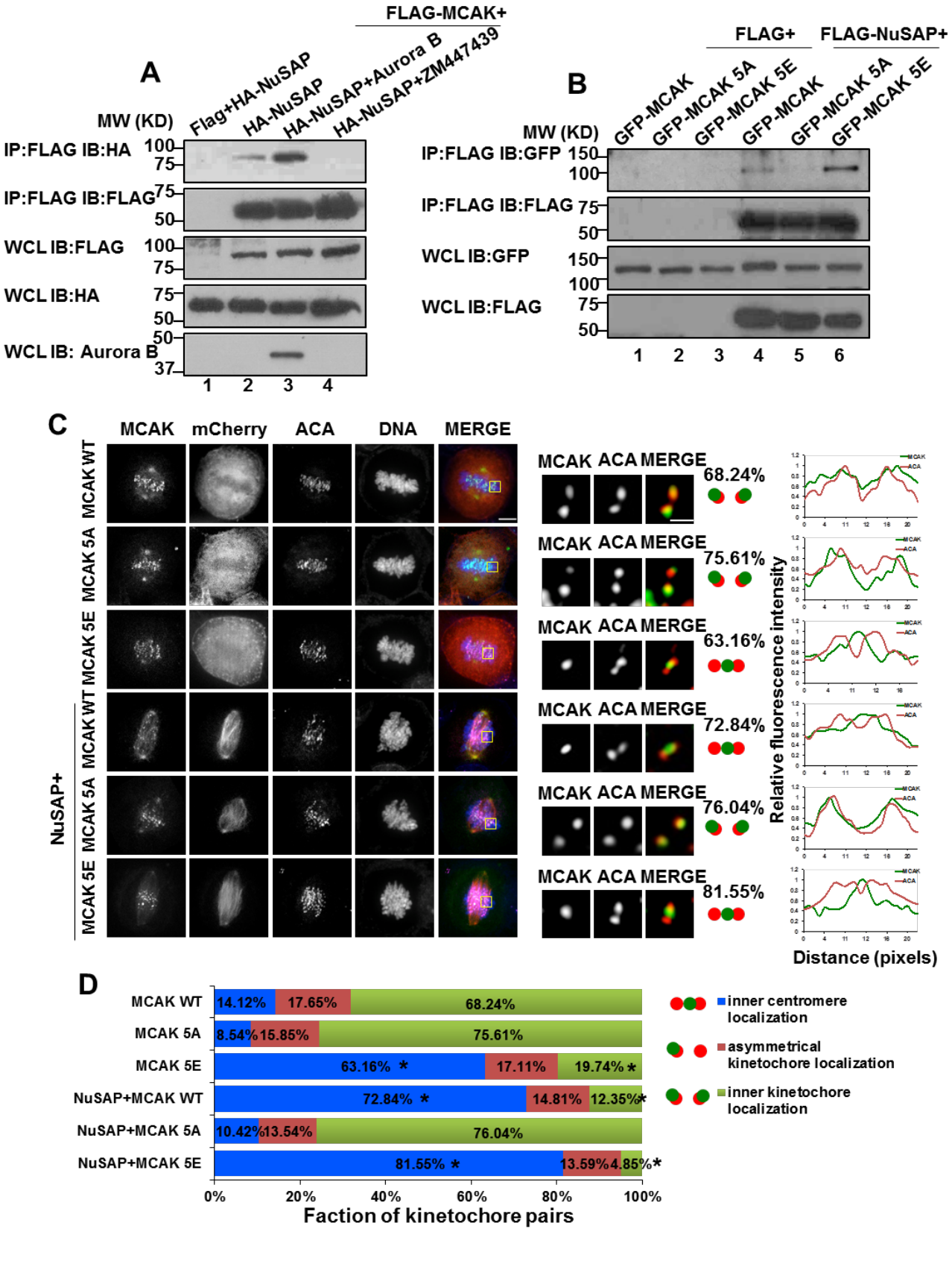
A
FLAG-MCAK+
Flag+HA-NuSAP
HA-NuSAP
HA-NuSAP+Aurora B
HA-NuSAP+ZM447439
MW (KD)
IP:FLAG IB:HA
IP:FLAG IB:FLAG
WCL IB:FLAG
WCL IB:HA
WCL IB: Aurora B
100
75
75
50
100
75
75
50
50
37
1 2 3 4
B
FLAG+
FLAG-NuSAP+
GFP-MCAK
GFP-MCAK 5A
GFP-MCAK 5E
GFP-MCAK
GFP-MCAK 5A
GFP-MCAK 5E
MW (KD)
IP:FLAG IB:GFP
IP:FLAG IB:FLAG
WCL IB:GFP
WCL IB:FLAG
150
100
75
50
150
100
75
50
1 2 3 4 5 6
C
MCAK
mCherry
ACA
DNA
MERGE
NuSAP+
MCAK WT
MCAK 5A
MCAK 5E
MCAK WT
MCAK 5A
MCAK 5E
MCAK ACA MERGE
68.24%
75.61%
63.16%
72.84%
76.04%
81.55%
Relative fluorescence intensity
Distance (pixels)
D
MCAK WT
MCAK 5A
MCAK 5E
NuSAP+MCAK WT
NuSAP+MCAK 5A
NuSAP+MCAK 5E
14.12%
17.65%
68.24%
8.54%
15.85%
75.61%
63.16% *
17.11%
19.74% *
72.84% *
14.81%
12.35%*
10.42%
13.54%
76.04%
81.55% *
13.59%
4.85%*
0%
20%
40%
60%
80%
100%
Faction of kinetochore pairs
inner centromere localization
asymmetrical kinetochore localization
inner kinetochore localization

**Figure 3.3.9. Aurora B regulates the binding and localization between NuSAP and MCAK.**

(A) Aurora B enhances the binding between NuSAP and MCAK. Whole cell lysates of 293T cells co-transfected with a FLAG vector or FLAG-MCAK and HA-NuSAP and Aurora B or treated with 2μM ZM447439 for 45min were collected for Co-IP using FLAG-M2 beads. Immunoprecipitated proteins and whole cell lysates were detected with anti-HA, anti-FLAG and anti-Aurora B antibodies. (B) Whole cell lysates of HEK 293T cells co-transfected with a FLAG vector or FLAG-NuSAP and GFP-MCAK WT, GFP-MCAK 5A or GFP-MCAK 5E were collected for Co-IP using FLAG M2-beads. Immunoprecipitated proteins and whole cell lysates were detected with anti-GFP and anti-FLAG antibodies. (C) MCAK localization at the kinetochore region in metaphase HeLa cells expressing GFP-MCAK WT, GFP-MCAK 5A or GFP-MCAK 5E and mCherry-NuSAP or mCherry-vector (control). Cells were stained with ACA and Hoechst 33342. Four laser channels were used to detect these signal intensities: 405nm for DNA, 488nm for MCAK, 568nm for mCherry, 640nm for ACA staining and seven z-stacks were merged. Scale bar, 5μm. The detailed MCAK localization at the plus-ends of kinetochore microtubules was imaged with single z-stack and enlarged in the middle panel and line profile was represented in the right graph. Scale bar, 1μm. (D) A bar chart represents the percentage of the kinetochore pairs with different types of MCAK localization according to ACA staining in HeLa cells expressing GFP-MCAK WT, GFP-MCAK 5A or GFP-MCAK 5E and mCherry-NuSAP or mCherry-vector (control) during metaphase. The number of kinetochore pairs quantified: n (MCAK WT)=85/11 cells, n (MCAK 5A)=82/11, n (MCAK 5E)=76/10, n (NuSAP+MCAK WT)=81/11, n (NuSAP+MCAK 5A)=95/13, n (NuSAP+MCAK 5E)=103/14. * $p<0.001$.

### 3.3.6 Aurora B dependent interaction of NuSAP and MCAK enhances microtubule stabilization

To explore whether the depolymerization activity of MCAK regulated by NuSAP is also dependent on the Aurora B-mediated phosphorylation, we performed an *in vitro* assay using purified recombinant NuSAP, MCAK, MCAK 5A and MCAK 5E proteins to analyze their depolymerizing activity in the taxol-stabilized microtubules(Lan et al., 2004) (Figure 3.3.10 A). A total of 20 nM MCAK WT, 5A or 5E caused time-dependent microtubule depolymerization (Figure 3.3.10 B, columns 2 to 4). Interestingly, the presence of NuSAP dramatically decreased the disassembling rate induced by MCAK WT or 5E (Figure 3.3.10 B, columns 5 and 7), but no detectable effect was found on the depolymerization activity of MCAK 5A (Figure 3.3.10 B, column 6). The extent of microtubule stability was quantified by counting the number of microtubules per image and our data showed that NuSAP inhibited the depolymerization activity of MCAK 5E (2.03 times) more prominently, compared to that of MCAK WT (1.30 times), but due to no interaction, NuSAP only has little effect on MCAK 5A (0.08 times) (Figure 3.3.10 C). Mechanistically, these results indicate that NuSAP can enhance the stability of microtubules by blocking the depolymerization activity of MCAK and MCAK 5E, but not MCAK 5A. In titration experiments scored at a single time point, the inhibitory effect of NuSAP was detected at the protein concentration as

low as 5nM, one-fourth the concentration of MCAK (Figure 3.3.11). Noticeably, these findings demonstrate that the phosphorylation of MCAK by Aurora B has a critical role on NuSAP-mediated MCAK depolymerization activity.

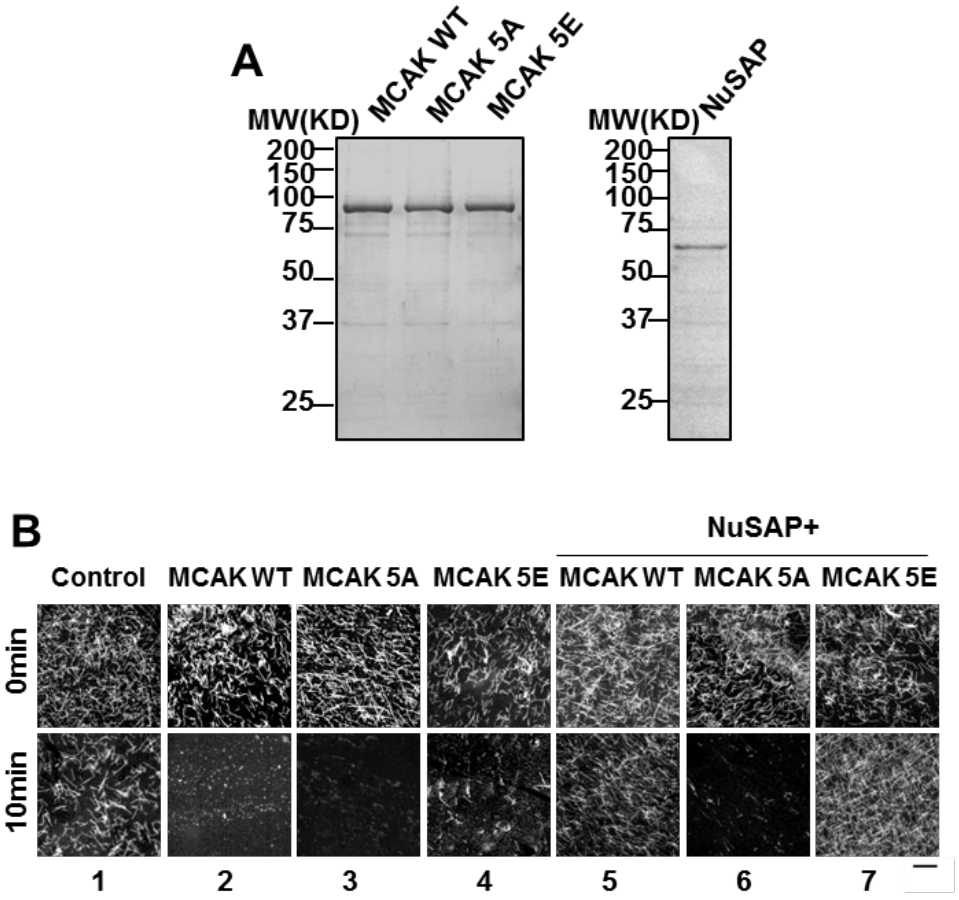
A
MCAK WT
MCAK 5A
MCAK 5E
MW(KD)
200
150
100
75
50
37
25
NuSAP
MW(KD)
200
150
100
75
50
37
25
B
NuSAP+
Control
MCAK WT
MCAK 5A
MCAK 5E
MCAK WT
MCAK 5A
MCAK 5E
0min
10min
1
2
3
4
5
6
7
C
Control
1.00
MCAK WT
0.22*
MCAK 5A
0.06*
MCAK 5E
0.35*
NuSAP+MCAK WT
1.30**
NuSAP+MCAK 5A
0.08*
NuSAP+MCAK 5E
2.03*
*
*
0
500
1000
1500
2000
Number of microtubules/field

**Figure 3.3.10. Aurora B promotes microtubule stabilization through positive regulation of NuSAP function on MCAK.**

(A) Purification of His-tagged NuSAP protein from bacteria and His-tagged MCAK WT, MCAK 5A, and MCAK 5E from insect sf9 cells. A total of 2.5μg of NuSAP, MCAK WT, MCAK 5A and MCAK 5E proteins were stained using Coomassie blue staining, respectively. (B) A microtubule depolymerization assay with MCAK and NuSAP. 100nM NuSAP and 20nM MCAK WT, MCAK 5A, or MCAK 5E proteins were incubated with 1.5μM microtubules at 37°C for 10min. Scale bar, 20μm. (C) A bar chart represents the number of microtubules per 63X field in control and MCAK WT, MCAK 5A, MCAK 5E with or without NuSAP protein at an incubating time of 10min. Three independent experiments were conducted. Error bars represent ±SD. * $p<0.001$, ** $p<0.05$.

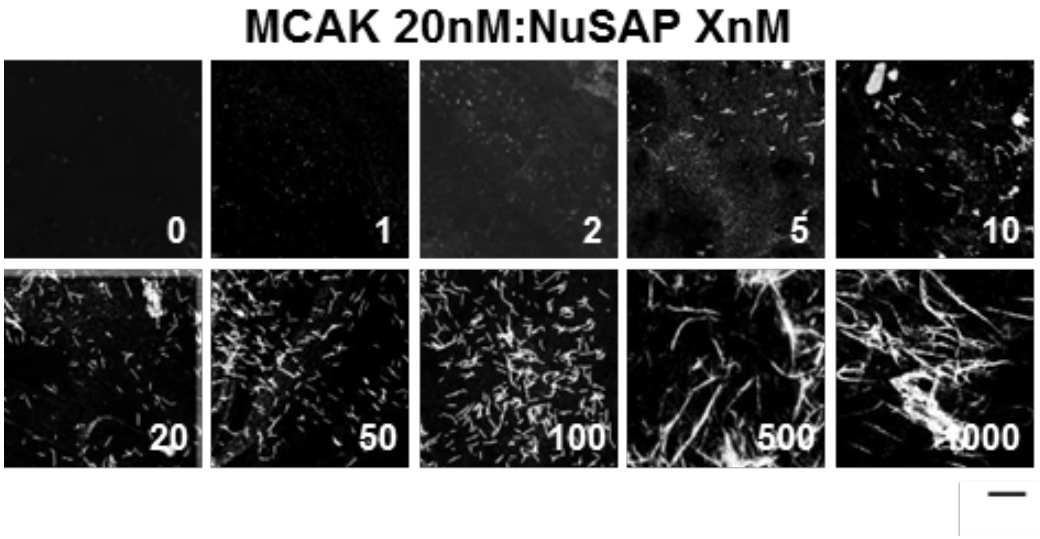


**Figure 3.3.11. NuSAP inhibits MCAK microtubule depolymerizing activity in vitro**

Different amounts of NuSAP (XnM) and 20nM MCAK WT proteins were incubated with 1.5μM microtubules at 37°C for 10min. Scale bar, 20μm.

## 3.4 Discussion

Here we have identified NuSAP as a specific kinetochore microtubule stabilizer. During metaphase, high numbers (25-40) of microtubules are required at kinetochores to correct chromosome positions and satisfy spindle assemble checkpoint (Skibbens et al., 1993b). The dynamics of kinetochore microtubules is critical, and must be within the narrow permissible boundaries to ensure both relatively stable kinetochore-microtubule attachment and permits error correction for accurate chromosome segregation (Bakhoum and Compton, 2012; Bouck et al., 2008). As a microtubule associated protein, NuSAP can stabilize microtubules *in vivo* (Figure 3.3.1 and Figure 3.3.2) and the function of NuSAP at kinetochore microtubules is specific through its regulation on MCAK (Figure 3.3.3 and Figure 3.3.4). Our results indicate that the NuSAP$^{delMCBD}$, with the MTBD but no MCBD, can still bind with microtubules but cannot stabilize kinetochore microtubules. Thus, the current study extends earlier findings by clearly identifying NuSAP not only functions as a strong microtubule stabilizer, but also specifically stabilizes kinetochore microtubules by decreasing the turnover rate of kinetochore microtubules during metaphase (Figure 3.3.5 and Figure 3.3.6). The temporal nature of the regulation indicates that NuSAP may specially regulate the length and stability of kinetochore microtubules in order to align chromosomes properly at metaphase plate.

In this study, we also clearly demonstrate that NuSAP directly binds MCAK through its MCAK binding domain (MCBD) and this binding is essential for maintaining the proper localization of MCAK at the kinetochore region (Figure 3.3.3). The localization of MCAK is tightly associated with the tension developed across sister kinetochores to correct kinetochore-microtubule attachment error (Andrews et al., 2004; Gorbsky, 2004; Kline-Smith et al., 2004; Lan et al., 2004). Overexpression of NuSAP leads to severe spindle elongation (Figure 3.3.1), resulting in the delocalization of MCAK at the centromere region. Herein, we carefully conducted the experiments with synchronized metaphase HeLa cells and only analyzed the kinetochore pairs at the metaphase plate region. However, since overexpression of NuSAP can induce the severe phenotypes of chromosome misalignment, the possibility of NuSAP overexpression leading to cell arrest at prometaphase was concerned. To address this question, we utilized $NuSAP^{1-233}$, the N-terminal domain, which leads to chromosome misalignment phenotype and $NuSAP^{delMCBD}$, the whole NuSAP sequence without a MCAK binding domain. Overexpression of $NuSAP^{1-233}$ or $NuSAP^{delMCBD}$ did not affect the localization of MCAK at the inner kinetochore region, consistent with the MCAK localization in control metaphase cell (Figure 3.3.3). Hence, the dislocalizaiton of MCAK at the inner centromere region is specific due to its interaction with NuSAP.

Since MCAK is highly activated as a robust microtubule depolymerizer (Domnitz et al., 2012; Helenius et al., 2006; Hunter et al., 2003; Maney et al., 1998), the negative regulation by NuSAP is pivotal to the stabilization of kinetochore microtubules once chromosomes are aligned during metaphase. Although several positive regulators of MCAK have been identified, for example ICIS (Inner Centromere KinI Stimulator) (Ohi et al., 2003), TIP150 (Jiang et al., 2009) and Kif18b (Tanenbaum et al., 2011), the negative regulators of MCAK have not been well studied. Here we reveal for the first time an important negative regulatory mechanism for the function of MCAK on the dynamics of kinetochore microtubules mediated by NuSAP during metaphase (Figure 3.3.6). NuSAP dramatically stabilized kinetochore microtubules by 5 times, compared to its regulation of MCAK dynamics by 1.5 times. The possible reason is that NuSAP itself can bundle and stabilize microtubules in addition to its regulation on MCAK. Also, although we focused to bleach an 1×1μm kinetochore region, we can not rule out that the cytosol diffused MCAK which unattached to the plus-ends of kinetochore microtubules at the kinetochore region had also been bleached and this undefined bleaching might lead to an underestimated affection of NuSAP on MCAK dynamics. Taken together, our results demonstrate that NuSAP has an indispensable role to ensure the precise MCAK function at the plus-ends of kinetochore microtubules by tightly regulating the localization (Figure 3.3.3), dynamics (Figure 3.3.6) and depolymerization activity (Figure

3.3.7) of MCAK. Though NuSAP concentrated at the metaphase plate region under the regulation of RanGTP, a very low level of NuSAP might also localize at the spindle pole region. Due to the nature of MCAK localizes at the both ends, it would be interesting to study how the pole localization of MCAK is indeed influenced by NuSAP in the future.

Aurora B plays a major role as a tension sensor in ensuring the proper dynamics of kinetochore microtubules and accurate kinetochore-microtubule attachment by regulating the phosphorylation of MCAK (Andrews et al., 2004; Gorbsky, 2004; Lan et al., 2004; Ohi et al., 2004). The phospho-mimicking MCAK 5E mutant with a dramatically decreased depolymerization activity was delocalized to inner centromere region during metaphase, compared to the phospho-deficient MCAK 5A mutant with a relatively high activity at the inner kinetochore region (Andrews et al., 2004). Our data markedly suggest that the phosphorylation of MCAK by Aurora B is vital in determining its interaction with NuSAP, resulting in subsequently sequestering its depolymerization activity (Figure 3.3.9 and Figure 3.3.10). Mechanistically, Aurora B, as a molecular switch, intensifies an extra temporally and spatially regulation on the NuSAP-MCAK machinery to further guarantee the rapid changes of kinetochore microtubules dynamics and precise chromosome alignment during metaphase. A recent report indicates that Aurora B phosphorylates MCAK resulting in inducing a specific conformational switch

(Ems-McClung et al., 2013); non-phosphorylated MCAK in an ADP-bound open state associates with kinetochore microtubules and depolymerizes tubulin dimers in an ATP-bound closed state, while phosphorylated MCAK by Aurora B switches to an open state which lowers its depolymerization activity. Thus, the association between NuSAP and MCAK might also depend on the conformation of MCAK. On the other hand, other reports indicate Aurora B can diffuse from centromeres with a gradient to phosphorylate other mitotic proteins (Liu et al., 2009; Wang et al., 2011) and that NuSAP can be phosphorylated by cdk1, causing a weak microtubule affinity (Chou et al., 2011). Hence, we could not rule out that in addition to Aurora B, other kinases may also involve in the phosphorylation of NuSAP or MCAK to regulate the kinetochore microtubule dynamics. Future studies would need to answer these questions.

Based on our results, we propose a schematic model that represents the role of NuSAP in stabilizing kinetochore microtubules by negatively regulating the activity of MCAK (Figure 3.3.12). In metaphase cells, the localization of NuSAP displays with a gradient on kinetochore microtubules under the regulation of RanGTP to stabilize kinetochore microtubules (Ribbeck et al., 2006a). MCAK diffuses into the kinetochore region to associate NuSAP at the kinetochore microtubule ends to depolymerize kinetochore microtubules and maintain the

proper dynamics of kinetochore microtubules for correcting the kinetochore-microtubule attachment error and ensuring accurate chromosome alignment. However, elevated levels of NuSAP elongate kinetochore microtubules. The strong interaction of NuSAP and MCAK subsequently causes MCAK inward collapses into the Aurora B activated region (Andrews et al., 2003; Lampson and Cheeseman, 2011; Welburn et al., 2010). The phosphorylation of MCAK by Aurora B further enhances the interaction between MCAK and NuSAP resulting in markedly reducing the depolymerization activity of MCAK. Therefore, the depolymerization activity of MCAK to intruded kinetochore microtubules in the inner centrosome region is compromised, which leads to NuSAP-promoted hyper-stabilized kinetochore microtubules. In short, understanding the role of NuSAP in the stability of kinetochore microtubules provides new insights into the control of accurate attachment of the microtubules to kinetochores during chromosome alignment, spindle assembly, cell division and cancer.

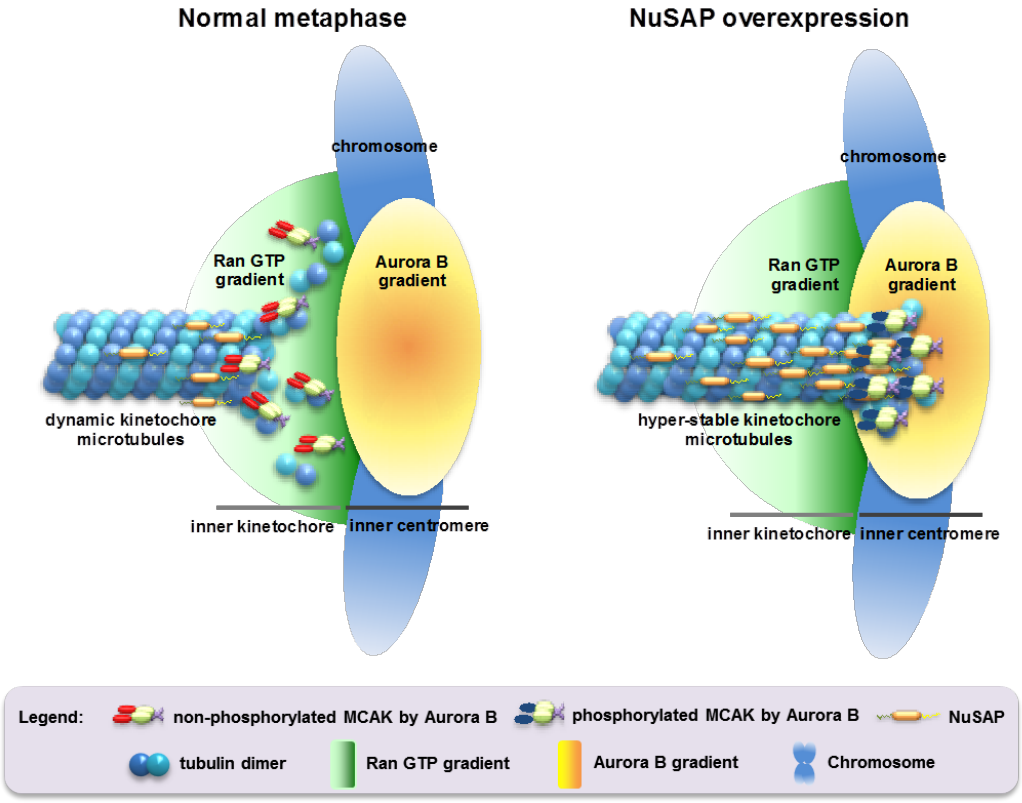


**Figure 3.3.12. A schematic model for NuSAP stabilizing kinetochore microtubules by attenuating MCAK depolymerization activity.**

A schematic model represents the role of NuSAP in stabilizing kinetochore microtubules through regulating MCAK, which is regulated by Aurora B kinase. In metaphase cells, NuSAP interacts with MCAK at the plus ends of the kinetochore microtubules to maintain proper kinetochore microtubule dynamics. In NuSAP-overexpressing cells, the delocalization of MCAK at the centromere region leads to the phosphorylation of MCAK by Aurora B and the enhanced binding between MCAK and NuSAP resulting in further reducing the depolymerization activity of MCAK.

# CHAPTER 4 NuSAP governs centrosome oscillation by regulating Kif22 generated polar ejection force

## 4.1 Abstract

In vertebrate cells, chromosomes oscillate to precisely align during metaphase. NuSAP as a microtubule associated protein, plays a critical role in stabilizing spindle microtubules during metaphase. However, the function of NuSAP in mitosis is largely unknown. In this study, we investigated the role of NuSAP in chromosome alignment, orientation and oscillation utilizing 3D live-cell imaging, which permits a general population of the centromeres with 3D information of the oscillation. Furthermore, we identified NuSAP as a pivotal regulator for the function of a chromokinesin—Kif22 in chromosome oscillation, and specifically investigated the impact of NuSAP on the polar ejection force generated by Kif22. Our findings revealed that NuSAP largely contributes to the polar ejection force generated by Kif22 ($I_{nusap}$=0.88) during chromosome movement. Taken together, our study provides new insights into the complicated regulation of chromosome oscillation at metaphase to ensure precise chromosome segregation during cell division.

## 4.2 Introduction

Chromosome oscillation is a unique feature at metaphase in vertebrate cells (Lewis, 1939). The movement of chromosome can be separated into poleward and anti-poleward, referring to the direction toward the pole or away from the pole (Skibbens et al., 1993a). The poleward motion is contributed by the polar force which is mainly generated by the depolymerization of the kinetochore microtubules (kMTs) (Hays and Salmon, 1990b); while, the anti-poleward motion is largely produced by the polar ejection force (PEF) which depends on the motors sliding along the chromosome arms at the interpolar microtubules (iMTs) (Rieder et al., 1986b). Although some studies focus on two-dimensional KT behaviors (Levesque and Compton, 2001; Stumpff et al., 2008; Stumpff et al., 2012; Wandke et al., 2012) and biophysical prediction of KT movement (Joglekar and Hunt, 2002; Liu et al., 2007; Sutradhar and Paul, 2014; Vladimirou et al., 2011), the underlying molecular mechanism of the KT oscillation is still largely elusive.

Microtubule associated proteins (MAPs) plays vital roles in regulating chromosome oscillation by tightly maintaining both the dynamics of kMTs and the surface properties of iMTs (Maiato et al., 2004). NuSAP (Nuclear and Spindle Associated Protein) (Raemaekers et al., 2003b), a RanGTP-regulated MAP, bundles microtubules (MTs) (Ribbeck et al., 2006a) and links microtubules to

chromosomes (Ribbeck et al., 2007b). In addition, NuSAP also functions in regulating spindle assembly, chromosome segregation and cytokinesis (Hussain et al., 2009; Raemaekers et al., 2003b). The protein levels of NuSAP are tightly regulated by APC/C during cell cycle (Li et al., 2007b; Song and Rape, 2010a) and upregulated in several kinds of cancers (Fujiwara et al., 2006; Gulzar et al., 2013; Iyer et al., 2011b; Kokkinakis et al., 2005b; Wadia et al., 2010; Xie et al., 2011). Despite previous studies identify the role of NuSAP on stabilizing MTs, the molecular mechanism leading to how NuSAP functions in mitosis is still poorly understood.

Human chromokinesins are plus-end directed motors contributing to the anti-poleward movement (Heald, 2000; Mazumdar and Misteli, 2005; Vanneste et al., 2011). Kif22 (kinesin-like DNA binding protein, Kid) is a chromokinesin with an N-terminal MT binding domain and a C-terminal chromosome interacting domain (Tokai et al., 1996). Kif22 functions as a MT-based motor to generate the PEF on chromosomes and regulates the orientation of chromosome arms and KT oscillation (Stumpff et al., 2012; Wandke et al., 2012; Yajima et al., 2003). The RanGTP gradient further promotes the accumulation of Kif22 on chromosomes (Trieselmann et al., 2003). Although a functional relationship between NuMA and Kif22 in spindle morphology and chromosome alignment has been reported (Levesque et al., 2003) and the MT localization of Kif22 is mediated by the

spindle protein CHICA (Santamaria et al., 2008), the regulatory mechanism of Kif22 in chromosome oscillation remains unclear.

In this study, we identify NuSAP as a novel regulator of Kif22 for the very first time. Also, we utilize 3D time-lapse live-cell imaging to analyze chromosome oscillation in a dynamically heterogeneous population. Our study shows that NuSAP facilitates the oscillation of chromosomes through the regulation of Kif22 and specifies the influence of NuSAP on the Kif22-generated PEF.

## 4.3 Result

### 4.3.1 NuSAP regulates chromosome alignment and orientation

To obtain insights into the function of NuSAP during metaphase, we investigated the localization of GFP-NuSAP along the spindle with the line profile (Figure 4.3.1 A). The result showed that NuSAP prominently localized at the central spindle MTs and the NuSAP overexpressing cells displayed a large proportion of misaligned chromosomes (Figure 4.3.1 B). To further quantify the data, we utilized the index of chromosome alignment (ICA) (Stumpff et al., 2012) to calculate the ratio of the fluorescence of ACA (Anti-Centromere Antibody) staining in the central spindle to the whole spindle (Figure 1B). In this assay, the ICA of the GFP-NuSAP overexpressing cells is significantly smaller (0.65±0.27) than that in the control cells (0.94±0.03), indicating a severe chromosome misalignment phenotype (Figure 4.3.1 C). The result suggests that the localization of NuSAP is mainly at the central spindle MTs where it may have a role in regulating the chromosome alignment.

To determine how NuSAP may disturb chromosome congression, we utilized 3D time-lapse live-cell imaging to monitor the movement of chromosome in the synchronized HeLa cells stably expressing mCherry-H2B (Figure 4.3.1 D and Movie S1). Strikingly, we found that the chromosomes in the cells overexpressing

NuSAP displayed prominent mis-orientation with the arms pointing to the spindle poles rather than perpendicular to the spindle axis (Figure 4.3.1 D, row 1) and selective misaligned chromosome was presented by a 3D reconstruction (row 2). The time-lapse projection for the lagging chromosome showed that the arms of the chromosome were rotating and stretching over the time (Figure 4.3.1 E), suggesting that the unbalanced forces on the arms disrupting the movement of chromosome. These results indicate that the up-regulated protein levels of NuSAP may induce unbalanced exaggerate forces on chromosome arms resulting in chromosome mis-orientation.

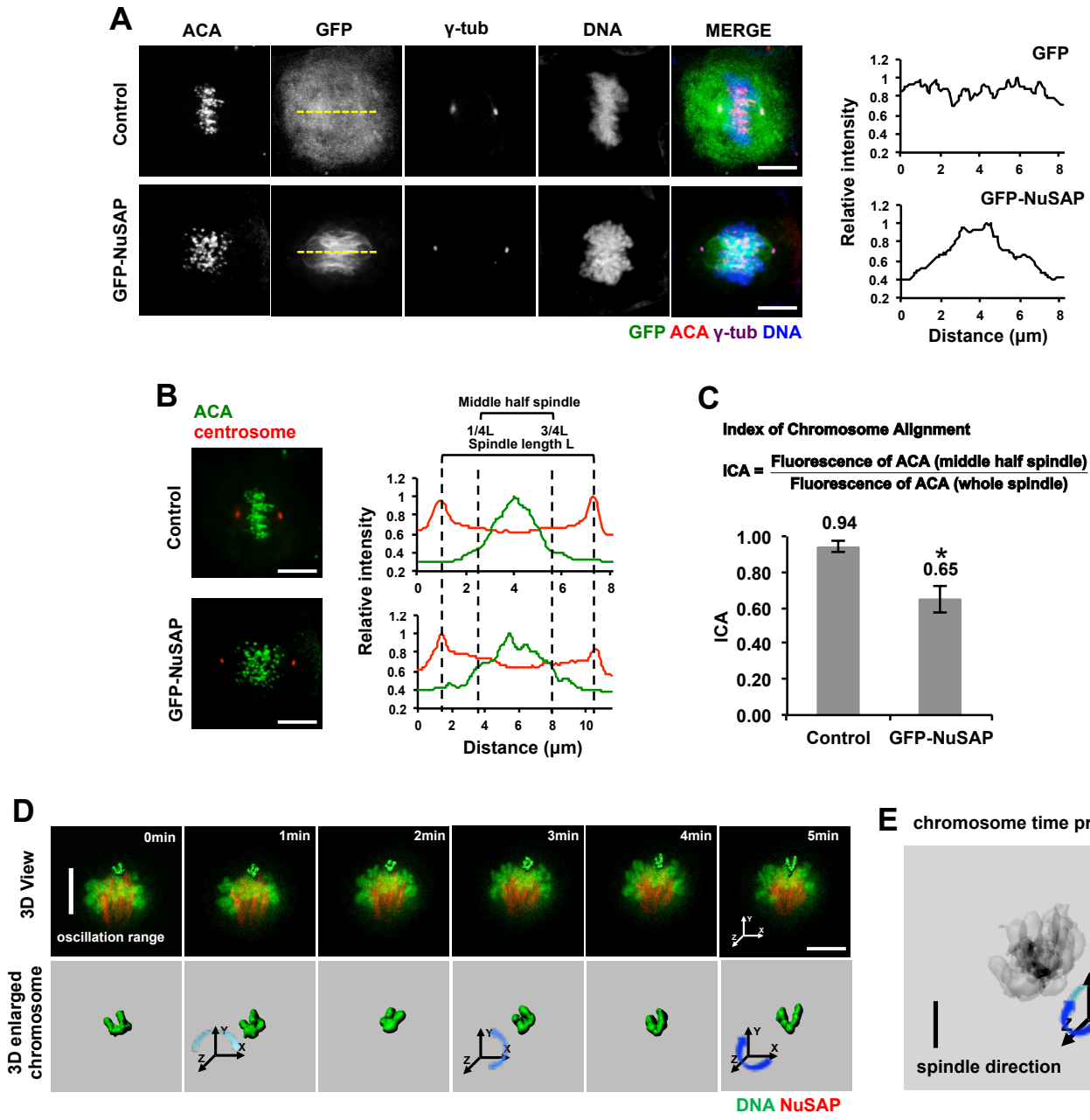
A
ACA
GFP
γ-tub
DNA
MERGE
Control
GFP-NuSAP
GFP ACA γ-tub DNA
GFP
GFP-NuSAP
Relative intensity
Distance (μm)
B
ACA
centrosome
Control
GFP-NuSAP
Middle half spindle
1/4L
3/4L
Spindle length L
Relative intensity
Distance (μm)
C
Index of Chromosome Alignment
ICA = Fluorescence of ACA (middle half spindle) / Fluorescence of ACA (whole spindle)
0.94
0.65
*
ICA
Control
GFP-NuSAP
D
3D View
0min
1min
2min
3min
4min
5min
oscillation range
3D enlarged chromosome
DNA NuSAP
E
chromosome time project
spindle direction

**Figure 4.3.1. NuSAP regulates chromosome alignment and orientation during metaphase**

(A) Fluorescent images of synchronized metaphase HeLa cells expressing GFP-NuSAP and GFP-vector (control) and the line profiles of the GFP channel were presented in the right graph. Mitotic spindles were labeled with anti-γ-tubulin, anti-Crest and DNA with Hoechst 333342. Scale bar, 5μm.
(B) Representative images with the ICA (Index of Chromosome Alignment) method utilized to analyze centromere alignment and a plot of ICAs in HeLa cells expressing GFP-NuSAP and GFP-vector only (control). The distribution of ACA fluorescence within the spindle region was measured along the spindle axis with the staining of anti-γ-tubulin and anti-Crest.
(C) ICAs in HeLa cells expressing GFP-NuSAP and GFP-vector only (control) were analyzed as in (B). Data were collected from 3 independent experiments and error bars represent ±SD. * $p<0.001$.
(D) 3D time-lapse imaging and 3D single chromosome surface of chromosome oscillation in synchronized metaphase stable mCherry-H2B HeLa cells expressing GFP-NuSAP. The changes of the chromosome orientation are indicated by arrows. Scale bar, 5μm.
(E) The time project image representing the single chromosome misorientation.

### 4.3.2 NuSAP interacts with Kif22 and facilitates its interaction with microtubules

The faulty orientation of chromosomes in NuSAP-overexpressing cells highly resembles the phenotype identified previously in the Kif22-depleted cells (Levesque and Compton, 2001; Wandke et al., 2012). This observation motivated us to investigate protein-protein interactions between NuSAP and Kif22. Our result showed that NuSAP interacted with the endogenous Kif22 (Figure 4.3.2 A). Reciprocally, NuSAP could also be pulled down by FLAG-Kif22 (Figure 4.3.2 B). In addition, to further access the interaction in the mitotic phase, cells were first arrested by thymidine/nocodazole treatment and then released (Figure 4.3.2 C). The result showed that NuSAP expressed relatively high throughout mitosis, while Kif22 highly expressed at metaphase and dramatically degraded afterwards. The immunoprecipitation indicated that Kif22 specifically interacts with NuSAP at metaphase (Figure 4.3.2 D).

The PEF generated by Kif22 during metaphase largely depends on the association of Kif22 to MTs (Shiroguchi et al., 2003; Tokai et al., 1996). Since NuSAP primarily localizes at the central spindle MTs, we wondered whether the interaction between NuSAP and Kif22 affects the interaction between Kif22 and MTs. As shown in Figure 4.3.2 E, although both the FLAG-Kif22 only (lane 2)

and FLAG-Kif22 co-overexpressing with HA-NuSAP (lane 4), but not FLAG-vector control (lane 1 and 3), can pull down endogenous a-tubulin, Kif22 interacts with more MTs in the NuSAP overexpressing cells (lane 4). To further confirm, the distribution of Kif22 on MTs and chromosomes was investigated in both control cells and GFP-NuSAP overexpressing cells. Kif22 interacts more with MTs in the GFP-NuSAP overexpressing metaphase cells (Figure 4.3.2 F) and monopolar cells (Figure 4.3.2 G) compared with control cells. The results indicate that NuSAP specifically interacts with Kif22 at metaphase and enhances the association between Kif22 and MTs.

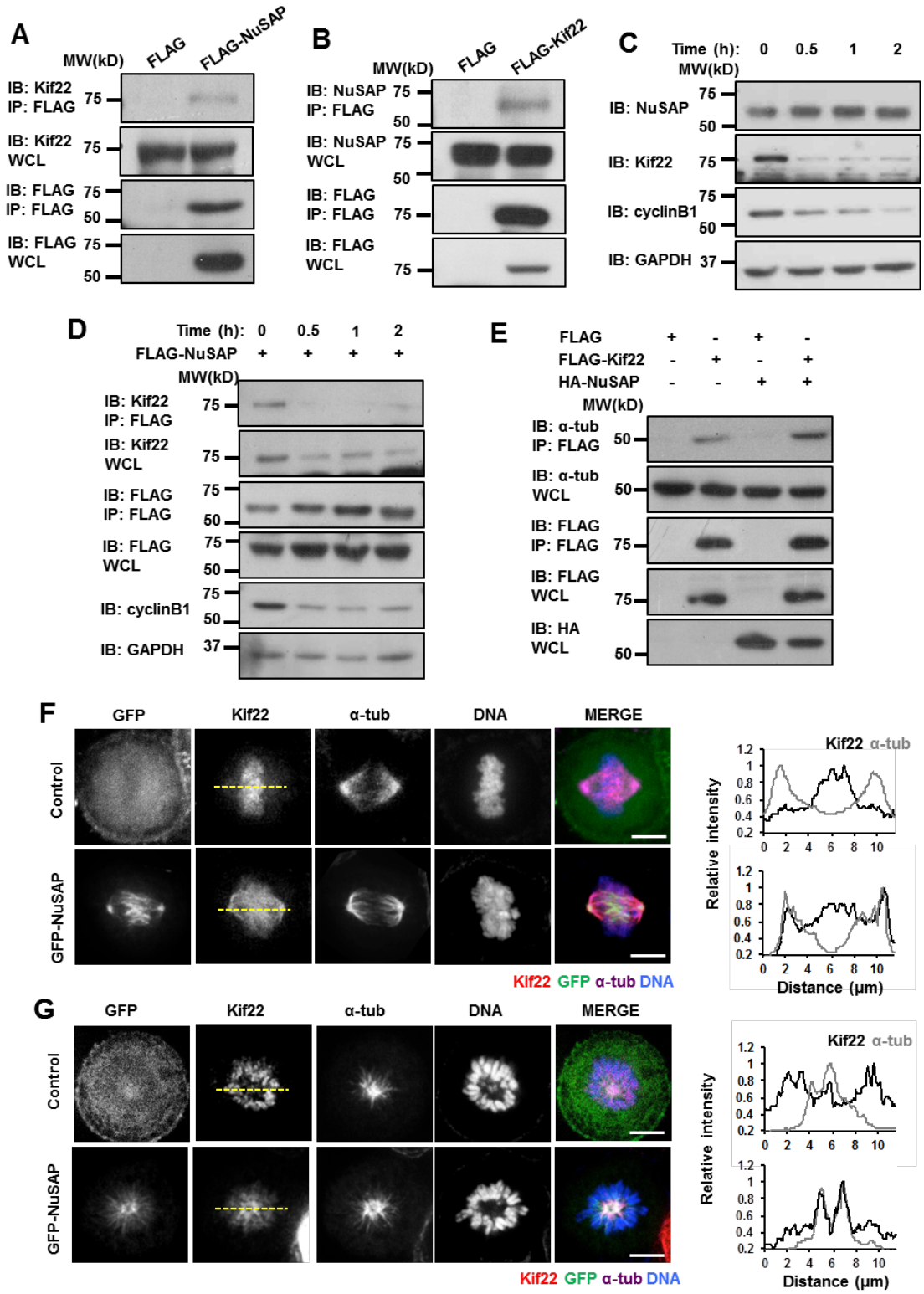
A
MW(kD)
FLAG
FLAG-NuSAP
IB: Kif22
IP: FLAG
IB: Kif22
WCL
IB: FLAG
IP: FLAG
IB: FLAG
WCL
B
MW(kD)
FLAG
FLAG-Kif22
IB: NuSAP
IP: FLAG
IB: NuSAP
WCL
IB: FLAG
IP: FLAG
IB: FLAG
WCL
C
Time (h): 0 0.5 1 2
MW(kD)
IB: NuSAP
IB: Kif22
IB: cyclinB1
IB: GAPDH
D
Time (h): 0 0.5 1 2
FLAG-NuSAP + + + +
MW(kD)
IB: Kif22
IP: FLAG
IB: Kif22
WCL
IB: FLAG
IP: FLAG
IB: FLAG
WCL
IB: cyclinB1
IB: GAPDH
E
FLAG + - + -
FLAG-Kif22 - + - +
HA-NuSAP - - + +
MW(kD)
IB: α-tub
IP: FLAG
IB: α-tub
WCL
IB: FLAG
IP: FLAG
IB: FLAG
WCL
IB: HA
WCL
F
GFP
Kif22
α-tub
DNA
MERGE
Control
GFP-NuSAP
Kif22 GFP α-tub DNA
Kif22 α-tub
Relative intensity
Distance (μm)
G
GFP
Kif22
α-tub
DNA
MERGE
Control
GFP-NuSAP
Kif22 GFP α-tub DNA
Kif22 α-tub
Relative intensity
Distance (μm)

**Figure 4.3.2. NuSAP binds with Kif22 and enhances its interaction with MTs**

(A) NuSAP immunoprecipitate contains Kif22. FLAG and FLAG-NuSAP immunoprecipitates from 293T cell lysate were blotted for Kif22.
(B) The reverse immunoprecipitation of Kif22 contains NuSAP detected by NuSAP antibody.
(C) NuSAP and Kif22 expression levels during the cell cycle. HeLa cells arrested in mitosis by thymidine/nocodazole were released into fresh medium for the indicated timepoints and blotted with anti-NuSAP, anti-Kif22, anti-cyclin B1 and anti-GAPDH antibodies.
(D) The immunoprecipitation of NuSAP with Kif22 were conducted with the whole-cell lysates of HeLa cells transfected with FLAG-NuSAP after release from thymidine/nocodazole arrest into fresh medium for the indicated timepoints. The immunoprecipitated protein and the whole-cell lysate were blotted with anti-Kif22, anti-FLAG, anti-cyclin B1 and anti-GAPDH antibodies.
(E) NuSAP enhances the interaction between Kif22 and MTs. The whole-cell lysates of 293T cells transfected with FLAG vector, FLAG-Kif22 with or without HA-NuSAP were incubated with FLAG M2 beads and both the immunoprecipitated proteins and the cell lysates were detected with anti-α-tubulin, anti-FLAG, anti-HA antibodies.
(F-G) Kif22 localization at KT region in bipolar metaphase HeLa cells (F) and monastrol treated monopolar cells (G) expressing GFP-NuSAP and GFP-vector (control). Cells were stained with anti-α-tubulin and Hoechst 33342. The line profile of Kif22 localization (black) according to α-tubulin (grey) was represented in the right graph. Scale bar, 5μm.

### 4.3.3 The depletion of NuSAP or Kif22 synergistically attenuates the amplitude and speed of centromere movements

To dissect how NuSAP regulates Kif22 in chromosome oscillation, the 3D time-lapse live-cell imaging was conducted with GFP-CENPA labeled centromeres in the synchronized HeLa cells stably expressing mCherry-H2B at metaphase and treated with control, NuSAP or Kif22 siRNA (Figure 4.3.3 A and B). Representative 3D images with xz and yz projections were shown in Figure 3A and Movie S2. To gain insight into the KT dynamics, the centromere positions were detected and tracked in 3D overtime during the oscillation by maximizing the signal-to-noise ratio with minimizing phototoxicity (Jaqaman et al., 2010) and color-coded by time (Figure 4.3.4 B, lane 1). Consistent with previous work (Stumpff et al., 2012; Wandke et al., 2012), centromeres in the Kif22-depleted cells displayed with a slower velocity as most of the tracks shown in blue and green (0-2μm/min) and less in red (2-3μm/min) color-coded by velocity, compared with the control cells (Figure 4.3.4 B, lane 2). The majority of the centromere velocity in the NuSAP-depleted cells was in the 0-2μm/min region with a similar pattern of the Kif22-depleted cells (Figure 4.3.4 B, lane 2). Taken together, these results indicate the depletion of NuSAP or Kif22 in cells decreases the velocity of the chromosome oscillation in metaphase cells.

To further investigate the function of NuSAP and Kif22 in chromosome movement, we characterized the inter-centromere distance (ICD) of sister centromeres and the half-period of the 3D time-lapse tracks. The ICDs in the NuSAP-depleted (0.69±0.09μm) and Kif22-depleted (0.71±0.10μm) cells were not significantly changed compared with that in the control siRNA cells (0.75±0.09μm, Table 1), and the average of the half-period displayed a rather similar range with 32.50±3.34s in the control siRNA cells, 32.56±3.55s in NuSAP-depleted cells and 31.73±4.14s in Kif22-depleted cells, respectively (Table 1), suggesting that the stiffness between the sister centromeres is not largely affected by the depletion of NuSAP or Kif22. To simplify the analysis, we set the projected 3D displacement of the center in a sister centromere with the time courses as the center point track to present the oscillation of a certain chromosome (Jaqaman et al., 2010; Vladimirou et al., 2011). The sketched spindles with the simplified forces at kMTs and iMTs on the projected center point were represented in Figure 3C. The polar force generated on kMTs was shown as $\Delta PF_{kMT}$ ($PF^{left}_{kMT}$- $PF^{right}_{kMT}$) in the control cells (Hays and Salmon, 1990b); while the $\Delta PF'_{kMT}$ indicates the putative influence of NuSAP on $\Delta PF_{kMT}$. In addition, the PEF generated on iMTs was shown as $\Delta PEF_{iMT}$ ($PEF^{left}_{iMT}$-$PEF^{right}_{iMT}$) in the control cells (Rieder et al., 1986b); the $\Delta PEF'_{iMT}$ indicates the possible influence of NuSAP on $\Delta PEF_{iMT}$ and the PEF generated by Kif22 was

indicated as $\Delta PEF_{Kif22}$ ($PEF^{left}_{Kif22}$- $PEF^{right}_{Kif22}$) (Rieder et al., 1986b; Stumpff et al., 2012; Wandke et al., 2012; Yajima et al., 2003).

We examined the kinetic features of the projected chromosome center point. As shown in Figure 3D, consistent with the previous reports (Levesque et al., 2003; Stumpff et al., 2012; Wandke et al., 2012), the oscillation amplitude of the center in Kif22-depleted cells was dramatically decreased (0.79±0.05μm) than that in the control cells (1.12±0.08μm). Similarly, the oscillation amplitude in NuSAP-depleted cells was reduced to 0.78±0.11μm (Figure 4.3.4 D). In addition, the distribution of the amplitude in the NuSAP or Kif22-depleted cells showed an increase in a lower range (0-1μm) and decrease in a larger range (1-2μm) compared to that in the control cells (Figure 4.3.4 E). Since the amplitude of the oscillation is directly correlated with the $\Delta PEF_{iMT}$ (Ke et al., 2009), the significant decrease of the amplitude in the NuSAP- and Kif22-depleted cells suggests the general elimination of the $\Delta PEF_{iMT}$. To further analysis the dynamics of the chromosome during oscillation, the velocity of the projected center point in control, NuSAP or Kif22-depleted cells was also calculated. As shown in Figure 3F, the depletion of either NuSAP (1.39±0.03μm/min) or Kif22 (1.54±0.06μm/min) significantly reduced the center oscillation velocity from 1.68±0.06μm/min in the control-depleted cells. The centromeres in the NuSAP or Kif22-depleted cells have less proportion in the large velocity range (2-4μm/min)

than that in the control cells (Figure 4.3.4 G), indicating that the depletion of NuSAP or Kif22 markedly reduces the high velocity of the oscillation. Since the velocity varies with the position during the oscillation and the maximum velocity is reached near the equator with the minimum ICD (Stumpff et al., 2012; Wan et al., 2012), we further investigated whether NuSAP and Kif22 can regulate the coupling of the velocity and ICD versus the time and position. As shown in Figure 3H, consistent with the previous study (Wan et al., 2012), the maximum velocity was reached near the minimum ICD with about twice the frequency in the control cells. However, in the NuSAP or Kif22-depleted cells, the change of the velocity was considerably irregular and the coupling between the velocity and ICD was abolished (Figure 4.3.4 H, row 2 and 3). Taken together, the data suggest that the depletion of NuSAP or Kif22 synergistically attenuates the overall motility and the coupling of centromere oscillation.

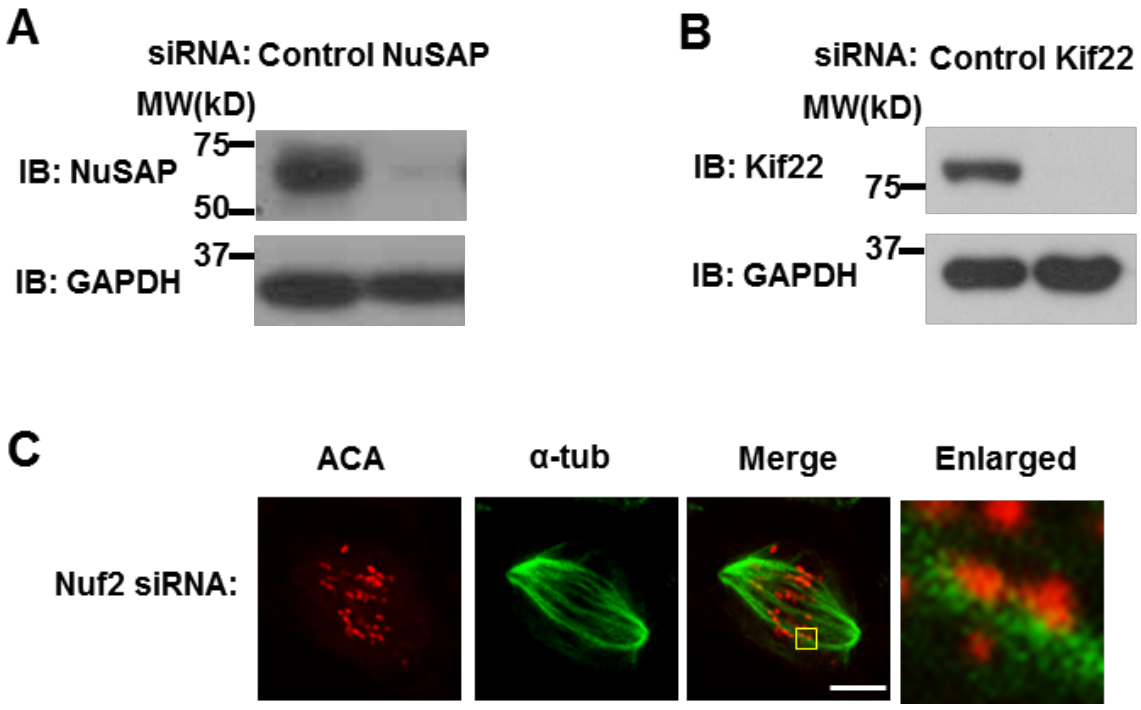


**Figure 4.3.3. NuSAP, Kif22 and Nuf2 depletions by siRNA**

(A-B) The effectiveness of NuSAP(A) or Kif22(B) depletion in HeLa cells was analyzed by western blot 48 hr after siRNA treatment. The cell lysate were blotted for NuSAP or Kif22. The amount of protein loading was detected using an anti-GAPDH antibody.
(C) The Nuf2 depletion in HeLa cells was visualized by immunofluorescence 48 hr after siRNA treatment. HeLa Cells were stained with anti-Crest, anti-α-tubulin and Hoechst 33342. The detailed centromere localization without kMT plus-ends attachment was enlarged in the right panel. Scale bar, 5μm.

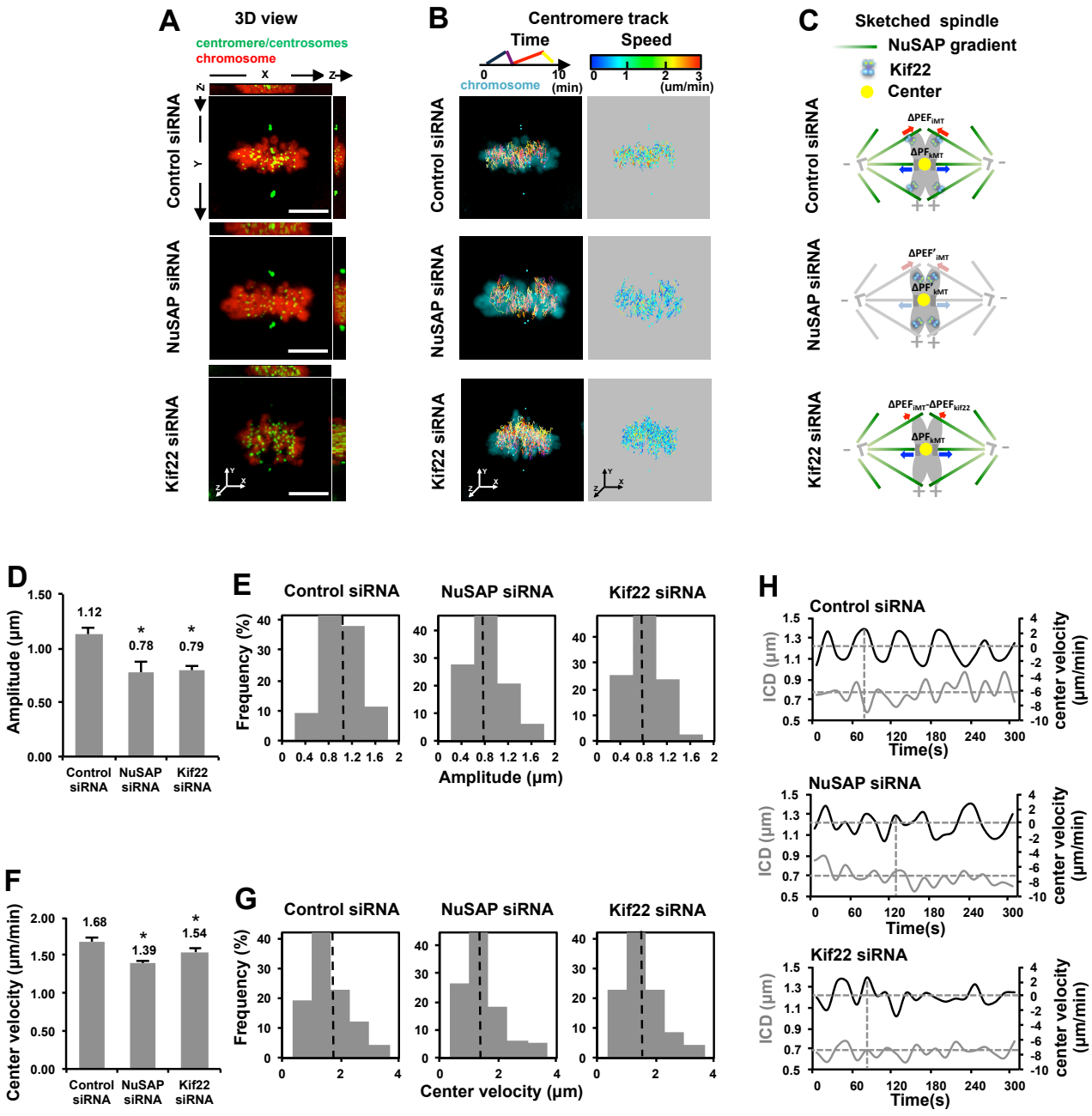
A
3D view
centromere/centrosomes
chromosome
Control siRNA
NuSAP siRNA
Kif22 siRNA
B
Centromere track
Time
Speed
chromosome
0
10
(min)
0
1
2
3
(um/min)
C
Sketched spindle
NuSAP gradient
Kif22
Center
D
Amplitude (μm)
1.12
0.78
0.79
Control siRNA
NuSAP siRNA
Kif22 siRNA
E
Frequency (%)
Amplitude (μm)
F
Center velocity (μm/min)
1.68
1.39
1.54
G
Center velocity (μm)
H
ICD (μm)
center velocity (μm/min)
Time(s)

**Figure 4.3.4. The depletion of NuSAP or Kif22 synergistically attenuates chromosome oscillation**

(A) Representative images of 3D view with xz and yz projections in control, NuSAP or Kif22 siRNA depleted synchronized metaphase stable mCherry-H2B HeLa cells. The centromeres were marked with GFP-CENPA and centrosomes with GFP-centrin. Scale bar, 5μm.
(B) Representative images of 3D centromere tracks color-coded with time and velocity as indicated by the color.
(C) Schematic spindle models illustrating the forces at kMTs and iMTs.
(D-E) The bar chart and the histogram represent the average (D) and the distribution (E) of the amplitude of the centromere oscillation in control, NuSAP or Kif22 siRNA depleted metaphase cells. Error bars represent +SED. * $p<0.001$.
(F-G) The bar chart and the histogram represent the average (F) and the distribution (G) of the center velocity. Error bars represent +SED. * $p<0.001$.
(H) Representative velocity (black line) and ICD (grey line) versus time plots of the projected center in a sister centromeres pair in control siRNA, NuSAP siRNA and Kif22 siRNA depleted metaphase cells. The sign of the velocity indicates the direction of the centromere movement. The average of the ICD (horizontal), the minimum (horizontal) and max velocity (vertical) are indicated by the dashed dot lines.

### 4.3.4 NuSAP and Kif22 specifically regulate centromere movement at interpolar microtubules

Our findings indicate that NuSAP and Kif22 correlately tune the amplitude and velocity of the centromere oscillation; however, as presented in Figure 3C, we could not rule out that the regulation of NuSAP on the chromosome movement may also result from its influence on $\Delta PF_{kMT}$. To examine this possibility, we depleted Nuf2 by siRNA to specifically diminish kMTs in the cells (Cai et al., 2009) and subsequently characterized the centromere oscillation in the NuSAP/Nuf2 or Kif22/Nuf2 double depleted cells using Nuf2-depleted cells as a control (Figure 4.3.3 C). Representative 3D time-lapse images were shown in Figure 4.3.5 A and Movie S3 and the centromere tracks color-coded by time were shown as Figure 4.3.5 B, lane 1. Consistent with previous work (Cai et al., 2009), the movement of the centromeres in the Nuf2-depleted cells displayed a faster velocity as more tracks shown in yellow-red (2-3μm/min) color-coded by velocity (Figure 4.3.5 B, lane 2), compared to that in the control cells (Figure 4.3.4 B, lane 2). On the other hand, the centromere velocities in the NuSAP/Nuf2 or Kif22/Nuf2 double depleted cells were mostly in the 0-2μm/min region (shown as blue and green in Figure 4.3.5 B, lane 2), indicating that the velocity of centromere movement was dramatically decreased by the co-depletion of NuSAP or Kif22 in the Nuf2-depleted cells.

The average of ICD and half-period of the centromere movement in the NuSAP/Nuf2 and Kif22/Nuf2 double depleted cells were similar with that in the Nuf2-depleted cells (Table 1). The sketched spindles with the projected center point were represented in Figure 5C. In Nuf2, NuSAP/Nuf2 or Kif22/Nuf2 depleted cells, the kMT generated polar force is diminished in the absence of kMTs and only the PEF generated on iMT exists (Cai et al., 2009; Rieder et al., 1986b).

We further examined the oscillation of the projected chromosome center point. The amplitude of the center oscillation in the NuSAP/Nuf2 or Kif22/Nuf2 depleted cells was dramatically decreased compared to Nuf2 depleted cells (Figure 4.3.5 D) and the proportion of the large oscillation amplitude (1-2μm) in the Nuf2-depleted cells was significantly decreased by the co-depletion with NuSAP or Kif22 (Figure 4.3.5 E). The velocity of the center was also significantly decreased in the NuSAP/Nuf2 or Kif22/Nuf2-depleted cells (Figure 4.3.5 F) and showed largely decreased proportion in the large velocity range, compared to that in Nuf2-depleted cells (2-4μm/min, Figure 4.3.5 G). The linkage within the maximum velocity with the minimum ICD is abolished in either Nuf2, NuSAP/Nuf2 or Kif22/Nuf2 depleted cells (Figure 4.3.5 H, doted lines), indicating that the coupling of the velocity and ICD requires kMT attachment.

Taken together, the overall attenuation of the oscillation in the absence of kMTs with the depletion of Nuf2 suggests the elimination of the chromosome oscillation by NuSAP or Kif22 is specifically at iMTs.

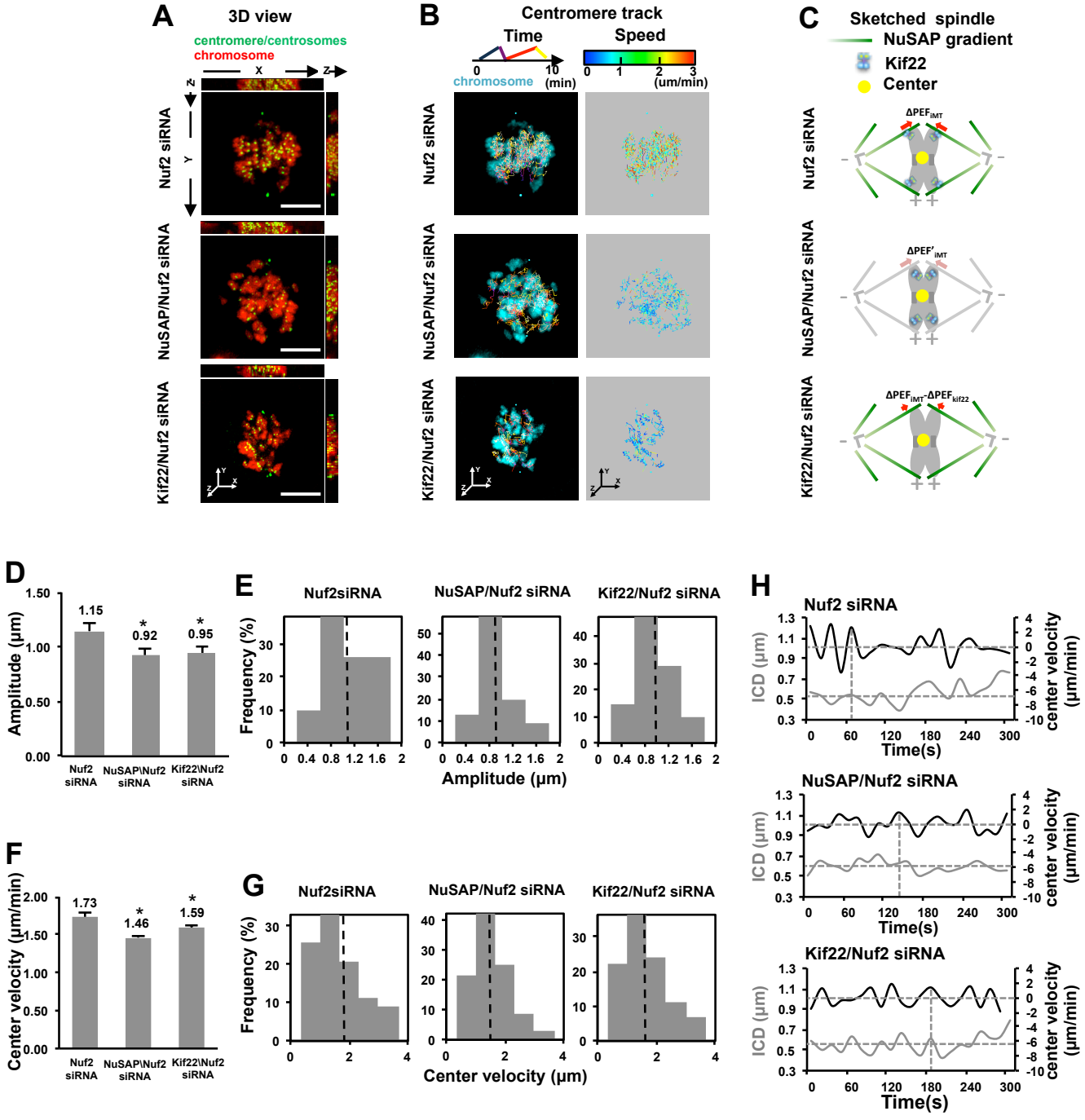
A
3D view
centromere/centrosomes
chromosome
Nuf2 siRNA
NuSAP/Nuf2 siRNA
Kif22/Nuf2 siRNA
B
Centromere track
Time
Speed
chromosome
(min)
(um/min)
C
Sketched spindle
NuSAP gradient
Kif22
Center
D
Amplitude (μm)
1.15
0.92
0.95
Nuf2 siRNA
NuSAP\Nuf2 siRNA
Kif22\Nuf2 siRNA
E
Nuf2siRNA
NuSAP/Nuf2 siRNA
Kif22/Nuf2 siRNA
Frequency (%)
Amplitude (μm)
F
Center velocity (μm/min)
1.73
1.46
1.59
G
Center velocity (μm)
H
ICD (μm)
center velocity (μm/min)
Time(s)

**Figure 4.3.5. NuSAP and Kif22 specifically regulate centromere movement at iMTs**

(A) Representative images of 3D view with xz and yz projections in Nuf2, NuSAP/Nuf2 or Kif22/Nuf2 siRNA depleted synchronized metaphase stable mCherry-H2B HeLa cells. The centromeres were marked with GFP-CENPA and centrosomes with GFP-centrin. Scale bar, 5μm.
(B) Representative images of 3D centromere tracks color-coded with time and velocity as indicated by the color.
(C) Schematic spindle models illustrating the forces at iMTs in the absence of kMTs in Nuf2, NuSAP/Nuf2 or Kif22/Nuf2 siRNA depleted metaphase cells.
(D-E) The bar chart and the histogram represent the average (D) and the distribution (E) of the amplitude of the centromere oscillation in Nuf2, NuSAP/Nuf2 or Kif22/Nuf2 siRNA depleted metaphase cells. Error bars represent +SED. * $p<0.001$.
(F-G) The bar chart and the histogram represent the average (F) and the distribution (G) of the center velocity. Error bars represent +SED. * $p<0.001$.
(H) Representative velocity (black line) and ICD (grey line) versus time plots of the projected center in a sister centromeres pair in Nuf2, NuSAP/Nuf2 or Kif22/Nuf2 siRNA depleted metaphase cells. The sign of the velocity indicates the direction of the centromere movement. The average of the ICD (horizontal), the minimum (horizontal) and max velocity (vertical) are indicated by the dashed dot lines.

### 4.3.5 NuSAP positively affect the amplitude and speed of centromere oscillation correlated with Kif22 in monopolar cells

In bipolar cells, the centromere oscillation is regulated by the motors, iMTs and kMTs from two poles with opposite directions as shown in Figure 4.3.4 C and 3.3.5 C. To further simplify the factors involved in the chromosome oscillation, we studied the movement of centromeres in the monastrol-treated monopolar cells with both iMTs and kMTs from one spindle pole with a single direction (Liu et al., 2007; Rieder et al., 1986b; Skibbens et al., 1993a; Wan et al., 2012).

The representative 3D time-lapse images (Figure 4.3.6 A) and centromere tracks color-coded by time (Figure 4.3.6 B, lane 1) of the control, NuSAP or Kif22 siRNA depleted cells were presented (Movie S4). The centromere tracks color-coded by velocity indicate that the centromeres in the NuSAP-depleted or Kif22-depleted cells are slowed down as more tracks shown in blue (0-1μm/min), compared to that in the control cells (Figure 4.3.6 B, lane 2).

The ICD and the half-period in NuSAP or Kif22-depleted monopolar cells were not significantly changed (Table 1). As shown in Figure 5C, the sketched spindles with the projected center point in the monopolar cells present a single direction

poleward polling force acting at the kMTs and the opposite PEF acting along the chromosome arms generated on iMT (Rieder et al., 1986b).

The depletion of NuSAP or Kif22 in monopolar cells resulted in even severer decrease in the oscillation amplitude (Figure 4.3.6 D) with more proportion in the 0-1μm range compared with control monopolar cells (Figure 4.3.6 E). Furthermore, the velocity of the center was significantly decreased in the NuSAP or Kif22 depleted monopolar cells with dramatically decreased propotion in 2-4μm/min (Figure 4.3.6 F and G). We noticed that the influence of Kif22 is larger than NuSAP on the oscillation amplitude and velocity in monopolar cells (Figure 4.3.6 D-G, lane 3). Since the PEF generated by Kif22 is directly related with the density of the iMTs at the function positions (Ke et al., 2009; Sutradhar and Paul, 2014), the higher density of MTs in the monopolar aster structure compared with the bipolar spindle might result in the increase of the Kif22 generated PEF, which is consistent with the previous finding that the mono-oriented chromosome arms are immediately ejected outward once cut free (Rieder et al., 1986b). The coupling of the velocity and ICD are abolished in the control, NuSAP-or Kif22 depleted monopolar cells (Figure 4.3.6 H), indicating that the nonrandom centromere oscillation also depends on the bipolar spindle structure. Taken together, these data suggests that both NuSAP and Kif22 positively affect the amplitude and velocity of centromere oscillation in the monopolar cells.

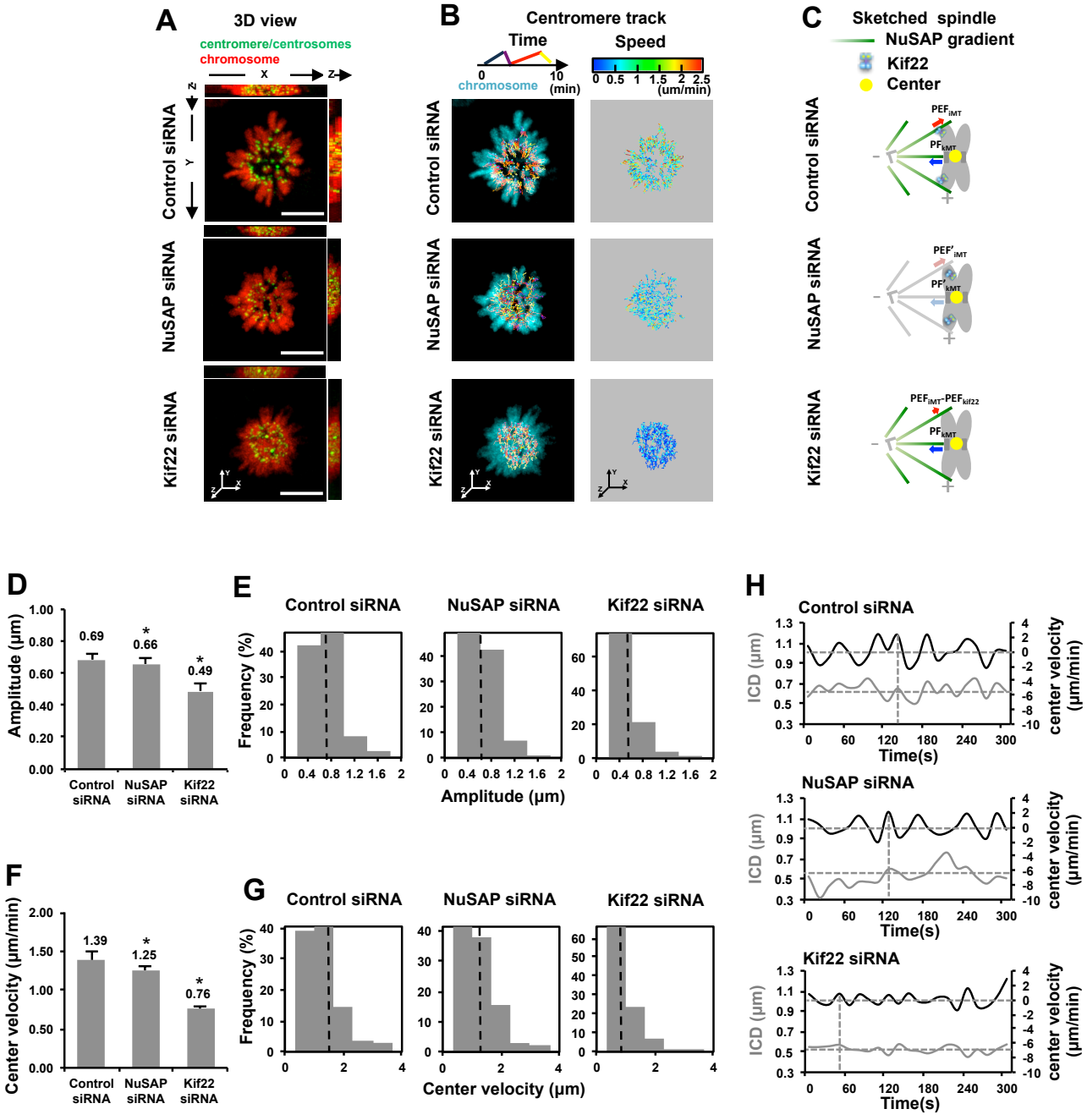
A
3D view
centromere/centrosomes
chromosome
Control siRNA
NuSAP siRNA
Kif22 siRNA
B
Centromere track
Time
Speed
chromosome
(min)
(um/min)
C
Sketched spindle
NuSAP gradient
Kif22
Center
D
Amplitude (μm)
0.69
0.66
0.49
Control siRNA
NuSAP siRNA
Kif22 siRNA
E
Frequency (%)
Amplitude (μm)
F
Center velocity (μm/min)
1.39
1.25
0.76
G
Center velocity (μm)
H
ICD (μm)
center velocity (μm/min)
Time(s)

**Figure 4.3.6. NuSAP positively affects the amplitude and velocity of centromere oscillation in monopolar cells correlated with Kif22**

(A) Representative images of 3D view with xz and yz projections in control, NuSAP or Kif22 siRNA depleted monastrol treated monopolar stable mCherry-H2B HeLa cells. The centromeres were marked with GFP-CENPA and centrosomes with GFP-centrin. Scale bar, 5μm.
(B) Representative images of 3D centromere tracks color-coded with time and velocity as indicated by the color.
(C) Schematic spindle models illustrating the forces at kMTs and iMTs in monopolar cells.
(D-E) The bar chart and the histogram represent the average (D) and the distribution (E) of the amplitude of the centromere oscillation in control, NuSAP or Kif22 siRNA depleted monopolar cells. Error bars represent +SED. * $p<0.001$.
(F-G) The bar chart and the histogram represent the average (F) and the distribution (G) of the center velocity. Error bars represent +SED. * $p<0.001$.
(H) Representative velocity (black line) and ICD (grey line) versus time plots of the projected center in a sister centromeres pair in control, NuSAP or Kif22 siRNA depleted monopolar cells. The sign of the velocity indicates the direction of the centromere movement. The average of the ICD (horizontal), the minimum (horizontal) and max velocity (vertical) are indicated by the dashed dot lines.

### 4.3.6 NuSAP collectively tunes polar ejection force with Kif22 at interpolar microtubules

Combining both the depletion of Nuf2 to disrupt kMT and monastrol treatment to form monopolar spindles, we specifically investigated the PEF on iMTs with a single direction in the Nuf2, NuSAP/Nuf2 or Kif22/Nuf2 siRNA depleted monopolar cells. The representative 3D time-lapse live-cell image (Figure 4.3.7 A and Movie S5) centromeres tracks (Figure 4.3.7 B and Movie S5) show that the oscillation was dramatically retarded with significant decreased velocity in the NuSAP/Nuf2 or Kif22/Nuf2 co-depleted cells.

The ICD and the half-period in the NuSAP/Nuf2 and Kif22/Nuf2 co-depleted monopolar cells were not significantly changed compared to that in Nuf2 depleted monopolar cells (Table 1). The sketched spindles with the projected center point in the monopolar cells present a single direction of the PEF on iMTs in the absence of kMTs (Figure 4.3.7 C). The amplitude of the center oscillation in the NuSAP/Nuf2 and Kif22/Nuf2 depleted monopolar cells is significantly retarded shown as the dramatically decreased of both the average (Figure 4.3.7 D) and the proportion of the 1-2μm range (Figure 4.3.7 E). Moreover, the center velocity was significantly attenuated in the NuSAP/Nuf2 or Kif22/Nuf2 depleted monopolar cells (Figure 4.3.7 F and G). The significant decreases of the oscillation velocity

and amplitude in both the NuSAP/Nuf2 and Kif22/Nuf2 depleted cells suggest that NuSAP strongly regulates the forces on iMTs, especially the PEF generated by Kif22. The linkage between the velocity and ICD during the oscillation is dramatically reduced in the Nuf2, NuSAP/Nuf2 or Kif22/Nuf2 depleted monopolar cells with severely random movement (Figure 4.3.7 H), which consistent with our previous results (Figure 4.3.4-3.3.7 H) that the kMT attachment and the bipolar spindle structure together are required for proper chromosome oscillation. Taken together, these data suggests that NuSAP governs the chromosome oscillation to strongly tune PEF with kif22 at iMTs.

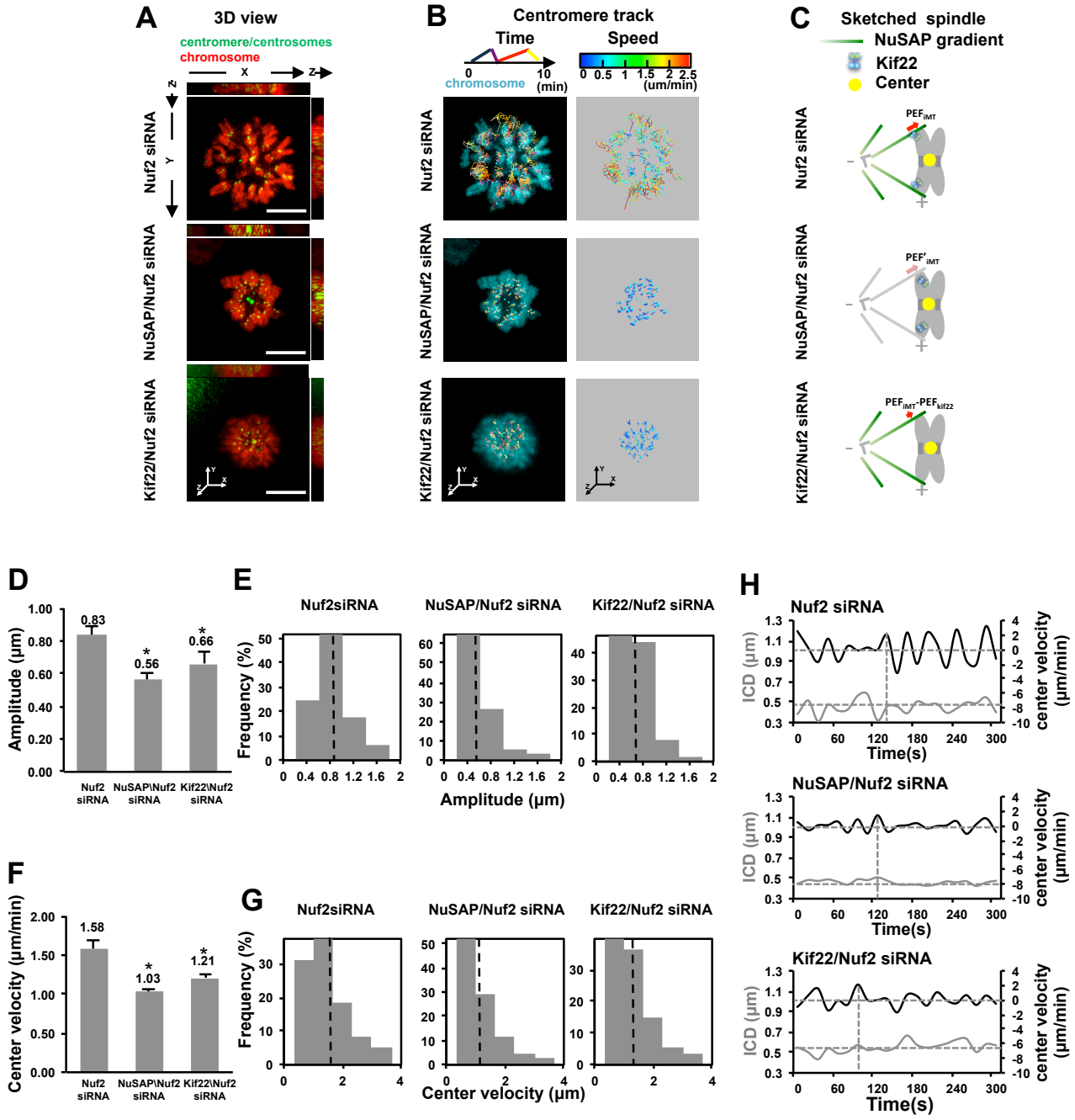


**Figure 4.3.7 . NuSAP collectively tunes PEF with kif22 at iMTs**

(A) Representative images of 3D view with xz and yz projections in Nuf2, NuSAP/Nuf2 or Kif22/Nuf2 siRNA depleted monastrol treated monopolar stable mCherry-H2B HeLa cells. The centromeres were marked with GFP-CENPA and centrosomes with GFP-centrin. Scale bar, 5μm.
(B) Representative images of 3D centromere tracks color-coded with time and velocity as indicated by the color.
(C) Schematic spindle models illustrating the forces at iMTs in the absence of kMTs in Nuf2, NuSAP/Nuf2 or Kif22/Nuf2 siRNA depleted monopolar cells.
(D-E) The bar chart and the histogram represent the average (D) and the distribution (E) of the amplitude of the centromere oscillation in Nuf2, NuSAP/Nuf2 or Kif22/Nuf2 siRNA depleted monopolar cells. Error bars represent +SED. * $p<0.001$.
(F-G) The bar chart and the histogram represent the average (F) and the distribution (G) of the center velocity. Error bars represent +SED. * $p<0.001$.
(H) Representative velocity (black line) and ICD (grey line) versus time plots of the projected center in a sister centromeres pair in control, NuSAP or Kif22 siRNA depleted monopolar cells. The sign of the velocity indicates the direction of the centromere movement. The average of the ICD (horizontal), the minimum (horizontal) and max velocity (vertical) are indicated by the dashed dot lines.

### 4.3.7 NuSAP governs the polar ejection force generated by Kif22 during centromere oscillation

To further specify the regulation of NuSAP in chromosome oscillation, we analyzed the influence of NuSAP on different forces generated on kMTs, iMTs and specifically by Kif22 using the force-balance approach (Joglekar and Hunt, 2002; Liu et al., 2007; Sutradhar and Paul, 2014; Vladimirou et al., 2011). At the subcellular level, the viscous forces dominate with the negligible inertial effects and a low Reynolds number (Joglekar and Hunt, 2002), thus all the forces on the chromosome can be equated to the viscous term that is proportional to the oscillation velocity as $F=k\times v$ (k as constant; v as velocity) (Vladimirou et al., 2011). As shown in Figure 3-6C, the forces on the 3D projected chromosome center were simplified as the polar force generated by kMT ($PF_{kMT}$), the PEF generated on iMTs ($PEF_{iMT}$) and the Kif22 generated PEF ($PEF_{kif22}$) as the same under different conditions (Hays and Salmon, 1990b; Ke et al., 2009; Rieder et al., 1986b; Skibbens et al., 1993a; Sutradhar and Paul, 2014; Wandke et al., 2012; Yajima et al., 2003). Taken together the 12 conditions we studied in Figure 3-6, the resulting forces on the chromosome center can be assembled as the 12 equations, which are directly related with the center velocity (Figure 4.3.8 A). In the simplest scenario, the influence of NuSAP in the chromosome oscillation can be proposed to be linear (Liu et al., 2007), as $K_{NuSAP}$—the impact of NuSAP on

$PF_{kMT}$, $I_{NuSAP}$—the impact of NuSAP on $PEF_{kif22}$ and $I'_{NuSAP}$—the impact of NuSAP on the other force at iMTs.

Taken together our result of the chromosome center velocity (Figure 4.3.4-3.3.7 F and Table 1), the influence of NuSAP in the chromosome oscillation—$K_{NuSAP}$ and $I_{NuSAP}$ can be calculated (as shown in Figure 7A and material and methods). The analysis indicates that the influence of NuSAP on the polar force at kMTs: $K_{NuSAP}$=0.20, the influence of NuSAP on the PEF generated by Kif22: $I_{NuSAP}$=0.88 (Figure 4.3.8 A).

**A**

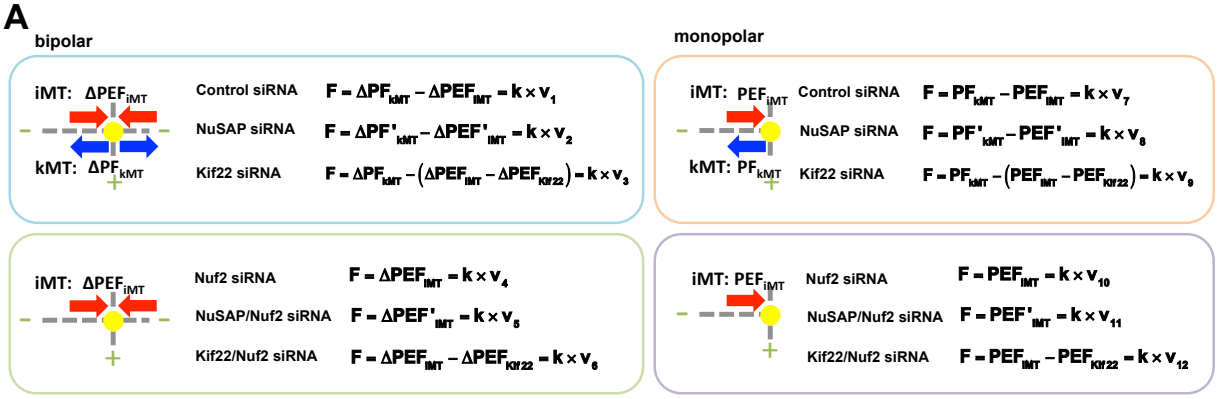


$I_{NuSAP}$ : Impact of NuSAP on Kif22 generated PEF at iMTs

$K_{NuSAP}$ : Impact of NuSAP on kMT generated force

$$\Delta PEF'_{iMT} = \Delta PEF_{iMT} - I_{NuSAP} \times \Delta PEF_{Kif22} - I'_{NuSAP} \times (\Delta PEF_{iMT} - \Delta PEF_{Kif22})$$

$$PEF'_{iMT} = PEF_{iMT} - I_{NuSAP} \times PEF_{Kif22} - I'_{NuSAP} \times (PEF_{iMT} - PEF_{Kif22})$$

$$\Delta PF'_{kMT} = \Delta PF_{kMT} - K_{NuSAP} \times \Delta PF_{kMT} \qquad PF'_{kMT} = PF_{kMT} - K_{NuSAP} \times PF_{kMT}$$

$$I_{NuSAP} = \frac{2v_4v_{12} - 2v_5v_{12} - 2v_6v_{10} + 2v_6v_{11}}{v_1v_{12} + v_4v_{12} - v_3v_{12} - v_6v_7 - v_6v_{10} + v_6v_9} = 0.88 \qquad K_{NuSAP} = 1 - \frac{(v_2 + v_5)(v_7 + v_{10}) + (v_1 + v_4)(v_8 + v_{11})}{2v_1v_7 + 2v_4v_7 + 2v_1v_{10} + 2v_4v_{10}} = 0.20$$

**B**

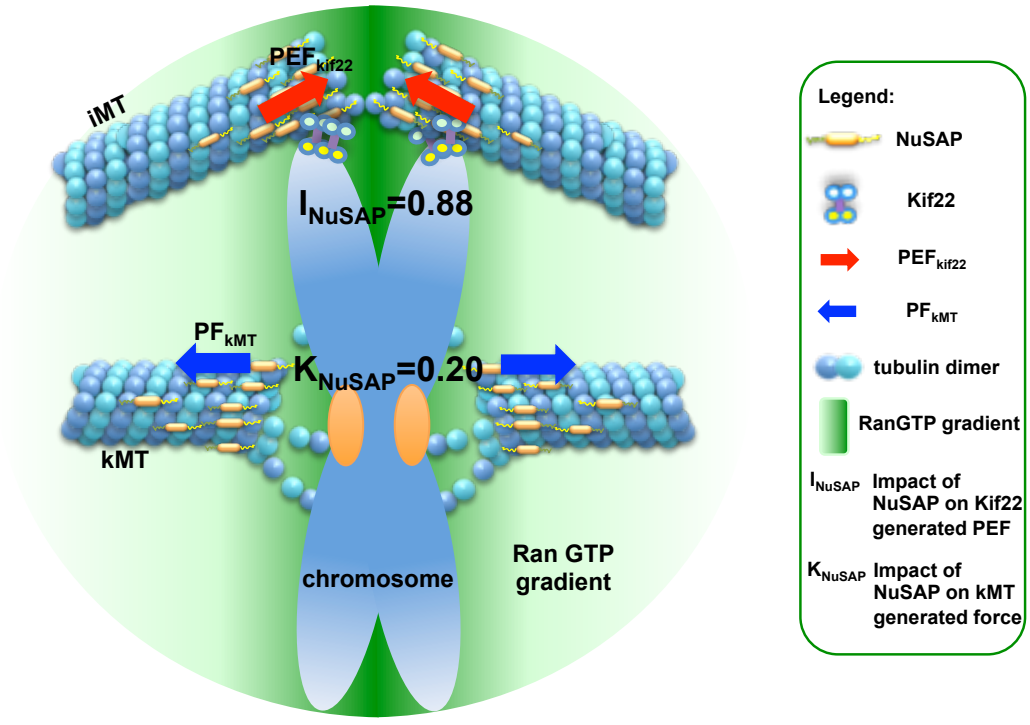

**Figure 4.3.8. NuSAP governs Kif22 generated PEF during chromosome oscillation**

(A) The sketched models of the forces on the projected center point and equations in 12 conditions—control siRNA, NuSAP siRNA, Kif22 siRNA ,Nuf2 siRNA, NuSAP/Nuf2 siRNA, Kif22/Nuf2 siRNA depleted bipolar metaphase cells and control siRNA, NuSAP siRNA, Kif22 siRNA, Nuf2 siRNA, NuSAP/Nuf2 siRNA, Kif22/Nuf2 siRNA depleted monopolar cells. $PF_{kMT}$: the force generated on kMTs. $PEF_{iMT}$: the force generated on iMTs. $PEF_{kif22}$: the PEF generated by Kif22. The influence of NuSAP is dessected into: the impact of NuSAP on $PF_{kMT}$ at kMTs— $K_{NuSAP}$, the impact of NuSAP on $PEF_{kif22}$ at iMTs—$I_{NuSAP}$ and the impact of NuSAP on the other force at iMTs—$I'_{NuSAP}$.
(B) A schematic model representing the role of NuSAP to govern Kif22 generated PEF in regulating Kif22 during chromosome oscillation.

**Table 1. A summary of the parameters defining centromere oscillation in bipolar and monopolar control, NuSAP, Kif22, Nuf2, Nuf2/NuSAP, Nuf2/Kif22 siRNA cells**

| | siRNA | Velocity (μm/min) | No.KT pairs/ No. cells | ICD (μm) | half-period (s) | Amplitude (μm) |
|---|---|---|---|---|---|---|
| bipolar | Control | $v_1$=1.68±0.06 | 298/12 | 0.75±0.09 | 32.50±3.34 | 1.12±0.08 |
| | NuSAP | $v_2$=1.39±0.03 | 226/8 | 0.69±0.09 | 32.56±3.55 | 0.78±0.11 |
| | Kif22 | $v_3$=1.54±0.06 | 344/11 | 0.71±0.10 | 31.73±4.14 | 0.79±0.05 |
| | Nuf2 | $v_4$=1.73±0.06 | 467/15 | 0.61±0.13 | 33.48±6.55 | 1.15±0.08 |
| | NuSAP/Nuf2 | $v_5$=1.46±0.03 | 257/11 | 0.60±0.08 | 33.24±2.93 | 0.92±0.06 |
| | Kif22/Nuf2 | $v_6$=1.59±0.04 | 238/9 | 0.58±0.10 | 33.34±2.89 | 0.95±0.06 |
| monopolar | Control | $v_7$=1.39±0.10 | 358/15 | 0.57±0.11 | 31.06±2.88 | 0.69±0.04 |
| | NuSAP | $v_8$=1.25±0.06 | 261/10 | 0.56±0.07 | 30.65±2.87 | 0.66±0.04 |
| | Kif22 | $v_9$=0.76±0.02 | 447/13 | 0.52±0.08 | 28.66±2.22 | 0.49±0.03 |
| | Nuf2 | $v_{10}$=1.58±0.09 | 341/15 | 0.52±0.09 | 29.97±3.04 | 0.83±0.05 |
| | NuSAP/Nuf2 | $v_{11}$=1.03±0.03 | 237/11 | 0.47±0.08 | 26.96±2.17 | 0.56±0.05 |
| | Kif22/Nuf2 | $v_{12}$=1.21±0.03 | 357/12 | 0.50±0.08 | 29.01±2.30 | 0.66±0.08 |

## 4.4 Discussion

Here we show that the MAP NuSAP functions importantly in the chromosome congression at metaphase. Previous studies indicate NuSAP is a MT stabilizer both in vitro and in vivo during mitosis (Raemaekers et al., 2003b; Ribbeck et al., 2006a; Ribbeck et al., 2007b). Our result shows that NuSAP associates with central spindle MTs to regulate the alignment and orientation of the chromosome at the metaphase plate (Figure 4.3.1). Thus, our findings extend earlier findings by clearly identifying NuSAP not only functions as a MT stabilizer, but also specifically facilitates the important chromosome congression process during metaphase.

We identify NuSAP as a novel regulator of the chromokinesin Kif22 for the very first time. NuSAP binds with Kif22 to facilitate its interaction with MTs (Figure 4.3.2). NuSAP and Kif22 are both highly expressed during mitosis (Feine et al., 2007; Song and Rape, 2010a) and regulated by the RanGTP gradient to accumulate at metaphase plate (Ribbeck et al., 2006a; Tahara et al., 2008b). Our immunoprecipitation results indicate that the pivotal role of NuSAP in regulating the functions of Kif22 during metaphase (Figure 4.3.2C and D) and the interaction facilitates the association of Kif22 with MTs (Figure 4.3.2E-G). The temporal and spatial feature of the regulation indicates that NuSAP is a vital regulator of Kif22 during metaphase.

Our quantitive live-cell imaging analyses show that NuSAP specifically regulates chromosome oscillation by governing the PEF generated by Kif22. Kif22 functions as a key force-producing agent for PEF (Brouhard and Hunt, 2005; Yajima et al., 2003). Here we reveal for the first time an important regulatory mechanism that NuSAP strongly governs the PEF generated by Kif22 during chromosomes oscillation. The depletion of NuSAP correlates with the Kif22 depletion in the regulation of the amplitude and velocity of chromosome oscillation in both bipolar and monopolar cells (Figure 4.3.4 and 3.3.6). The regulation of NuSAP in the centromere movement is specifically at iMTs synergistially with Kif22 in the absence of kMTs by the depletion of Nuf2 (Figure 4.3.5 and 3.3.7). With a simplified force-balance approach, we analyzed the impact of NuSAP on the PEF generated by Kif22 (Figure 4.3.8 A). The analysis indicates the regulation of NuSAP on the Kif22 generated PEF is dominant ($I_{NuSAP}$=0.88), compared to the regulation of NuSAP on the other force on iMTs ($I'_{NuSAP}$=0.09, Material and Methods), suggesting that the PEF produced by Kif22 significantly depends on the specific regulation of NuSAP.

Our analysis shows that NuSAP also regulates the kMT generated polar force ($K_{NuSAP}$=0.20). Previous studies indicate that NuSAP can stabilize MTs and link MTs with chromosomes (Raemaekers et al., 2003b; Ribbeck et al., 2006a;

Ribbeck et al., 2007b). Thus NuSAP may facilitate the polar force generated by kMT through its regulation of kMT dynamics and the attachment between KT and kMTs.

Though our result indicates the general influence of NuSAP on the other forces besides $PEF_{kif22}$ on iMTs is small ($I'_{NuSAP}$=0.09, Material and Methods), we can not rule out the possibility that NuSAP might have other significant functions on certain specific forces at iMTs, for example the forces generated by Kif4a (Stumpff et al., 2012; Wandke et al., 2012), dyneins (King et al., 2000b) or the dynamics of iMTs (Ke et al., 2009).

Here we propose a simplified chromosome center projected force-balance approach. Our data suggest that the average of the ICD and period did not change significantly in NuSAP or Kif22 depleted cell (Table 1). However, the distributions of the ICD and the period are influenced and the coupling of the ICD and velocity is abolished by the depletion of NuSAP or Kif22 (Figure 4.3.4-3.3.7 H). However, other factors might also involve in the complicated situation of chromosome oscillation; for example, the stiffness of KTs absolves one portion of the imbalanced force upon the chromosome during oscillation (Jaqaman et al., 2010; Joglekar and Hunt, 2002; McClelland et al., 2007; Vladimirou et al., 2011). The MT density changes in the absence of kMT or monopolar MT asters might

also lead to the changes of PEF (Joglekar and Hunt, 2002; Ke et al., 2009; Rieder et al., 1986b; Skibbens et al., 1993a). Future studies would need to answer these questions.

In summary, we generated a schematic model representing the role of NuSAP in governing the PEF generated by Kif22 (Figure 4.3.8 B). Our result shows that NuSAP facilitates chromosome congression and interacts with Kif22 to regulate its localization during metaphase. Our quantitive analyses indicate that NuSAP regulates both the forces generated on kMTs and iMTs with different impacts. The non-NuSAP coated kMTs generate about 0.8 fold ($K_{NuSAP}$=0.20) of the force generated by NuSAP coated kMTs. In the absence of NuSAP, the Kif22 generated PEF is only 0.12 fold ($I_{NuSAP}$=0.88) compared with the normal cells. Thus, the PEF generated by Kif22 mostly depends on NuSAP during chromosome oscillation.

# CHAPTER 5 NuSAP facilitates midzone microtubule formation through negative regulation of Kif4a

## 5.1 Abstract

The central spindle formation is critical for segregating chromosomes during anaphase and required for cytokinesis. Although many studies focus on the stability of microtubules during metaphase, very few investigate the dynamics of central spindle microtubule during anaphase. NuSAP (Nucleolar and Spindle associated protein), a microtubule associated protein, functions importantly in mitosis. In our study, we show that NuSAP plays an important role in stabilizing midzone microtubule during anaphase and chromosome bridge at the midzone region. Furthermore, we identify NuSAP as a novel binding partner of Kif4a to facilitate its localization to midzone microtubules. Since Kif4a has been reported as a key regulator for central spindle microtubule stability, the regulation of NuSAP on Kif4a is vital for accurate midzone formation during anaphase. Further studies are required to confirm the important role of NuSAP in modulating Kif4a to promote efficient cytokinesis.

## 5.2 Introduction

Cytokinesis is the key process to accurate segregate the genetic material into two daughter cells (Glotzer, 2005). The central spindle (spindle midzone) are formed with a complex microtubule structure which consists with two masses of parallel microtubule bundles with opposite directionalities in the center of the interchromosomal region (McDonald et al., 1979). In anaphase, multiple mitotic kinesins and microtubule associated proteins are recruited to the antiparallel array of microtubules at the central spindle (Saxton and McIntosh, 1987). However, it's still largely unclear how the interpolar microtubules are prepared for central spindle formation.

NuSAP has been identified as a microtubule associated protein to stabilize microtubules both *in vivo* and *in vitro* (Raemaekers et al., 2003a; Ribbeck et al., 2006b; Ribbeck et al., 2007a). The depletion of NuSAP leads to severe defects in mitosis, which indicates its important role in mitosis (Raemaekers et al., 2003a). The protein level of NuSAP is tightly regulated by the APC/C complex and specifically up-regulated during mitosis (Li et al., 2007a; Song and Rape, 2010b). Furthermore, the association of NuSAP with microtubules is tightly regulated by RanGTP gradient (Ribbeck et al., 2006b). The function of NuSAP during anaphase has been unclear.

Kif4a is a kinesin-4 family chromokinesin member (Oh et al., 2000) and functions as microtubule depolymerizer to regulate the length of the microtubules at the central spindle region (Hu et al., 2011). During cytokinesis, Kif4a interacts with PRC1 at the midzone and control the formation of central spindle under the regulation of Aurora B and cdk1 (Hu et al., 2012; Kurasawa et al., 2004; Zhu and Jiang, 2005; Zhu et al., 2006). Though the function of Kif4a at cytokinesis is largely investigated, the role of Kif4a at anaphase is still not understood.

In this study, we identified the important function of NuSAP for stabilizing midzone microtubule during anaphase. With high levels of NuSAP in the cells, the interpolar microtubule at the central spindle is hyper-stabled with severe chromosome bridge phenotypes. Furthermore, we show that NuSAP interacts with Kif4a and is essential for Kif4a to target midzone microtubules from chromosomes during anaphase. Our result presents an important role of NuSAP in mediating midzone formation during anaphase.

## 5.3 Result

### 5.3.1 Overexpression of NuSAP results in lagging chromosomes during anaphase

To study the role of NuSAP during mitosis, we first investigated the expression pattern of endogenous NuSAP during different stages in mitosis. As shown in Figure 5.3.1A row 1, NuSAP associated with microtubules during the whole mitosis process from prophase to telophase. However, NuSAP specifically targets at the midzone region during anaphase (Figure 5.3.1 A, lane 3). We further studied the protein expression level of NuSAP during mitosis utilizing metaphase synchronized HeLa cells releasing in the fresh medium for the indicated time points (Figure 5.3.1 B). The result indicated that although NuSAP expressed in different stages of mitosis, the protein levels were relatively higher after metaphase (Figure 5.3.1 B, lane 2-4). We utilized the 3D live-cell imaging to track the cell division in the GFP-NuSAP overexpressing mCherry-H2B stable HeLa cells. As shown in Figure 5.3.1 C, the NuSAP overexpressed cells showed severe lagging chromosome phenotypes with several chromosomes stuck and elongated interpolar microtubules at midzone region during anaphase (indicated by the arrows). Taken together, the results show that NuSAP is specifically highly expressed and targets at midzone microtubules at anaphase and may function in chromosome segregation during anaphase.

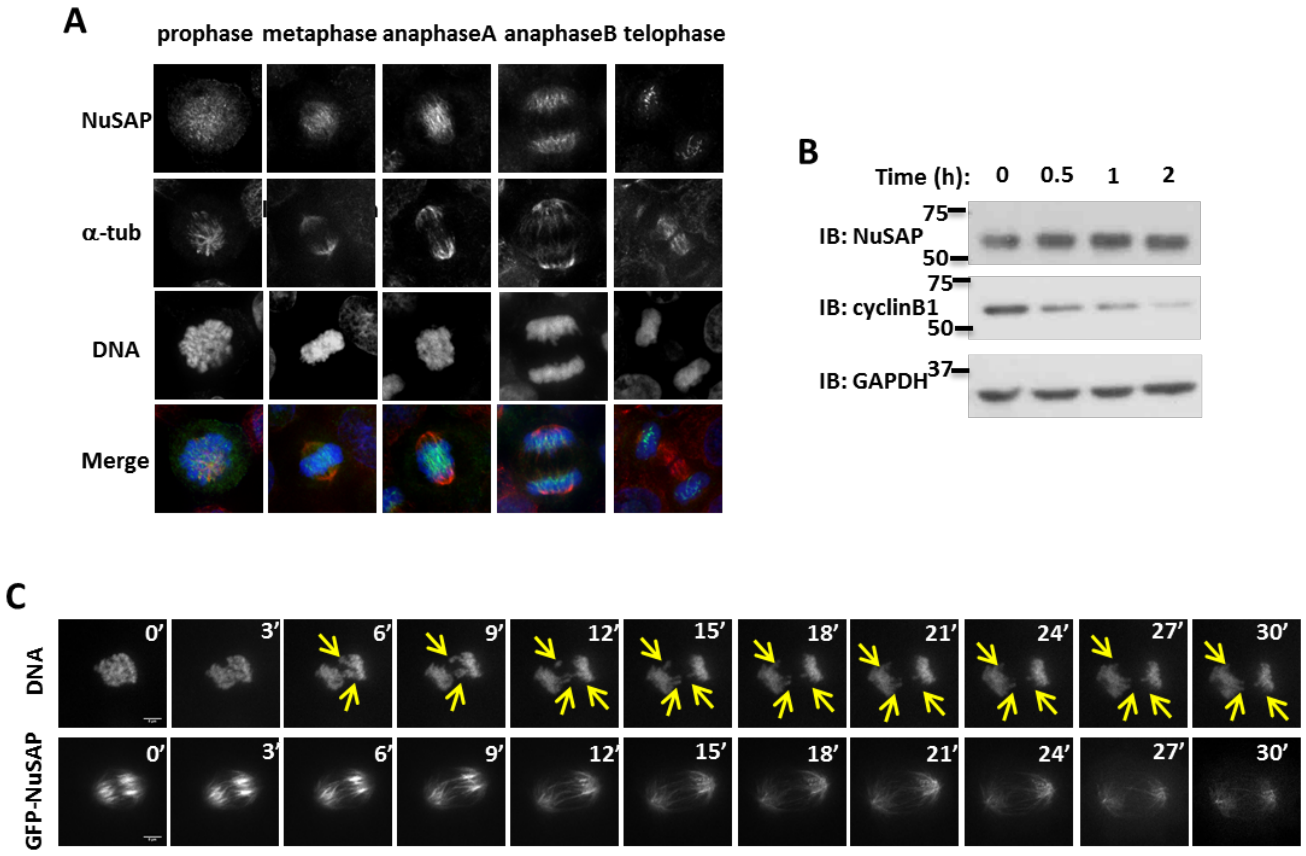


**Figure 5.3.1 NuSAP localizes at midzone region and regulates chromosome separation during anaphase**

(A) NuSAP localization during mitosis. Fluorescent images of metaphase HeLa cells were stained with an anti-NuSAP antibody, an anti-α-tubulin antibody for microtubules and DNA with Hoechst 333342. (B) NuSAP protein expression level during mitosis. HeLa cells arrested in mitosis by thymidine/nocodazole were released into fresh medium for the indicated timepoints (hr) and blotted with anti-NuSAP, anti-cyclin B1 and anti-GAPDH antibodies. (C) 3D time-lapse imaging of chromosome oscillation in synchronized metaphase stable mCherry-H2B HeLa

cells expressing GFP-NuSAP. The lagging chromosomes are indicated by arrows. Scale bar, 5μm.

### **5.3.2** NuSAP stabilizes midzone microtubules

The elongated interpolar microtubules at midzone region in NuSAP overexpressing cells indicate that NuSAP might modulate the stability of the midzone microtubules at the central spindle region. Thus, we further investigated the midzone microtubule structure at anaphase. As shown in Figure 5.3.2 A, compared with control cells, the NuSAP overexpressing cells showed elongated interpolar microtubules with severe misaligned chromosomes at midzone region (enlarged right panel). To further confirm the function of NuSAP in regulating midzone microtubule stability, we utilized the treatment of monastrol/flavopiridol to form ectopic furrow of microtubules mimicking the midzone microtubule formation (Figure 5.3.2 B). The results show that with elevated levels of NuSAP in cells, the number of the robust membrane blabbing was dramatically increased at the site of polarization and along the periphery (arrows). Also, the microtubule bundle at the mimic midzone region was largely elongated with recognizable ectopic furrows in NuSAP overexpressing cells. The result indicates that NuSAP functions as a microtubule stabilizer during midzone formation at anaphase.

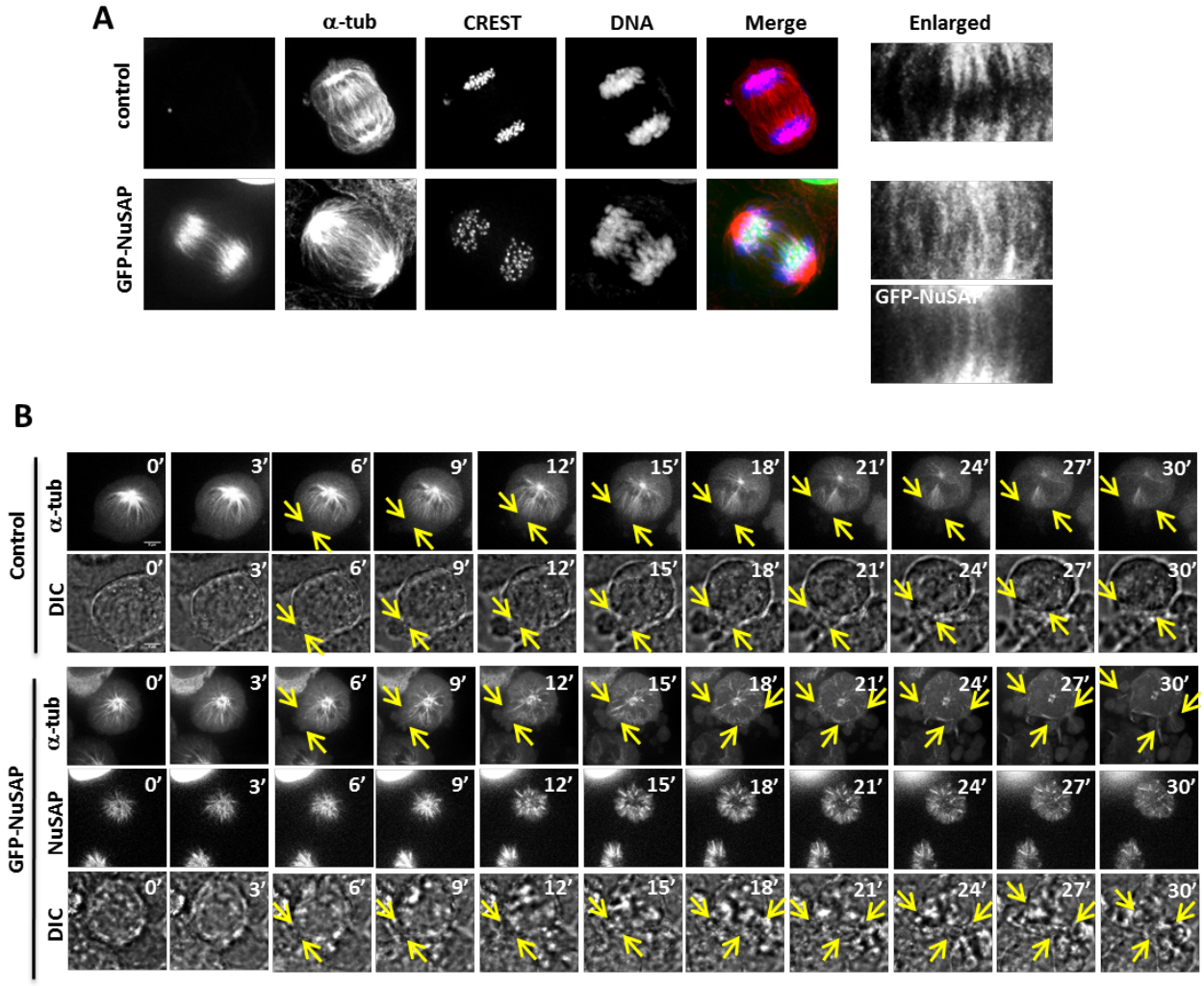


**Figure 5.3.2 NuSAP regulates the central spindle microtubule stability at midzone region.**

(A) NuSAP stabilizes interpolar microtubule at midzone region during anaphase. Fluorescent images of anaphase control cells or HeLa cells were transfected with GFP-NuSAP were stained with an anti-α-tubulin antibody for microtubules, ACA antibody for kinetochores and DNA with Hoechst 333342. (B) The time-lapse imaging of the dynamic ectopic furrow formation in control or stable mCherry-α-tubulin HeLa cells expressing GFP-NuSAP following monastrol/flavopiridol treatment. The positions of ectopic furrow formations are indicated by arrows.

### **5.3.3** NuSAP interacts with Kif4a and regulates its localization at midzone

Previous studies indicate the stability of the interpolar microtubule at the midzone region during anaphase is specifically regulated by the kinesin-Kif4a, which depletion also leads to severe lagging chromosomes similar to the NuSAP overexpression phenotypes (Hu et al., 2011; Kurasawa et al., 2004; Nunes Bastos et al., 2013; Shrestha et al., 2012; Zhu and Jiang, 2005). Thus, to understand the molecular mechanism of how NuSAP regulates the stability of midzone microtubules, immunoprecipitation was utilized (Figure 5.3.3 A and B). Our result showed that NuSAP interacted with Kif4a. We further investigated the localization of Kif4a in the NuSAP overexpressing cells from metaphase to telophase (Figure 5.3.3 C). The result indicated that the chromosome localization of Kif4a during metaphase was not affected by the overexpression of NuSAP (Figure 5.3.3 C, lane 1). However, in the NuSAP overexpressing cells, the midzone localization of Kif4a was dramatically abolished, compared with the central spindle localization of Kif4a in control cells from anaphase to telophase (Figure 5.3.3 C). The intensity of Kif4a was further investigated with the kymograph specifically at the midzone region. As shown in Figure 5.3.3 D, Kif4a specifically concentrated at the midzone region in control cells (Figure 5.3.3 D, left panel). However, in NuSAP overexpressing cells, the intensity of Kif4a was largely decreased at the central spindle (Figure 5.3.3 D, right panel). Taken

together, our result indicates that NuSAP associates with Kif4a and specifically regulates its localization at midzone region during anaphase.

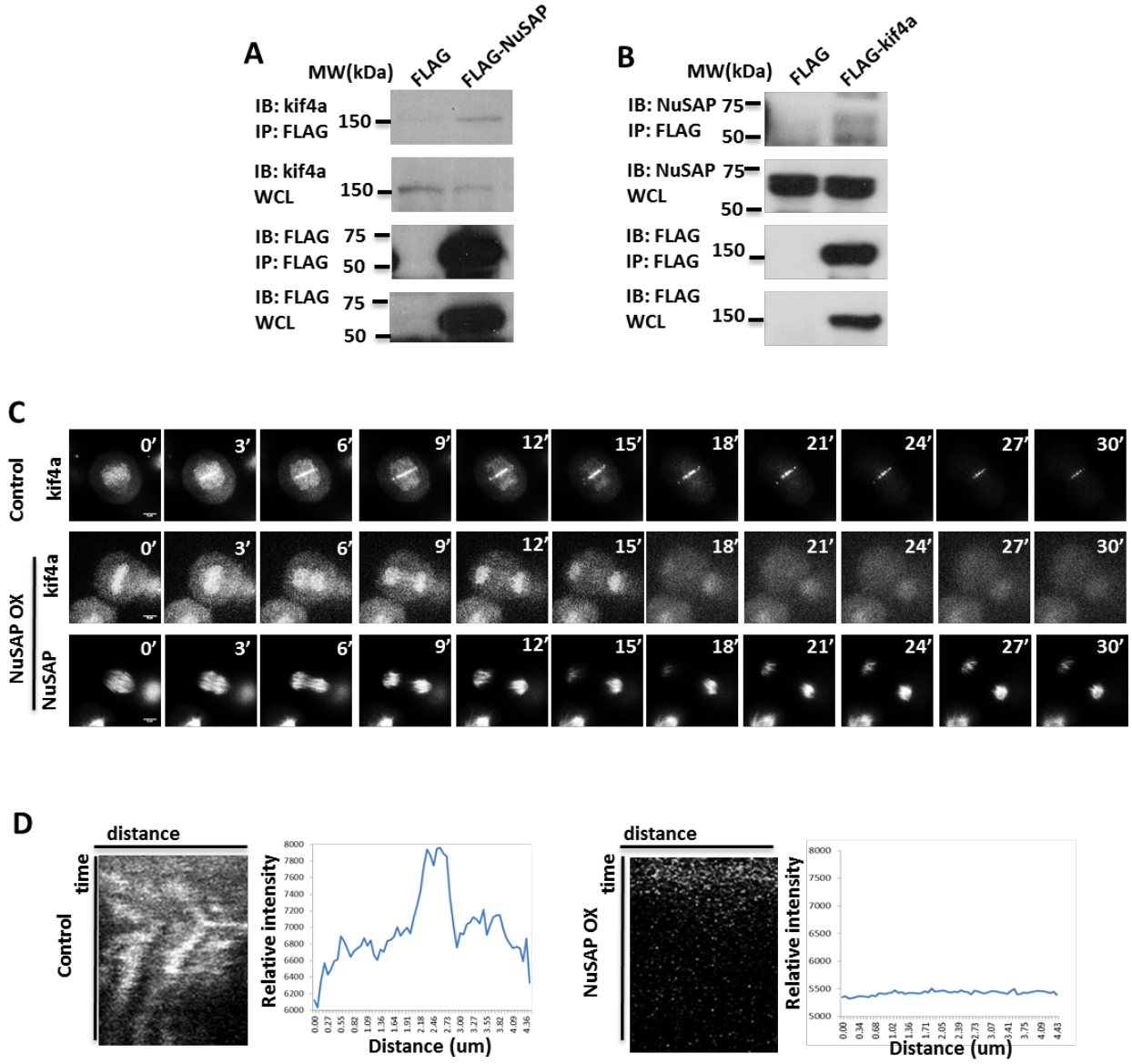


**Figure 5.3.3 NuSAP interacts with Kif4a and regulates its localization at midzone region**

(A) NuSAP immunoprecipitates contain Kif4a. FLAG and FLAG-NuSAP immunoprecipitates from HEK 293T cell lysate were blotted with either an anti-Kif4a or anti-FLAG antibody. (B) The endogenous NuSAP is pulled-down by

FLAG-Kif4a. FLAG and FLAG-Kif4a immunoprecipitates from HEK 293T cell lysate were blotted with NuSAP antibody. (C) The time-lapse imaging of the dynamic localization of Kif4a from metaphase to telophase in control or HeLa cells expressing GFP-NuSAP. (D) The kymographs of Kif4a at midzone region in control cells or GFP-NuSAP overexpressingHeLa cells. The intensities of Kif4a in control and NuSAP overexpressing cells were shown in the right panel.

## 5.4 Discussion

The precise formation of the central spindle is critical for the signaling machinery in cytokinesis. Our finding shows that NuSAP specifically e regulate the stability of central spindle microtubules. Since the interaction between NuSAP and Kif4a tightly modulates the localization of Kif4a at midzone region. The result indicates that the function of NuSAP on midzone microtubule stability might through its regulation on Kif4a.

We identify NuSAP regulates the midzone microtubule stability. Previous studies indicate that NuSAP as a microtubule associated protein stabilizes microtubules both *in vivo* and *in vitro* (Raemaekers et al., 2003a; Ribbeck et al., 2006b; Ribbeck et al., 2007a). Our results show that NuSAP localizes at the midzone and stabilizes the central spindle microtubules during anaphase (Figure 5.3.1 and Figure 5.3.2). Thus, our study strongly extents previous findings, that NuSAP specifically controls the stability of inter-microtubules at central spindle during cytokinesis.

Our study presents NuSAP as a novel regulator of Kif4a at the midzone region during cell division. Kif4a has been reported as a key regulator of the midzone microtubule stability during cytokinesis (Hu et al., 2011; Kurasawa et al., 2004; Nunes Bastos et al., 2013; Shrestha et al., 2012; Zhu and Jiang, 2005). Our study shows that NuSAP specifically controls the midzone targeting of Kif4a during anaphase to telophase (Figure 5.3.3). Thus, the role of NuSAP in stabilizing midzone microtubules during anaphase might through its negative regulation of Kif4a. To reach this point, further experiments are required.

The central spindle formation during anaphase is critical for chromosome segregation during anaphase and is important for accurate cytokinesis. Our study indicates that NuSAP specifically functions as a central microtubule stabilizer through its interaction and regulation of Kif4a during anaphase (Figure 5.3.4). Hence, this study provides insights into a novel role of NuSAP in midzone formation during anaphase which disruption might related with cancer formation.

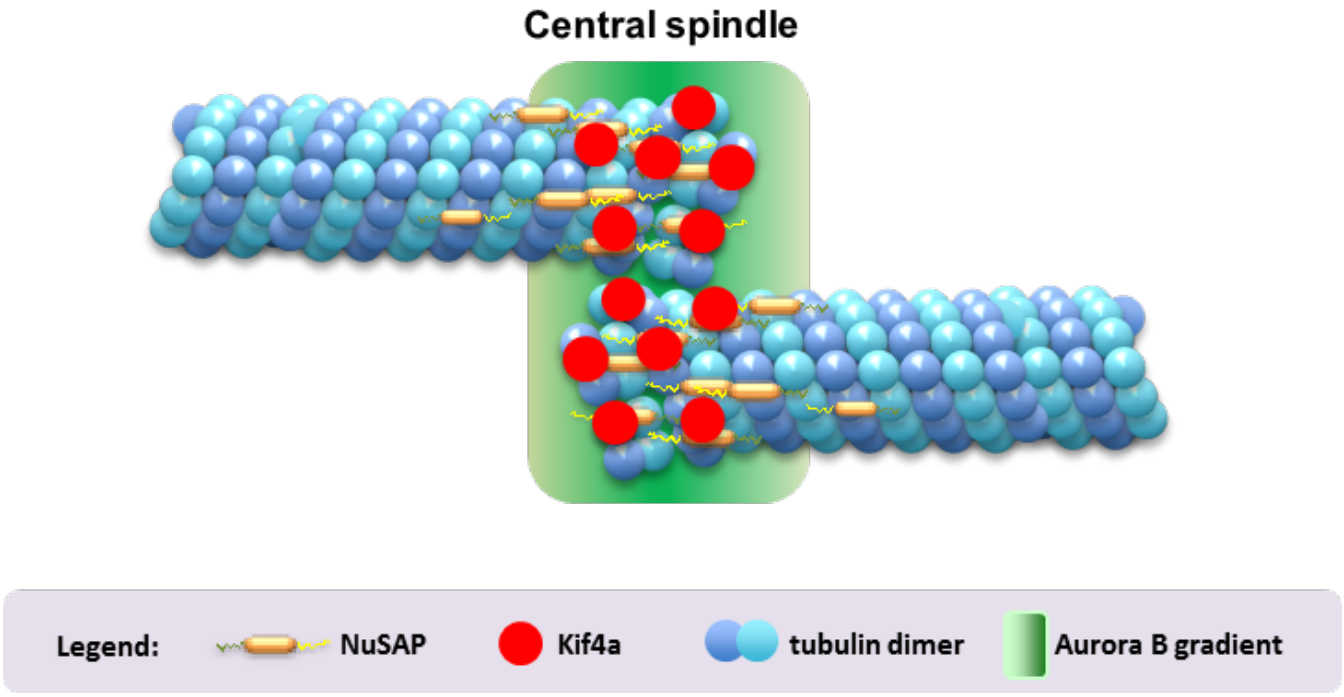


**Figure 5.3.4. Model of NuSAP regulating midzone microtubule stability through interaction with Kif4a during anaphase.**

# CHAPTER 6 Discussion and conclusions

## 6.1 Discussion

Mitosis is essential to maintain the consistent genetic material in daughter cells and microtubule associated proteins play important roles in the regulation of mitosis. NuSAP as a MAP, functions as a microtubule stabilizer both *in vivo* and *in vitro*. Our results show that NuSAP specifically stabilizes kinetochore microtubules during metaphase through the interaction and regulation of the microtubule depolymerizer—MCAK. Our finding demonstrates that NuSAP regulates the dynamics of kinetochore microtubules through its MCBD binding domain and the interaction between NuSAP and MCAK is under the tightly regulation of Aurora B. The dynamics of kinetochore microtubules are key to the correct kinetochore microtubule attachment and the chromosome alignment during metaphase. Thus, our study provides insights into the critical role of the MAP—NuSAP in kinetochore microtubule dynamics and attachment, which defects might lead to cancer formation.

The depletion of NuSAP leads to severe chromosome oscillation defects. NuSAP regulates the alignment, orientation and oscillation of the chromosomes during metaphase through the regulation of Kif22. Furthermore, we elucidate the influence of NuSAP on the polar ejection force generated by Kif22. Our results show that NuSAP is essential for Kif22 generated PEF (I=0.88) and partially

regulate the kinetochore microtubule generated polar force (K=0.20). Taken together the NuSAP regulation on kinetochore microtubule dynamics, the influence of NuSAP on kinetochore microtubule forces might be from its regulation on MCAK depolymerization activity to further regulation the dynamics of kinetochore microtubules. Thus, NuSAP plays a key role in chromosome oscillation through both the regulation of kinetochore microtubule dynamics and the Kif22 generate force during metaphase.

NuSAP facilitates the stability of midzone microtubules and regulates the localization of Kif4a to the central spindle region during anaphase. Our study indicates the important role of NuSAP in modulating the dynamics of midzone microtubule during anaphase. However, further studies are needed to confirm the function of NuSAP at midzone formation.

In summary, our study indicates the temporal and spatial function of NuSAP at different kinds of microtubules during different stages of mitosis, suggesting the vital role of NuSAP during mitosis. The different roles of NuSAP during mitosis might be controlled by the mitotic kinases, such as cdk1, Aurora B or Aurora A. The modification on NuSAP might further contribute to its different roles during mitosis. In addition, the RanGTP gradient can modulate the association of NuSAP on microtubules, and contribute to the different roles of NuSAP.

As a microtubule associated protein, the function of NuSAP in regulating MCAK, Kif22 and Kif4a might not be totally independent and the three parts of the study are tightly connected. The dynamics of kinetochore microtubules involves in the chromosome oscillation during metaphase and the accurate interaction between kinetochores and microtubules are the pre-condition of the correct chromosome oscillation. Thus, the regulation of NuSAP on MCAK depolymerization activity might also contribute to the chromosome oscillation. Moreover, during anaphase, MCAK targets at both ends of the kinetochore microtubules and interpolar microtubules, which might also contribute to the dynamics regulation of NuSAP on midzone microtubules. Furthermore, Kif22 mainly generates the polar ejection force during chromosome oscillation and has important functions in spindle formation. The regulation of NuSAP on Kif22 might not only at the polar ejection force, but might involve in the spindle formation. In the meantime, Kif4a localizes at chromosome during metaphase and antagonize the function of Kif22 during the chromosome oscillation. The regulation of NuSAP on the translocalization of Kif4a from chromosome to midzone microtubules might also contributes to the chromosome movement during metaphase and anaphase.

There are several future studies can be proposed to reveal the important roles of NuSAP. In this study, we focus on the function of NuSAP in metaphase and

anaphase. We also notice that NuSAP localizes at nucleus during interphase and specifically targets at the nuclear membrane, which might show its possible role in the nuclear matrix formation during interphase. In addition,, in the recent proteome-wide poly(ADP-Ribosyl)ation study, NuSAP is listed as a target, suggesting that NuSAP might be post-translational modified by PARylation (Jungmichel et al. 2013). To validate the proteomics results, we shows that NuSAP can be PARylated at its N-terminal domain, the 1-233 region under specific genotoxic stress treatments. PARylation has been reported to be specifically related in the regulation of chromatin structure modulation, DNA repair and transcription (Hassa et al., 2006, Luo et al. 2012), suggesting that NuSAP may engage in the DNA repair machinery during cell cycle. Furthermore, a previous report indicates NuSAP can be phosphorylated by Aurora A kinase at the S240 residue (Sardon et al., 2010). Aurora A functions at the spindle pole region as a key regulator in spindle pole formation. Our preliminary data also indicates the overexpression of NuSAP in cells leads to dramatic spindle pole fragments. Further studies on the role of NuSAP in the spindle pole formation might enhance our understanding in mitosis. Yet as mentioned, aberrantly high expression levels of NuSAP have been found in several kinds of cancers (Fujiwara et al., 2006; Gulzar et al., 2013; Iyer et al., 2011b; Kokkinakis et al., 2005b; Wadia et al., 2010; Xie et al., 2011). Thus, studies on the role of NuSAP in cancer development and cancer prognosis may facilitate our knowledge about

the relationship of microtubule-associated proteins such as NuSAP and cancer biology.

## 6.2 Conclusions

This study was aimed to explore the underlying mechanism of how does NuSAP function during mitosis. To address this question, we investigate the function of NuSAP in three essential processes in mitosis: the stability of kinetochore microtubules during metaphase, the regulation of chromosome oscillation and the midzone formation during anaphase (Figure 6.2.1). Our results indicate that NuSAP specifically stabilizes kinetochore microtubules during metaphase and the regulation of the kinetochore microtubule dynamics is through its negative modulation of MCAK, the microtubule depolymerizer. With the middle spindle localization during metaphase, NuSAP also regulates the chromosome oscillation through the interaction with Kif22 to govern the generation of polar ejection force at interpolar microtubules. NuSAP expresses at the midzone region during anaphase and facilitates the central spindle localization of Kif4a by stabilizing the midzone microtubules. In summary, we describe for the very first time the multiple roles of NuSAP in regulating three kinesins at interpolar microtubules, kinetochore microtubules and midzone microtubules during different stages mitosis, respectively. The spatial and temporal function of NuSAP reveals the complicated regulation of spindle microtubules during mitosis. Hence, understanding the role of NuSAP would provide new insights into the mechanism of mitosis and cancer formation.

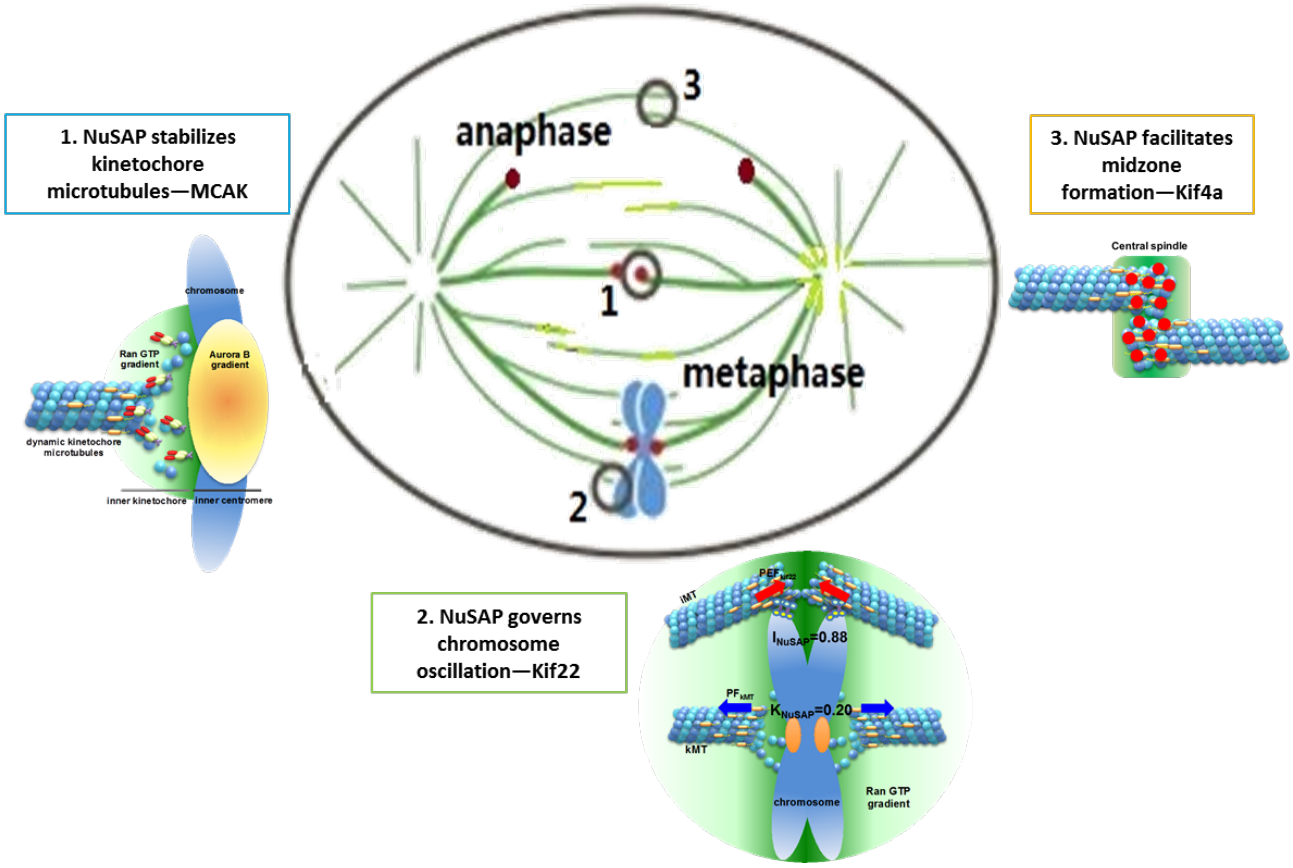


**Figure 6.2.1. The functions of NuSAP in kinetochore microtubule stability, chromosome oscillation and midzone formation during mitosis.**

## References


Andrews, P.D., E. Knatko, W.J. Moore, and J.R. Swedlow. 2003. Mitotic mechanics: the auroras come into view. *Current opinion in cell biology*. 15:672-683.

Andrews, P.D., Y. Ovechkina, N. Morrice, M. Wagenbach, K. Duncan, L. Wordeman, and J.R. Swedlow. 2004. Aurora B regulates MCAK at the mitotic centromere. *Developmental cell*. 6:253-268.

Aravind, L., and E.V. Koonin. 2000. SAP - a putative DNA-binding motif involved in chromosomal organization. *Trends in biochemical sciences*. 25:112-114.

Bakhoum, S.F., and D.A. Compton. 2012. Kinetochores and disease: keeping microtubule dynamics in check! *Current opinion in cell biology*. 24:64-70.

Bakhoum, S.F., G. Genovese, and D.A. Compton. 2009. Deviant kinetochore microtubule dynamics underlie chromosomal instability. *Current biology : CB*. 19:1937-1942.

Biggins, S., and C.E. Walczak. 2003. Captivating capture: how microtubules attach to kinetochores. *Current biology : CB*. 13:R449-460.

Bouck, D.C., A.P. Joglekar, and K.S. Bloom. 2008. Design features of a mitotic spindle: balancing tension and compression at a single microtubule kinetochore interface in budding yeast. *Annual review of genetics*. 42:335-359.

Boyden, E.D., A.B. Campos-Xavier, S. Kalamajski, T.L. Cameron, P. Suarez, G. Tanackovic, G. Andria, D. Ballhausen, M.D. Briggs, C. Hartley, D.H. Cohn, H.R. Davidson, C. Hall, S. Ikegawa, P.S. Jouk, R. Konig, A. Megarbane, G. Nishimura, R.S. Lachman, G. Mortier, D.L. Rimoin, R.C. Rogers, M. Rossi, H. Sawada, R. Scott, S. Unger, E.R. Valadares, J.F. Bateman, M.L. Warman, A. Superti-Furga, and L. Bonafe. 2011. Recurrent dominant mutations affecting two adjacent residues in the motor domain of the monomeric kinesin KIF22 result in skeletal dysplasia and joint laxity. *American journal of human genetics*. 89:767-772.

Brouhard, G.J., and A.J. Hunt. 2005. Microtubule movements on the arms of mitotic chromosomes: polar ejection forces quantified in vitro. *Proceedings of the National Academy of Sciences of the United States of America*. 102:13903-13908.

Cai, S., C.B. O'Connell, A. Khodjakov, and C.E. Walczak. 2009. Chromosome congression in the absence of kinetochore fibres. *Nature cell biology*. 11:832-838.

Carmena, M., and W.C. Earnshaw. 2003. The cellular geography of aurora kinases. *Nature reviews. Molecular cell biology*. 4:842-854.

Chapman, M.J., M.F. Dolan, and L. Margulis. 2000. Centrioles and kinetosomes: form, function, and evolution. *The Quarterly review of biology*. 75:409-429.

Chou, H.Y., T.H. Wang, S.C. Lee, P.H. Hsu, M.D. Tsai, C.L. Chang, and Y.M. Jeng. 2011. Phosphorylation of NuSAP by Cdk1 regulates its interaction with microtubules in mitosis. *Cell cycle*. 10:4083-4089.

Cimini, D. 2007. Detection and correction of merotelic kinetochore orientation by Aurora B and its partners. *Cell cycle*. 6:1558-1564.

Cimini, D., L.A. Cameron, and E.D. Salmon. 2004. Anaphase spindle mechanics prevent mis-segregation of merotelically oriented chromosomes. *Current biology : CB*. 14:2149-2155.

Civelekoglu-Scholey, G., B. He, M. Shen, X. Wan, E. Roscioli, B. Bowden, and D. Cimini. 2013. Dynamic bonds and polar ejection force distribution explain kinetochore oscillations in PtK1 cells. *The Journal of cell biology*. 201:577-593.

DeLuca, J.G. 2010. Kinetochore-microtubule dynamics and attachment stability. *Methods in cell biology*. 97:53-79.

Desai, A., and A. Hyman. 1999. Microtubule cytoskeleton: No longer an also Ran. *Current biology : CB*. 9:R704-707.

Domnitz, S.B., M. Wagenbach, J. Decarreau, and L. Wordeman. 2012. MCAK activity at microtubule tips regulates spindle microtubule length to promote robust kinetochore attachment. *The Journal of cell biology*. 197:231-237.

Dorn, J.F., G. Danuser, and G. Yang. 2008. Computational processing and analysis of dynamic fluorescence image data. *Methods in cell biology*. 85:497-538.

Ems-McClung, S.C., S.G. Hainline, J. Devare, H. Zong, S. Cai, S.K. Carnes, S.L. Shaw, and C.E. Walczak. 2013. Aurora B inhibits MCAK activity through a phosphoconformational switch that reduces microtubule association. *Current biology : CB*. 23:2491-2499.

Endow, S.A. 1991. The emerging kinesin family of microtubule motor proteins. *Trends in biochemical sciences*. 16:221-225.

Feine, O., A. Zur, H. Mahbubani, and M. Brandeis. 2007. Human Kid is degraded by the APC/C(Cdh1) but not by the APC/C(Cdc20). *Cell cycle*. 6:2516-2523.

Friedman, J.R., B.M. Webster, D.N. Mastronarde, K.J. Verhey, and G.K. Voeltz. 2010. ER sliding dynamics and ER-mitochondrial contacts occur on acetylated microtubules. *The Journal of cell biology*. 190:363-375.

Fujiwara, T., H. Harigae, Y. Okitsu, S. Takahashi, H. Yokoyama, M.F. Yamada, K. Ishizawa, J. Kameoka, M. Kaku, and T. Sasaki. 2006. Expression analyses and transcriptional regulation of mouse nucleolar spindle-associated protein gene in erythroid cells: essential role of NF-Y. *British journal of haematology*. 135:583-590.

Gall, J.G. 1966. Microtubule fine structure. *The Journal of cell biology*. 31:639-643.

Gardner, M.K., D.J. Odde, and K. Bloom. 2008. Kinesin-8 molecular motors: putting the brakes on chromosome oscillations. *Trends in cell biology*. 18:307-310.

Geiman, T.M., U.T. Sankpal, A.K. Robertson, Y. Chen, M. Mazumdar, J.T. Heale, J.A. Schmiesing, W. Kim, K. Yokomori, Y. Zhao, and K.D. Robertson. 2004. Isolation and characterization of a novel DNA methyltransferase complex linking DNMT3B with components of the mitotic chromosome condensation machinery. *Nucleic acids research*. 32:2716-2729.

Glotzer, M. 2005. The molecular requirements for cytokinesis. *Science*. 307:1735-1739.

Gorbsky, G.J. 2004. Mitosis: MCAK under the aura of Aurora B. *Current biology : CB*. 14:R346-348.

Gordon, M.B., L. Howard, and D.A. Compton. 2001. Chromosome movement in mitosis requires microtubule anchorage at spindle poles. *The Journal of cell biology*. 152:425-434.

Gulzar, Z.G., J.K. McKenney, and J.D. Brooks. 2013. Increased expression of NuSAP in recurrent prostate cancer is mediated by E2F1. *Oncogene*. 32:70-77.

Hays, T.S., and E.D. Salmon. 1990a. Poleward force at the kinetochore in metaphase depends on the number of kinetochore microtubules. *The Journal of cell biology*. 110:391-404.

Hays, T.S., and E.D. Salmon. 1990b. Poleward force at the kinetochore in metaphase depends on the number of kinetochore microtubules. *J Cell Biol*. 110:391-404.

Heald, R. 2000. Motor function in the mitotic spindle. *Cell*. 102:399-402.

Helenius, J., G. Brouhard, Y. Kalaidzidis, S. Diez, and J. Howard. 2006. The depolymerizing kinesin MCAK uses lattice diffusion to rapidly target microtubule ends. *Nature*. 441:115-119.

Hinkle, B., M.M. Rolls, P. Stein, T. Rapoport, and M. Terasaki. 2000. Ran is associated with chromosomes during starfish oocyte meiosis and embryonic mitoses. *Zygote*. 8 Suppl 1:S91.

Hornick, J.E., K. Karanjeet, E.S. Collins, and E.H. Hinchcliffe. 2010. Kinesins to the core: The role of microtubule-based motor proteins in building the mitotic spindle midzone. *Seminars in cell & developmental biology*. 21:290-299.

Hu, C.K., M. Coughlin, C.M. Field, and T.J. Mitchison. 2011. KIF4 regulates midzone length during cytokinesis. *Current biology : CB*. 21:815-824.

Hu, C.K., N. Ozlu, M. Coughlin, J.J. Steen, and T.J. Mitchison. 2012. Plk1 negatively regulates PRC1 to prevent premature midzone formation before cytokinesis. *Molecular biology of the cell*. 23:2702-2711.

Hunter, A.W., M. Caplow, D.L. Coy, W.O. Hancock, S. Diez, L. Wordeman, and J. Howard. 2003. The kinesin-related protein MCAK is a microtubule depolymerase that forms an ATP-hydrolyzing complex at microtubule ends. *Molecular cell*. 11:445-457.

Hussain, S., S.B. Benavente, E. Nascimento, I. Dragoni, A. Kurowski, A. Gillich, P. Humphreys, and M. Frye. 2009. The nucleolar RNA methyltransferase Misu (NSun2) is required for mitotic spindle stability. *The Journal of cell biology*. 186:27-40.

Inoue, S. 1960. On the physical properties of the mitotic spindle. *Annals of the New York Academy of Sciences*. 90:529-530.

Iyer, J., S. Moghe, M. Furukawa, and M.Y. Tsai. 2011a. What's Nu(SAP) in mitosis and cancer? *Cellular signalling*. 23:991-998.

Iyer, J., S. Moghe, M. Furukawa, and M.Y. Tsai. 2011b. What's Nu(SAP) in mitosis and cancer? *Cellular signalling*. 23:991-998.

Jaqaman, K., E.M. King, A.C. Amaro, J.R. Winter, J.F. Dorn, H.L. Elliott, N. McHedlishvili, S.E. McClelland, I.M. Porter, M. Posch, A. Toso, G. Danuser, A.D. McAinsh, P. Meraldi, and J.R. Swedlow. 2010. Kinetochore alignment within the metaphase plate is regulated by centromere stiffness and microtubule depolymerases. *The Journal of cell biology*. 188:665-679.

Jiang, K., J. Wang, J. Liu, T. Ward, L. Wordeman, A. Davidson, F. Wang, and X. Yao. 2009. TIP150 interacts with and targets MCAK at the microtubule plus ends. *EMBO reports*. 10:857-865.

Joglekar, A.P., K.S. Bloom, and E.D. Salmon. 2010. Mechanisms of force generation by end-on kinetochore-microtubule attachments. *Current opinion in cell biology*. 22:57-67.

Joglekar, A.P., and A.J. Hunt. 2002. A simple, mechanistic model for directional instability during mitotic chromosome movements. *Biophysical journal*. 83:42-58.

Jungmichel, S., F. Rosenthal, M. Altmeyer, J. Lukas, M.O. Hottiger, and M.L. Nielsen. 2013. Proteome-wide identification of poly(ADP-

Ribosyl)ation targets in different genotoxic stress responses. *Molecular cell*. 52:272-285.
Kalab, P., R.T. Pu, and M. Dasso. 1999. The ran GTPase regulates mitotic spindle assembly. *Current biology : CB*. 9:481-484.
Ke, K., J. Cheng, and A.J. Hunt. 2009. The distribution of polar ejection forces determines the amplitude of chromosome directional instability. *Current biology : CB*. 19:807-815.
King, J.M., T.S. Hays, and R.B. Nicklas. 2000a. Dynein is a transient kinetochore component whose binding is regulated by microtubule attachment, not tension. *The Journal of cell biology*. 151:739-748.
King, J.M., T.S. Hays, and R.B. Nicklas. 2000b. Dynein is a transient kinetochore component whose binding is regulated by microtubule attachment, not tension. *J Cell Biol*. 151:739-748.
Kitajima, T.S., M. Ohsugi, and J. Ellenberg. 2011. Complete kinetochore tracking reveals error-prone homologous chromosome biorientation in mammalian oocytes. *Cell*. 146:568-581.
Kline-Smith, S.L., A. Khodjakov, P. Hergert, and C.E. Walczak. 2004. Depletion of centromeric MCAK leads to chromosome congression and segregation defects due to improper kinetochore attachments. *Molecular biology of the cell*. 15:1146-1159.
Kline-Smith, S.L., S. Sandall, and A. Desai. 2005. Kinetochore-spindle microtubule interactions during mitosis. *Current opinion in cell biology*. 17:35-46.
Knowlton, A.L., W. Lan, and P.T. Stukenberg. 2006. Aurora B is enriched at merotelic attachment sites, where it regulates MCAK. *Current biology : CB*. 16:1705-1710.
Kokkinakis, D.M., X. Liu, and R.D. Neuner. 2005a. Modulation of cell cycle and gene expression in pancreatic tumor cell lines by methionine deprivation (methionine stress): implications to the therapy of pancreatic adenocarcinoma. *Molecular cancer therapeutics*. 4:1338-1348.
Kokkinakis, D.M., X. Liu, and R.D. Neuner. 2005b. Modulation of cell cycle and gene expression in pancreatic tumor cell lines by methionine deprivation (methionine stress): implications to the therapy of pancreatic adenocarcinoma. *Molecular cancer therapeutics*. 4:1338-1348.
Kurasawa, Y., W.C. Earnshaw, Y. Mochizuki, N. Dohmae, and K. Todokoro. 2004. Essential roles of KIF4 and its binding partner PRC1 in organized central spindle midzone formation. *The EMBO journal*. 23:3237-3248.

Lampson, M.A., and I.M. Cheeseman. 2011. Sensing centromere tension: Aurora B and the regulation of kinetochore function. *Trends in cell biology*. 21:133-140.

Lan, W., X. Zhang, S.L. Kline-Smith, S.E. Rosasco, G.A. Barrett-Wilt, J. Shabanowitz, D.F. Hunt, C.E. Walczak, and P.T. Stukenberg. 2004. Aurora B phosphorylates centromeric MCAK and regulates its localization and microtubule depolymerization activity. *Current biology : CB*. 14:273-286.

Lara-Chacon, B., M.B. de Leon, D. Leocadio, P. Gomez, L. Fuentes-Mera, I. Martinez-Vieyra, A. Ortega, D.A. Jans, and B. Cisneros. 2010. Characterization of an Importin alpha/beta-recognized nuclear localization signal in beta-dystroglycan. *Journal of cellular biochemistry*. 110:706-717.

Lee, Y.M., S. Lee, E. Lee, H. Shin, H. Hahn, W. Choi, and W. Kim. 2001. Human kinesin superfamily member 4 is dominantly localized in the nuclear matrix and is associated with chromosomes during mitosis. *The Biochemical journal*. 360:549-556.

Levesque, A.A., and D.A. Compton. 2001. The chromokinesin Kid is necessary for chromosome arm orientation and oscillation, but not congression, on mitotic spindles. *J Cell Biol*. 154:1135-1146.

Levesque, A.A., L. Howard, M.B. Gordon, and D.A. Compton. 2003. A functional relationship between NuMA and kid is involved in both spindle organization and chromosome alignment in vertebrate cells. *Molecular biology of the cell*. 14:3541-3552.

Levin, M.J., R. Rossi, G. Levitus, E. Mesri, S. Bonnefoy, N. Kerner, and M. Hontebeyrie-Joskowicz. 1990. The cloned C-terminal region of a Trypanosoma cruzi P ribosomal protein harbors two antigenic determinants. *Immunology letters*. 24:69-73.

Lewis, W.H. 1939. Changes of viscosity and cell activity. *Science*. 89.

Li, L., Y. Zhou, L. Sun, G. Xing, C. Tian, J. Sun, L. Zhang, and F. He. 2007a. NuSAP is degraded by APC/C-Cdh1 and its overexpression results in mitotic arrest dependent of its microtubules' affinity. *Cellular signalling*. 19:2046-2055.

Li, L., Y. Zhou, L. Sun, G. Xing, C. Tian, J. Sun, L. Zhang, and F. He. 2007b. NuSAP is degraded by APC/C-Cdh1 and its overexpression results in mitotic arrest dependent of its microtubules' affinity. *Cellular signalling*. 19:2046-2055.

Liu, D., G. Vader, M.J. Vromans, M.A. Lampson, and S.M. Lens. 2009. Sensing chromosome bi-orientation by spatial separation of aurora B kinase from kinetochore substrates. *Science*. 323:1350-1353.

Liu, J., A. Desai, J.N. Onuchic, and T. Hwa. 2007. A mechanobiochemical mechanism for monooriented chromosome oscillation in mitosis. *Proceedings of the National Academy of Sciences of the United States of America*. 104:16104-16109.

Maddox, P., E. Chin, A. Mallavarapu, E. Yeh, E.D. Salmon, and K. Bloom. 1999. Microtubule dynamics from mating through the first zygotic division in the budding yeast Saccharomyces cerevisiae. *The Journal of cell biology*. 144:977-987.

Magidson, V., C.B. O'Connell, J. Loncarek, R. Paul, A. Mogilner, and A. Khodjakov. 2011. The spatial arrangement of chromosomes during prometaphase facilitates spindle assembly. *Cell*. 146:555-567.

Maiato, H., P. Sampaio, and C.E. Sunkel. 2004. Microtubule-associated proteins and their essential roles during mitosis. *International review of cytology*. 241:53-153.

Maney, T., A.W. Hunter, M. Wagenbach, and L. Wordeman. 1998. Mitotic centromere-associated kinesin is important for anaphase chromosome segregation. *The Journal of cell biology*. 142:787-801.

Mazumdar, M., and T. Misteli. 2005. Chromokinesins: multitalented players in mitosis. *Trends in cell biology*. 15:349-355.

Mazumdar, M., S. Sundareshan, and T. Misteli. 2004. Human chromokinesin KIF4A functions in chromosome condensation and segregation. *The Journal of cell biology*. 166:613-620.

McClelland, S.E., S. Borusu, A.C. Amaro, J.R. Winter, M. Belwal, A.D. McAinsh, and P. Meraldi. 2007. The CENP-A NAC/CAD kinetochore complex controls chromosome congression and spindle bipolarity. *The EMBO journal*. 26:5033-5047.

McDonald, K.L., M.K. Edwards, and J.R. McIntosh. 1979. Cross-sectional structure of the central mitotic spindle of Diatoma vulgare. Evidence for specific interactions between antiparallel microtubules. *The Journal of cell biology*. 83:443-461.

Min, B.J., N. Kim, T. Chung, O.H. Kim, G. Nishimura, C.Y. Chung, H.R. Song, H.W. Kim, H.R. Lee, J. Kim, T.H. Kang, M.E. Seo, S.D. Yang, D.H. Kim, S.B. Lee, J.I. Kim, J.S. Seo, J.Y. Choi, D. Kang, D. Kim, W.Y. Park, and T.J. Cho. 2011. Whole-exome sequencing identifies mutations of KIF22 in spondyloepimetaphyseal dysplasia with joint laxity, leptodactylic type. *American journal of human genetics*. 89:760-766.

Nam, H.S., and R. Benezra. 2009. High levels of Id1 expression define B1 type adult neural stem cells. *Cell stem cell*. 5:515-526.

Nie, J., H. Wang, F. He, and H. Huang. 2010. Nusap1 is essential for neural crest cell migration in zebrafish. *Protein & cell*. 1:259-266.

Nishimoto, T. 1999. A new role of ran GTPase. *Biochemical and biophysical research communications*. 262:571-574.

Nunes Bastos, R., S.R. Gandhi, R.D. Baron, U. Gruneberg, E.A. Nigg, and F.A. Barr. 2013. Aurora B suppresses microtubule dynamics and limits central spindle size by locally activating KIF4A. *The Journal of cell biology*. 202:605-621.

Oh, S., H. Hahn, T.A. Torrey, H. Shin, W. Choi, Y.M. Lee, H.C. Morse, and W. Kim. 2000. Identification of the human homologue of mouse KIF4, a kinesin superfamily motor protein. *Biochimica et biophysica acta*. 1493:219-224.

Ohi, R., M.L. Coughlin, W.S. Lane, and T.J. Mitchison. 2003. An inner centromere protein that stimulates the microtubule depolymerizing activity of a KinI kinesin. *Developmental cell*. 5:309-321.

Ohi, R., T. Sapra, J. Howard, and T.J. Mitchison. 2004. Differentiation of cytoplasmic and meiotic spindle assembly MCAK functions by Aurora B-dependent phosphorylation. *Molecular biology of the cell*. 15:2895-2906.

Parra, M.T., R. Gomez, A. Viera, J. Page, A. Calvente, L. Wordeman, J.S. Rufas, and J.A. Suja. 2006. A perikinetochoric ring defined by MCAK and Aurora-B as a novel centromere domain. *PLoS genetics*. 2:e84.

Raemaekers, T., K. Ribbeck, J. Beaudouin, W. Annaert, M. Van Camp, I. Stockmans, N. Smets, R. Bouillon, J. Ellenberg, and G. Carmeliet. 2003a. NuSAP, a novel microtubule-associated protein involved in mitotic spindle organization. *The Journal of cell biology*. 162:1017-1029.

Raemaekers, T., K. Ribbeck, J. Beaudouin, W. Annaert, M. Van Camp, I. Stockmans, N. Smets, R. Bouillon, J. Ellenberg, and G. Carmeliet. 2003b. NuSAP, a novel microtubule-associated protein involved in mitotic spindle organization. *The Journal of cell biology*. 162:1017-1029.

Ribbeck, K., A.C. Groen, R. Santarella, M.T. Bohnsack, T. Raemaekers, T. Kocher, M. Gentzel, D. Gorlich, M. Wilm, G. Carmeliet, T.J. Mitchison, J. Ellenberg, A. Hoenger, and I.W. Mattaj. 2006a. NuSAP, a mitotic RanGTP target that stabilizes and cross-links microtubules. *Molecular biology of the cell*. 17:2646-2660.

Ribbeck, K., A.C. Groen, R. Santarella, M.T. Bohnsack, T. Raemaekers, T. Kocher, M. Gentzel, D. Gorlich, M. Wilm, G. Carmeliet, T.J. Mitchison, J. Ellenberg, A. Hoenger, and I.W. Mattaj. 2006b. NuSAP, a mitotic RanGTP target that stabilizes and cross-links microtubules. *Molecular biology of the cell*. 17:2646-2660.

Ribbeck, K., T. Raemaekers, G. Carmeliet, and I.W. Mattaj. 2007a. A role for NuSAP in linking microtubules to mitotic chromosomes. *Current biology : CB*. 17:230-236.

Ribbeck, K., T. Raemaekers, G. Carmeliet, and I.W. Mattaj. 2007b. A role for NuSAP in linking microtubules to mitotic chromosomes. *Current biology : CB*. 17:230-236.

Rieder, C.L. 1990. Formation of the astral mitotic spindle: ultrastructural basis for the centrosome-kinetochore interaction. *Electron microscopy reviews*. 3:269-300.

Rieder, C.L., E.A. Davison, L.C. Jensen, L. Cassimeris, and E.D. Salmon. 1986a. Oscillatory movements of monooriented chromosomes and their position relative to the spindle pole result from the ejection properties of the aster and half-spindle. *The Journal of cell biology*. 103:581-591.

Rieder, C.L., E.A. Davison, L.C. Jensen, L. Cassimeris, and E.D. Salmon. 1986b. Oscillatory movements of monooriented chromosomes and their position relative to the spindle pole result from the ejection properties of the aster and half-spindle. *J Cell Biol*. 103:581-591.

Ruchaud, S., M. Carmena, and W.C. Earnshaw. 2007. Chromosomal passengers: conducting cell division. *Nature reviews. Molecular cell biology*. 8:798-812.

Sanhaji, M., C.T. Friel, L. Wordeman, F. Louwen, and J. Yuan. 2011. Mitotic centromere-associated kinesin (MCAK): a potential cancer drug target. *Oncotarget*. 2:935-947.

Santamaria, A., S. Nagel, H.H. Sillje, and E.A. Nigg. 2008. The spindle protein CHICA mediates localization of the chromokinesin Kid to the mitotic spindle. *Current biology : CB*. 18:723-729.

Sardon, T., R.A. Pache, A. Stein, H. Molina, I. Vernos, and P. Aloy. 2010. Uncovering new substrates for Aurora A kinase. *EMBO reports*. 11:977-984.

Saxton, W.M., and J.R. McIntosh. 1987. Interzone microtubule behavior in late anaphase and telophase spindles. *The Journal of cell biology*. 105:875-886.

Schaerer-Brodbeck, C., and H. Riezman. 2000. Interdependence of filamentous actin and microtubules for asymmetric cell division. *Biological chemistry*. 381:815-825.

Shiroguchi, K., M. Ohsugi, M. Edamatsu, T. Yamamoto, and Y.Y. Toyoshima. 2003. The second microtubule-binding site of monomeric kid enhances the microtubule affinity. *The Journal of biological chemistry*. 278:22460-22465.

Shrestha, S., L.J. Wilmeth, J. Eyer, and C.B. Shuster. 2012. PRC1 controls spindle polarization and recruitment of cytokinetic factors during monopolar cytokinesis. *Molecular biology of the cell*. 23:1196-1207.

Skibbens, R.V., V.P. Skeen, and E.D. Salmon. 1993a. Directional instability of kinetochore motility during chromosome congression and segregation in mitotic newt lung cells: a push-pull mechanism. *J Cell Biol*. 122:859-875.

Skibbens, R.V., V.P. Skeen, and E.D. Salmon. 1993b. Directional instability of kinetochore motility during chromosome congression and segregation in mitotic newt lung cells: a push-pull mechanism. *The Journal of cell biology*. 122:859-875.

Slep, K.C., and R.D. Vale. 2007. Structural basis of microtubule plus end tracking by XMAP215, CLIP-170, and EB1. *Molecular cell*. 27:976-991.

Song, L., and M. Rape. 2010a. Regulated degradation of spindle assembly factors by the anaphase-promoting complex. *Molecular cell*. 38:369-382.

Song, L., and M. Rape. 2010b. Regulated degradation of spindle assembly factors by the anaphase-promoting complex. *Molecular cell*. 38:369-382.

Stumpff, J., G. von Dassow, M. Wagenbach, C. Asbury, and L. Wordeman. 2008. The kinesin-8 motor Kif18A suppresses kinetochore movements to control mitotic chromosome alignment. *Developmental cell*. 14:252-262.

Stumpff, J., M. Wagenbach, A. Franck, C.L. Asbury, and L. Wordeman. 2012. Kif18A and chromokinesins confine centromere movements via microtubule growth suppression and spatial control of kinetochore tension. *Developmental cell*. 22:1017-1029.

Sturgill, E.G., and R. Ohi. 2013. Kinesin-12 differentially affects spindle assembly depending on its microtubule substrate. *Current biology : CB*. 23:1280-1290.

Sudakin, V., and T.J. Yen. 2007. Targeting mitosis for anti-cancer therapy. *BioDrugs : clinical immunotherapeutics, biopharmaceuticals and gene therapy*. 21:225-233.

Sutradhar, S., and R. Paul. 2014. Tug-of-war between opposing molecular motors explains chromosomal oscillation during mitosis. *Journal of theoretical biology*. 344:56-69.

Tahara, K., M. Takagi, M. Ohsugi, T. Sone, F. Nishiumi, K. Maeshima, Y. Horiuchi, N. Tokai-Nishizumi, F. Imamoto, T. Yamamoto, S. Kose, and N. Imamoto. 2008a. Importin-beta and the small guanosine

triphosphatase Ran mediate chromosome loading of the human chromokinesin Kid. *The Journal of cell biology*. 180:493-506.

Tahara, K., M. Takagi, M. Ohsugi, T. Sone, F. Nishiumi, K. Maeshima, Y. Horiuchi, N. Tokai-Nishizumi, F. Imamoto, T. Yamamoto, S. Kose, and N. Imamoto. 2008b. Importin-beta and the small guanosine triphosphatase Ran mediate chromosome loading of the human chromokinesin Kid. *J Cell Biol*. 180:493-506.

Tanenbaum, M.E., L. Macurek, B. van der Vaart, M. Galli, A. Akhmanova, and R.H. Medema. 2011. A complex of Kif18b and MCAK promotes microtubule depolymerization and is negatively regulated by Aurora kinases. *Current biology : CB*. 21:1356-1365.

Tokai-Nishizumi, N., M. Ohsugi, E. Suzuki, and T. Yamamoto. 2005. The chromokinesin Kid is required for maintenance of proper metaphase spindle size. *Molecular biology of the cell*. 16:5455-5463.

Tokai, N., A. Fujimoto-Nishiyama, Y. Toyoshima, S. Yonemura, S. Tsukita, J. Inoue, and T. Yamamota. 1996. Kid, a novel kinesin-like DNA binding protein, is localized to chromosomes and the mitotic spindle. *EMBO Journal*. 15:457-467.

Toso, A., J.R. Winter, A.J. Garrod, A.C. Amaro, P. Meraldi, and A.D. McAinsh. 2009. Kinetochore-generated pushing forces separate centrosomes during bipolar spindle assembly. *The Journal of cell biology*. 184:365-372.

Trieselmann, N., S. Armstrong, J. Rauw, and A. Wilde. 2003. Ran modulates spindle assembly by regulating a subset of TPX2 and Kid activities including Aurora A activation. *J Cell Sci*. 116:4791-4798.

Vader, G., R.H. Medema, and S.M. Lens. 2006. The chromosomal passenger complex: guiding Aurora-B through mitosis. *The Journal of cell biology*. 173:833-837.

Vanden Bosch, A., T. Raemaekers, S. Denayer, S. Torrekens, N. Smets, K. Moermans, M. Dewerchin, P. Carmeliet, and G. Carmeliet. 2010. NuSAP is essential for chromatin-induced spindle formation during early embryogenesis. *Journal of cell science*. 123:3244-3255.

Vanneste, D., V. Ferreira, and I. Vernos. 2011. Chromokinesins: localization-dependent functions and regulation during cell division. *Biochemical Society transactions*. 39:1154-1160.

Verbakel, W., G. Carmeliet, and Y. Engelborghs. 2011. SAP-like domain in nucleolar spindle associated protein mediates mitotic chromosome loading as well as interphase chromatin interaction. *Biochemical and biophysical research communications*. 411:732-737.

Vernos, I., and E. Karsenti. 1996. Motors involved in spindle assembly and chromosome segregation. *Curr. Opin. Cell Biol.* 8:4-9.

Vladimirou, E., E. Harry, N. Burroughs, and A.D. McAinsh. 2011. Springs, clutches and motors: driving forward kinetochore mechanism by modelling. *Chromosome research : an international journal on the molecular, supramolecular and evolutionary aspects of chromosome biology*. 19:409-421.

Wadia, P.P., M. Coram, R.J. Armstrong, M. Mindrinos, A.J. Butte, and D.B. Miklos. 2010. Antibodies specifically target AML antigen NuSAP1 after allogeneic bone marrow transplantation. *Blood*. 115:2077-2087.

Walczak, C.E. 2000. Molecular mechanisms of spindle function. *Genome biology*. 1:REVIEWS101.

Wan, X., D. Cimini, L.A. Cameron, and E.D. Salmon. 2012. The coupling between sister kinetochore directional instability and oscillations in centromere stretch in metaphase PtK1 cells. *Molecular biology of the cell*. 23:1035-1046.

Wandke, C., M. Barisic, R. Sigl, V. Rauch, F. Wolf, A.C. Amaro, C.H. Tan, A.J. Pereira, U. Kutay, H. Maiato, P. Meraldi, and S. Geley. 2012. Human chromokinesins promote chromosome congression and spindle microtubule dynamics during mitosis. *J Cell Biol*. 198:847-863.

Wang, E., E.R. Ballister, and M.A. Lampson. 2011. Aurora B dynamics at centromeres create a diffusion-based phosphorylation gradient. *The Journal of cell biology*. 194:539-549.

Waters, J.C., R.V. Skibbens, and E.D. Salmon. 1996. Oscillating mitotic newt lung cell kinetochores are, on average, under tension and rarely push. *Journal of cell science*. 109 ( Pt 12):2823-2831.

Welburn, J.P., M. Vleugel, D. Liu, J.R. Yates, 3rd, M.A. Lampson, T. Fukagawa, and I.M. Cheeseman. 2010. Aurora B phosphorylates spatially distinct targets to differentially regulate the kinetochore-microtubule interface. *Molecular cell*. 38:383-392.

Wilde, A., and Y. Zheng. 1999. Stimulation of microtubule aster formation and spindle assembly by the small GTPase Ran. *Science*. 284:1359-1362.

Wordeman, L., and T.J. Mitchison. 1995. Identification and partial characterization of mitotic centromere-associated kinesin, a kinesin-related protein that associates with centromeres during mitosis. *The Journal of cell biology*. 128:95-104.

Xie, P., L. Li, G. Xing, C. Tian, Y. Yin, F. He, and L. Zhang. 2011. ATM-mediated NuSAP phosphorylation induces mitotic arrest. *Biochemical and biophysical research communications*. 404:413-418.

Yajima, J., M. Edamatsu, J. Watai-Nishii, N. Tokai-Nishizumi, T. Yamamoto, and Y.Y. Toyoshima. 2003. The human chromokinesin Kid is a plus end-directed microtubule-based motor. *The EMBO journal*. 22:1067-1074.

Ye, F., L. Tan, Q. Yang, Y. Xia, L.W. Deng, M. Murata-Hori, and Y.C. Liou. 2011. HURP regulates chromosome congression by modulating kinesin Kif18A function. *Current biology : CB*. 21:1584-1591.

Yu, Y., X.Y. Wang, L. Sun, Y.L. Wang, Y.F. Wan, X.Q. Li, and Y.M. Feng. 2014. Inhibition of KIF22 suppresses cancer cell proliferation by delaying mitotic exit through upregulating CDC25C expression. *Carcinogenesis*. 35:1416-1425.

Zhai, Y., P.J. Kronebusch, and G.G. Borisy. 1995. Kinetochore microtubule dynamics and the metaphase-anaphase transition. *The Journal of cell biology*. 131:721-734.

Zhang, C., M. Hughes, and P.R. Clarke. 1999. Ran-GTP stabilises microtubule asters and inhibits nuclear assembly in Xenopus egg extracts. *Journal of cell science*. 112 ( Pt 14):2453-2461.

Zhang, M., D. Yang, X. Liu, Y. Liu, J. Liang, H. He, K. Zhong, L. Lin, G. Tao, C. Zhang, and J. Zhou. 2013. [Expression of Nusap1 in the surgical margins of hepatocellular carcinoma and its association with early recurrence]. *Nan fang yi ke da xue xue bao = Journal of Southern Medical University*. 33:937-938, inside back cover.

Zhang, X., and C.E. Walczak. 2006. Chromosome segregation: correcting improperly attached chromosomes. *Current biology : CB*. 16:R677-679.

Zhu, C., and W. Jiang. 2005. Cell cycle-dependent translocation of PRC1 on the spindle by Kif4 is essential for midzone formation and cytokinesis. *Proceedings of the National Academy of Sciences of the United States of America*. 102:343-348.

Zhu, C., E. Lau, R. Schwarzenbacher, E. Bossy-Wetzel, and W. Jiang. 2006. Spatiotemporal control of spindle midzone formation by PRC1 in human cells. *Proceedings of the National Academy of Sciences of the United States of America*. 103:6196-6201.

## Appendix

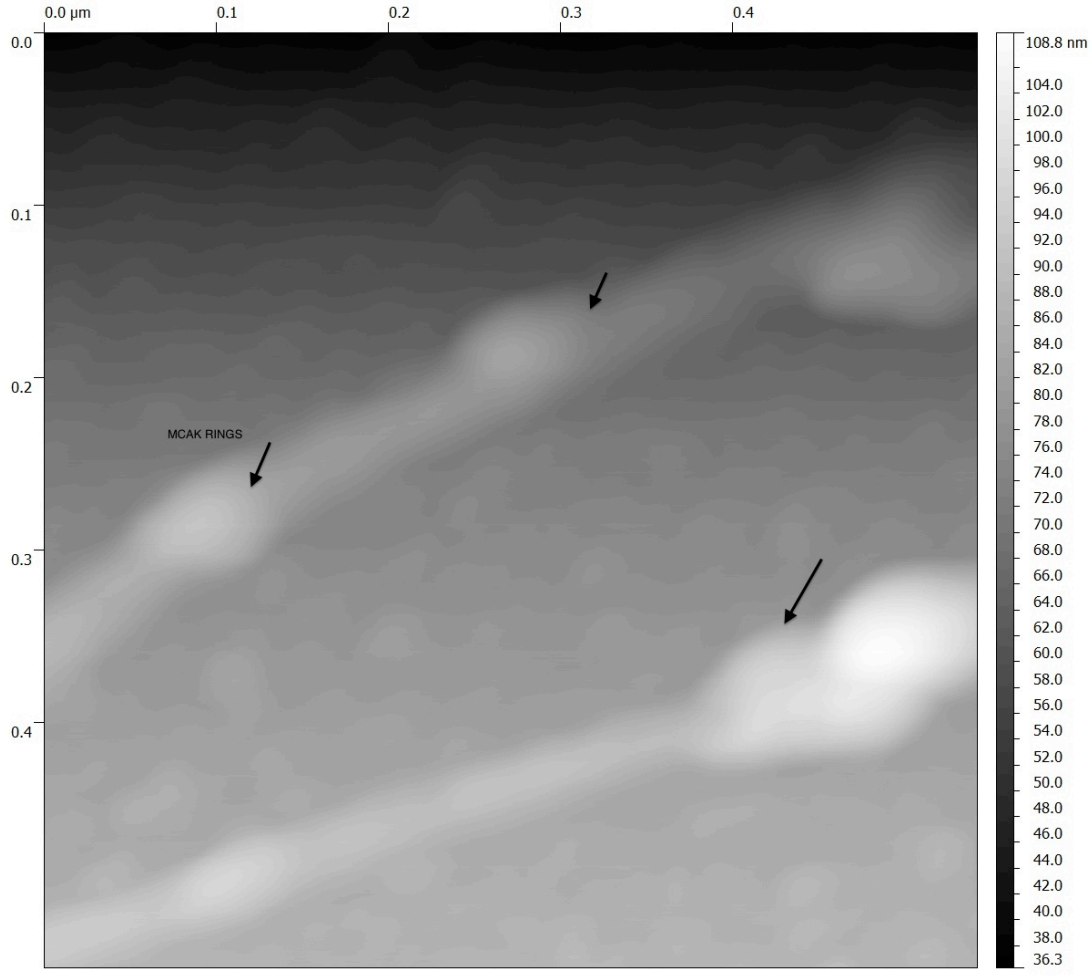


**Figure S1. MCAK bracelet on microtubules (AFM).**

In vitro microtubules were incubated with MCAK protein and fixed on grids. The imaging was acquired with AFM. MCAK protein forms rings on the surface of MTs. The arrow indicates MCAK bracelets.

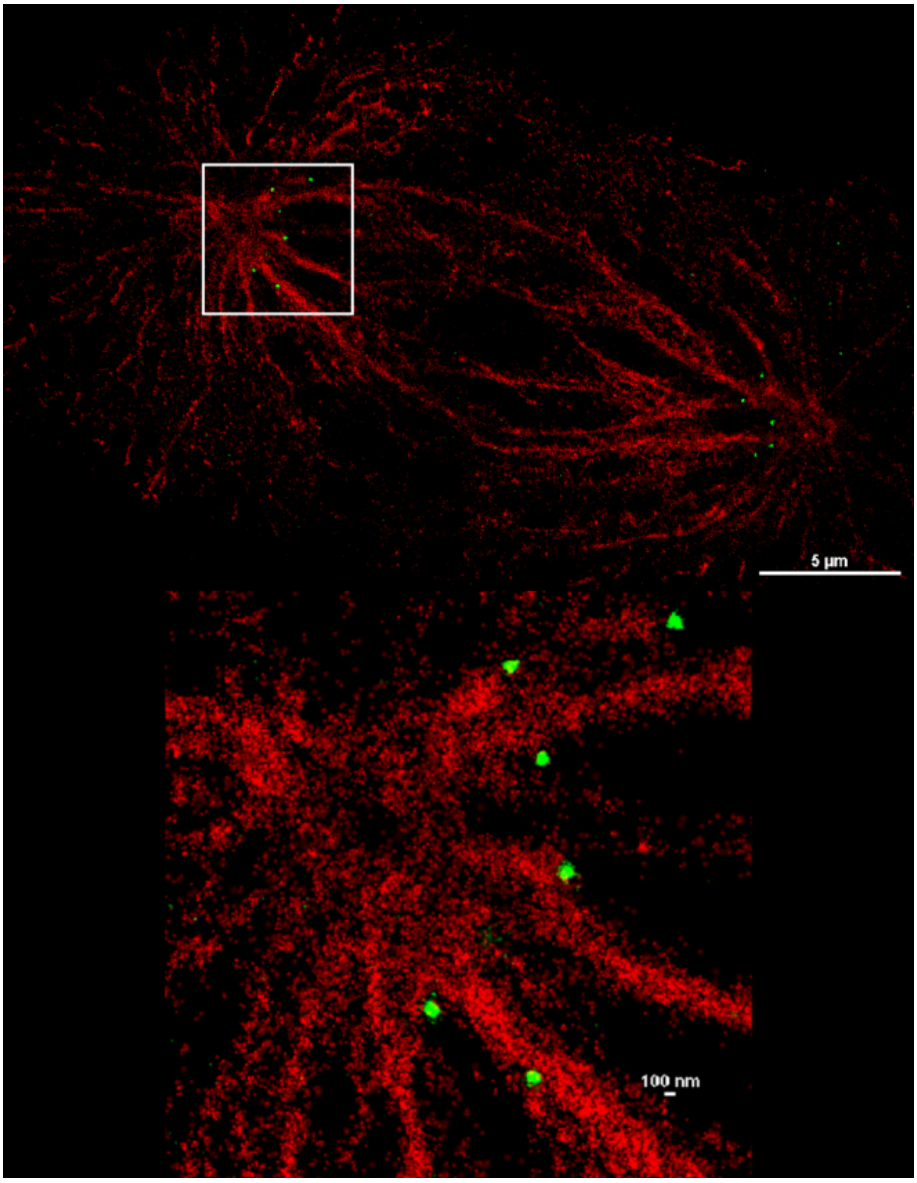


**Figure S2. Anaphase spindle structure.**

Anaphase PTK2 cells were cultured on 18mm cover glass and stained with mouse anti-alpha-tubulin (1:2000, Sigma) for microtubules and CREST (1:2000, Invision) for centromeres. The images were taken with N-STROM.

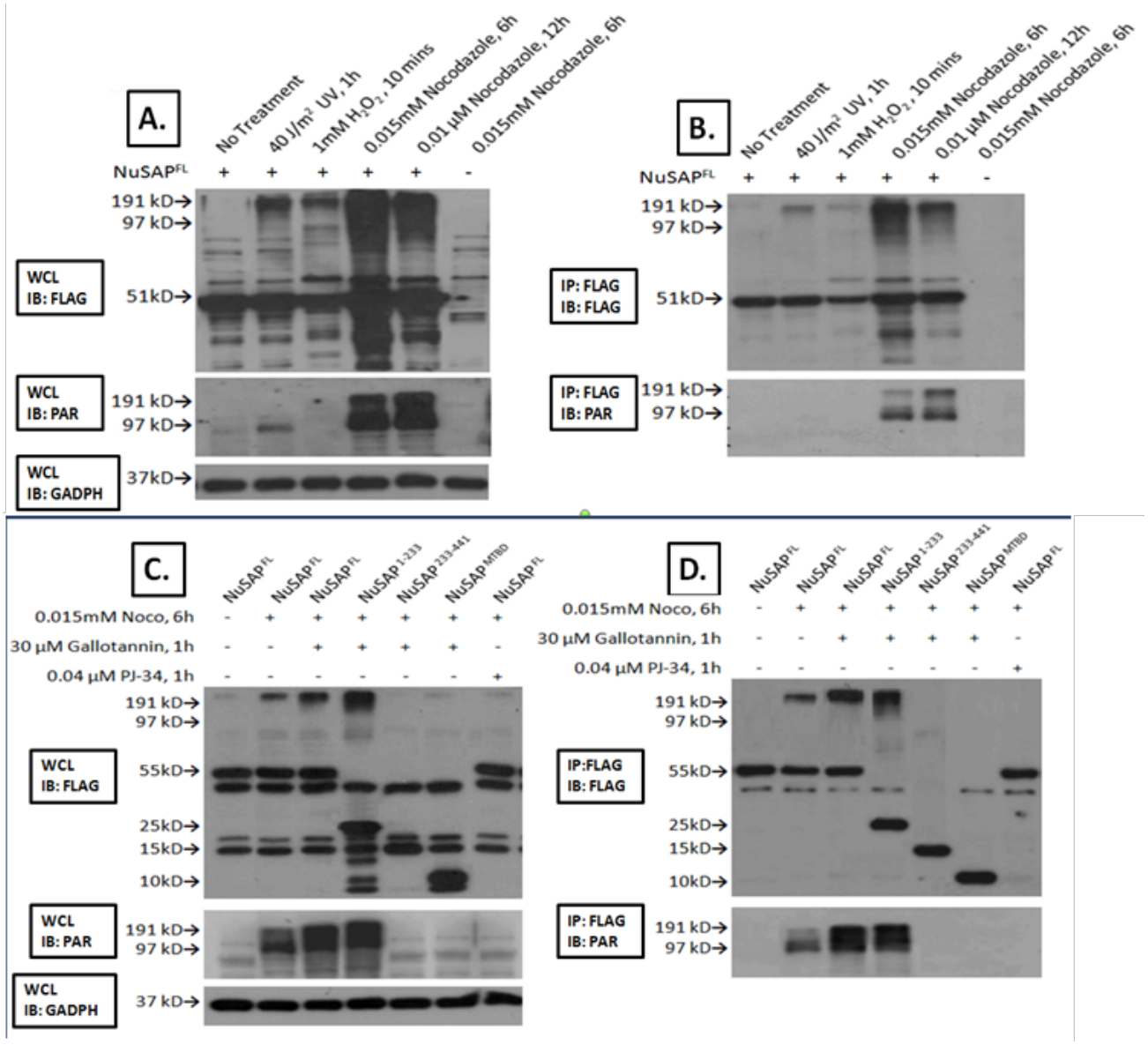


**Figure S3. NuSAP is PAR modified at its N1-233 domain (done by FYP student, Sandra Yeo).**

(A-B) The immunoprecipitation of NuSAP were treated with nocodazole, H2O2 or UV for the indicated conditions. The immunoprecipitated protein and the

whole-cell lysate were blotted with anti-FLAG, anti-PAR and anti-GAPDH antibodies.
(C-D) The immunoprecipitation of NuSAP, $NuSAP^{1-233}$, $NuSAP^{233-441}$ and $NuSAP^{MTBD}$ were treated with nocodazole for the indicated conditions. The immunoprecipitated protein and the whole-cell lysate were blotted with anti-FLAG, anti-PAR and anti-GAPDH antibodies.

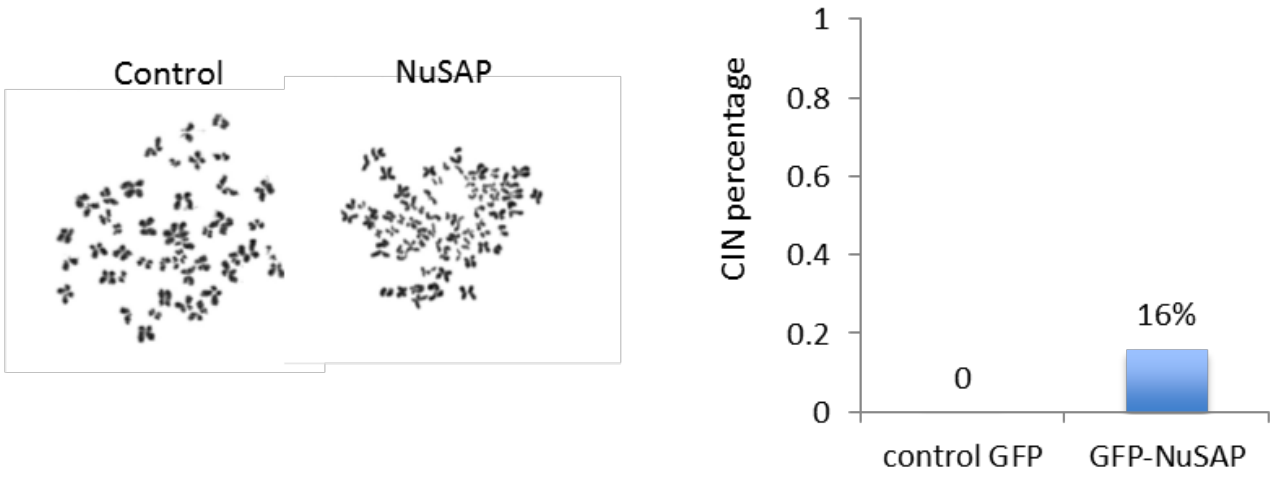


**Figure S4. Overexpression of NuSAP induces chromosome instability in normal cells.**

IMR90 cells were transfected with GFP-NuSAP or GFP vector as a control and the GFP positive cells were separated with FACS and stained with Giemsa. The number of the chromosomes were analyzed and the cells with NuSAP overexpression show severe chromosome instability phenotype.

**Movie S1. Representative 3D movie of chromosome movement in GFP-NuSAP transfected metaphase cells.**

Stable mCherry-H2B HeLa cells were transfected with GFP-NuSAP and synchronized with nocodazole/MG132 before imaging. Frames were acquired in a 5s interval for 5min. The 3D view of both channels, 3D view with the chromosome marked and the 3D single chromosome movement tracks color-coded with time were presented.

**Movie S2. Representative 3D movie of centromere oscillation in control siRNA, NuSAP siRNA and Kif22 siRNA depleted synchronized metaphase cells.**

Stable mCherry-H2B HeLa cells were transfected with GFP-CENPA to mark the centromeres, GFP-centrin for centrosomes and depleted with control siRNA, NuSAP siRNA and Kif22 siRNA. The cells were synchronized with nocodazole/MG132 before imaging. Frames were acquired in a 15s interval for 10min. The 3D view, 3D centromeres tracks color-coded with time and speed were presented.

**Movie S3. Representative 3D movie of centromere oscillation in Nuf2 siRNA, NuSAP/Nuf2 siRNA and Kif22/Nuf2 siRNA depleted synchronized metaphase cells.**

Stable mCherry-H2B HeLa cells were transfected with GFP-CENPA to mark the centromeres, GFP-centrin for centrosomes and depleted with Nuf2 siRNA, NuSAP/Nuf2 siRNA and Kif22/Nuf2 siRNA. The cells were synchronized with nocodazole/MG132 before imaging. Frames were acquired in a 15s interval for 10min. The 3D view, 3D centromeres tracks color-coded with time and speed were presented. Movie corresponds to Figure 5A and B.

**Movie S4. Representative 3D movie of centromere oscillation in control siRNA, NuSAP siRNA and Kif22 siRNA depleted monopolar cells.**

Stable mCherry-H2B HeLa cells were transfected with GFP-CENPA to mark the centromeres, GFP-centrin for centrosomes and depleted with control siRNA, NuSAP siRNA and Kif22 siRNA. The cells were treated with monastrol before imaging. Frames were acquired in a 15s interval for 10min. The 3D view, 3D centromeres tracks color-coded with time and speed were presented.

**Movie S5. Representative 3D movie of centromere oscillation in Nuf2 siRNA, NuSAP/Nuf2 siRNA and Kif22/Nuf2 siRNA depleted monopolar cells.**

Stable mCherry-H2B HeLa cells were transfected with GFP-CENPA to mark the centromeres, GFP-centrin for centrosomes and depleted with Nuf2 siRNA, NuSAP/Nuf2 siRNA and Kif22/Nuf2 siRNA. The cells were treated with monastrol before imaging. Frames were acquired in a 15s interval for 10min. The 3D view, 3D centromeres tracks color-coded with time and speed were presented.

**Movie S6. The overexpression of NuSAP leads to chromosome mis-segregation in anaphase.**

Stable mCherry-H2B HeLa cells were transfected with GFP-NuSAP. The 3D view of the anaphase cell was presented and frames were acquired in a 15s interval for 30min.

**Movie S7. The localization of Kif4a at midzone region during the cell cycle.**

HeLa cells were transfected with GFP-Kif4a. Frames were acquired in a 15s interval for 30min.

**Movie S8. NuSAP regulates the localization of Kif4a at midzone region.**

HeLa cells were transfected with GFP-Kif4a and mCherry-NuSAP. Frames were acquired in a 15s interval for 30min.

**Movie S9. The midzone formation in monopolar anaphase cells.**

HeLa cells were transfected with GFP-α-tubulin. The cells were treated with monastrol for 2h and flavopiridol for 30min before imaging. Frames were acquired in a 15s interval for 30min.

**Movie S10. NuSAP stabilizes midzone microtubule in monopolar anaphase cells.**

HeLa cells were transfected with GFP-α-tubulin and mCherry-NuSAP. The cells were treated with monastrol for 2h and flavopiridol for 30min before imaging. Frames were acquired in a 15s interval for 30min.

**Movie S11. The dynamics of mitochondria in NuSAP overexpressing metaphase cells.**

Stable mito-red HeLa cells were transfected with GFP-α-tubulin or GFP-NuSAP. Frames were acquired in a 10s interval for 10min.

**Movie S12. The dynamics of mitochondria in NuSAP overexpressing anaphase cells.**

Stable mito-red HeLa cells were transfected with GFP-α-tubulin or GFP-NuSAP. Frames were acquired in a 10s interval for 10min.